**ANALYSIS AND DESIGN OF MICROSTRIP PRINTED STRUCTURES
ON ELECTROMAGNETIC BANDGAP SUBSTRATES**

**A THESIS SUBMITTED TO
THE GRADUATE SCHOOL OF NATURAL AND APPLIED SCIENCES
OF
MIDDLE EAST TECHNICAL UNIVERSITY**

BY

TAMER GÜDÜ

**IN PARTIAL FULFILLMENT OF THE REQUIREMENTS
FOR
THE DEGREE OF DOCTOR OF PHILOSOPHY
IN
ELECTRICAL AND ELECTRONICS ENGINEERING**

MARCH 2008

Approval of the thesis:

**ANALYSIS AND DESIGN OF MICROSTRIP PRINTED STRUCTURES
ON ELECTROMAGNETIC BANDGAP SUBSTRATES**

submitted by **TAMER GÜDÜ** in partial fulfillment of the requirements for the degree of **Doctor of Philosophy in Electrical and Electronics Engineering Department, Middle East Technical University** by,

Prof. Dr. Canan Özgen _____
Dean, Graduate School of **Natural and Applied Sciences**

Prof. Dr. İsmet Erkmen _____
Head of Department, **Electrical and Electronics Engineering**

Assist. Prof. Dr. Lale Alatan _____
Supervisor, **Electrical and Electronics Enginnering Dept., METU**

Examining Committee Members:

Assoc. Prof. Dr. Sencer Koç _____
Electrical and Electronics Engineering Dept., METU

Assist. Prof. Dr. Lale Alatan _____
Electrical and Electronics Engineering Dept., METU

Prof. Dr. Mustafa Kuzuoğlu _____
Electrical and Electronics Engineering Dept., METU

Assoc. Prof. Dr. Özlem Çivi _____
Electrical and Electronics Engineering Dept., METU

Assoc. Prof. Dr. Vakur. B. Ertürk _____
Electrical and Electronics Engineering Dept., Bilkent Univ.

Date: March, 7, 2008

I hereby declare that all information in this document has been obtained and presented in accordance with academic rules and ethical conduct. I also declare that, as required by these rules and conduct, I have fully cited and referenced all material and results that are not original to this work.

Name, Last Name: Tamer GÜDÜ

Signature   :

ABSTRACT

ANALYSIS AND DESIGN OF MICROSTRIP PRINTED STRUCTURES ON ELECTORMAGNETIC BANDGAP SUBSTRATES

GÜDÜ, Tamer

Ph.D., Department of Electrical and Electronics Engineering

Supervisor: Assist. Prof. Dr. Lale Alatan

March 2008, 124 pages

In the first part of the thesis, the 2-D structures in stratified media are analyzed using an efficient MoM technique. The method is used to optimize transmitted or reflected electric fields from the 2-D structures. The genetic algorithm is used in the optimization process. In the second part a 3-D MoM technique is implemented to analyze multilayered structures with periodically implanted material blocks. Using the method, the dispersion and reflection characteristics of the structure are calculated for different configurations. The results are compared with the results found in the literature and it is seen that they are in good agreement. Asymptotic Waveform Evaluation (AWE) technique is utilized to obtain the Pade approximation of the solution in terms of frequency. The high order derivatives that are required by the AWE technique are calculated through Automatic Differentiation technique. Using the AWE method, the dispersion diagram and reflection characteristics of the periodic structures are obtained in a shorter time. The results are compared with the ones obtained through direct calculation and it

is seen that they are in perfect agreement. The reflection coefficients that are obtained from the 3-D MoM procedure are used to calculate Green's functions that approximate electric field of an infinitesimal dipole on the periodically implanted substrate. Using the calculated Green's functions and the spectral domain MoM procedure, dispersion characteristics of a microstrip line on the periodically implanted substrate are obtained.

ÖZ

ELEKTROMANYETİK BANT ARALIKLI KATMAN ÜZERİNDEKİ BASKILI MİKROŞERİT YAPILARIN ANALİZ VE TASARIMI

GÜDÜ, Tamer

Doktora, Elektrik ve Elektronik Mühendisliği Bölümü

Tez Yöneticisi: Yrd. Doçent Dr. Lale Alatan

Mart 2008, 124 sayfa

Bu tezin ilk kısmında öncelikle iki boyutlu mikroşerit yapılar verimli bir moment metodu kullanılarak analiz edilmiştir. Bu method bu yapılardan yansıyan ve iletilen eletrik alanı optimize etmek için kullanılmıştır. Optimizasyon işleminde genetik algortitma kullanılmıştır. İkinci kısımda içinde tekarlı olarak gömülü yalıtkan bulunan çok katmanlı yapıları analiz etmek üzere bir üç boyutlu moment tekniği uygulaması yapılmıştır. Bu metod kullanılarak bu yapıların dispersiyon ve yansıma karakteritikleri hesaplanmıştır. Bulunan sonuçlar literatürdeki sonuçlar ile karşılaştırılmış ve mükemmel bir uyum içinde olduğu görülmüştür. Dispersion ve yansıma karakteristiklerini daha kısa bir zamanda elde etmek amacıyla asimptotik dalga hesaplama (AWE) methodu önerilmiştir. AWE metodu için gerekli olan yüksek dereceli türevler otomatik türev alma teorisi kullanılarak hesaplanmıştır. AWE metodu kullanılarak söz konusu tekrarlı yapıların karakteristikleri daha kısa sürede hesaplanmıştır. Elde edilen sonuçlar doğrudan hesaplama yöntemi ile elde edilen sonuçlar ile karşılaştırılmış ve mükemmel bir

uyum içinde olduğu gözlenmiştir. Üç boyutlu moment metodu ile elde edilen yansıma katsayıları, içinde tekrarlı olarak gömülü yalıtkan bulunan katman üzerindeki küçük dipollerin Green fonksiyonlarını hesaplamak üzere kullanılmıştır. Hesaplanan bu Green fonksiyonları ve spektral alan yaklaşımlı moment tekniği kullanılarak yalıtkan gömülü katman üzerindeki bir mikroşerit transmissyon hattının dispersiyon karakteristikleri elde edilmiştir.

Anahtar kelimeler: tekrarlı yapılar, elektromanyetik bant aralığı, moment metodu, Green fonksiyonları, mikroşerit yapılar.

ACKNOWLEDGEMENTS

TABLE OF CONTENTS

x

LIST OF FIGURES

FIGURES

LIST OF TABLES

TABLES

CHAPTER 1

INTRODUCTION

Periodic structures that prohibit the propagation of electromagnetic and light waves at some frequencies have been widely used in electromagnetics. Frequency selective surfaces (FSS) are the planar versions of such structures used in filters and antennas extensively for many years. Generally speaking, FSS are surfaces designed by putting periodic metallic patch elements on a dielectric substrate or aperture elements on a metallic screen. At some resonance frequencies FSSs totally reflect or transmit the incoming waves and behave as planar electromagnetic filters. A typical FSS geometry is shown in Fig. 1.1.

Periodic Cell
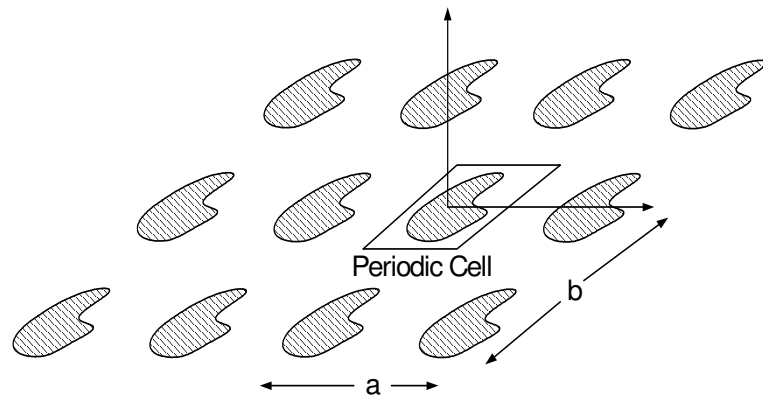
Fig. 1.1 General geometry of frequency selective surfaces

Planar gratings used in the design of leaky wave antennas are another type of frequency selective structure used for many years in electromagnetics. However, with the invention of Yablonovitch [1] in the late 1980's periodic structures have received much more attention than in the past. In his paper [1], Yablonovitch showed that 3-D face centered cubic cell structures prohibit the transmission of light at some frequency bands and this invention opened new possibilities to use periodic structures in optical applications. Due to the structural and behavioral resemblance to the bandgap structures in semiconductors, such materials are given a name as "Photonic Bandgap structures (PBG)". Note that some authors also use the term "Photonic Crystals(PC)" instead of PBG. The term PBG generally refers to the periodic structures operating at optical frequencies. To define the structures operating in microwave frequencies another term Electromagnetic Bandgap structures (EBG) is used. However there is no strict distinction between the two terms and PBG term is also very commonly used to define periodic structures operating in microwave frequency regime.

The definition of EBG structures is given in [2] as:

"Electromagnetic Band-gap structures (EBG) are 3-D periodic objects that prevent the propagation of the electromagnetic waves in a specified band of frequency for all angles of arrival and for all polarization states of electromagnetic waves"

The definition given above refers to ideal EBG structures. In practice it is difficult to obtain 3-D periodic structures with a complete bandgap such that they prevent the radiation for all angles of arrival and all polarizations. Most EBG materials that are used in practice have partial bandgap, such that they prevent the radiation not for all angles but some angles and polarizations. As an example the artificial dielectrics used as antenna substrates have partials bandgaps. The periodic substrates that are analyzed in this work also have partial bandgaps. The complete bandgap is easily obtainable in 2-D structures but notice that the term 2-D also includes an abstract idealism because there is no 2-D object in reality. Due

to the reasons listed above through this work the term "Electromagnetic Band-gap Structures (EBG)" is used to define 3-D objects that prevent propagation of electromagnetic waves in a specified band of frequency for some angles and some polarization states.

"Metamaterials" is another term generally used to refer periodic structures. "Meta" means beyond in Greek and the term "metamaterials" often refers to artificial materials, that exhibit the electromagnetic properties that are not observed in nature [3]. The history of metamaterials is older than the history of electromagnetic bandgap structures and starts in 1968 with the question asked by Veselago: "What happens if there is a material in nature with negative permittivity and permeability?" [4]. In nature the ordinary materials have positive permittivity and positive permeability. Although there are some materials with negative permittivity, there is not any material in nature with negative permeability. In [4] Veselago showed that in a material with negative permittivity and permeability, the phase velocity and group velocity have different directions. In such materials Snell's Law and Doppler effect are reversed. Therefore by using a material with negative permittivity and permeability, it is possible to use a flat slab as a superlens since it refracts the light in the negative direction. In year 2000, Smith et. al. [5] discovered that negative permittivity and permeability can be obtained by forming a periodic structure in a similar way that a matter is composed in terms of atoms. In macroscopic scale these structures show material properties that are not found in nature [6], hence they are called metamaterials. These materials are sometimes referred as "Left-Handed Materials (LHM)", and/or "Double Negative Materials (DNG)", as well. The detailed history of metamaterials is given in [7].

Although some authors attempted to make clear definitions of "metamaterials" [8] and "electromagnetic bandgap structures (EBG)" [2], still there is not complete agreement on the proper usage of these terms. It is difficult to make a clear distinction between metamaterials and EBG structures because both of the terms refer to periodic structures composed of wires and dielectrics. Also the authors are contradicts with each other. [2] and [8] are two of the references among many other examples which show that a consensus about the

classification of periodic structures has not been reached by the researchers of the field. Similar periodic structures are classified under the terminology of EBG in [2], whereas they are referred as metamaterials in. [8].

Generally, the distinction between metamaterials and EBG structures are based on two concepts: The distance between periodic elements compared to the wavelength and the electromagnetic properties of the periodic structure as far as the specific application is concerned.

When the wavelength is comparable to the distance between the periodic elements, complex scattering and refraction take place in the structure. If the structure is properly designed partial or complete bandgaps are observed. The local parameters of the periodic elements such as their shape and dimension play an important role in the scattering process. Therefore to predict the electromagnetic properties of such structures, rigorous and full-wave analysis methods that consider the whole structure should be preferred. EBG structures are fall into this category. However, when the wavelength is much longer than the periodicity, the overall structure resembles an ordinary material with atoms periodically arranged in it. For this case the macroscopic properties such as effective permittivity and permeability are more important than the scatterings and refractions that occur in the microscopic scale. Therefore approximate methods like effective medium theory or homogenization approach that replaces the periodic structure with a homogeneous medium, can be used to analyze the electromagnetic characteristics of such structures. Metamaterials fall into this category.

Another distinction between the metamaterials and EBG-related structures can be made by looking at the properties used in the applications. For applications where the metamaterials are used macroscopic properties like effective permittivity and permeability are the main parameters of interest. On the other hand for EBG structures, the important parameters are the frequency range where the propagation is prohibited as explained in the next section.

1.1 Applications of EBG Structures

EBG structures allow us to control and manipulate the propagation of electromagnetic waves. This property of the structures is incorporated into several applications in electromagnetics and photonics, such as high efficiency antennas, wideband filters, high Q resonators, waveguides, lasers etc.

Microstrip patch antennas are widely used in communication systems due to their unique features such as the ease of fabrication, being light weight, having small dimensions, and the adaptability to aero dynamical and wearable systems that require conformal antennas. Microstrip patch antenna is basically a half wavelength resonant cavity which is open circuited at two ends. When the antenna is excited by some means, most of the power is radiated via fringing electric fields at the edges. Patch antennas are narrow band and lower gain antennas compared to other antenna types. The radiation efficiency of the patch antennas might be degraded when the surface waves propagating through the antenna interfere with the fields radiated from the end points. Recently it has been shown that these drawbacks of the microstrip antennas can be eliminated by using electromagnetic bandgap structures to design efficient antennas with good radiation characteristics and smaller dimensions [9]-[11]. Such an antenna is manufactured by drilling periodic holes around the patch [10].

In two-dimensional photonic bandgap structures, within bandgaps, no modes of propagation are allowed. However, by perturbing the structure we can permit some set of modes inside the bandgap. This property of EBG structures can be used to make directive resonator antennas. Such an antenna design has been demonstrated by Cheype et al [12]. It has been reported that with the use of EBG structure, the gain of the conventional patch antenna is increased from 7 dB to 20.5 dB.

The EBG structures are also applicable to other antenna types. Thevenot has presented a photonic reflector antenna built with seven dielectric dishes separated with a slab of air [13]. It has been shown that PBG reflector antenna has equal gain with conventional metallic antenna over the bandgap of the reflector. Such an

5

antenna design enables filtering of unwanted electromagnetic signals outside the operation frequency.

The application of EBG structures to dipole antenna is given in [14]. In this work the dipole antenna is mounted on PBG substrate to prevent spurious radiation in terahertz imaging arrays used in astronomy.

EBG structures can be used to guide light or electromagnetic waves in sharp bends. This is achieved by etching holes in the guiding direction. In the bandgap region wave is trapped in the channel and cannot be scattered through the EBG structure [15]. Such a waveguide could be used in RF designs to reduce the area of printed circuit boards.

EBG technology, allows the production of high Q filters with high isolation, low insertion loss and wideband. Recently resonators and filters that use EBG technology have been proposed as an alternative to the current technologies for optic and electromagnetic applications [16]-[18].

1.2   Numerical Modeling of Electromagnetic Bandgap Structures

Initially, in the design of EBG structures cut and try method was applied because of lack of reliable analysis methods. With the theoretical description of Maxwell's equation in periodic structures, several techniques have been proposed to analyze EBG structures.

The most commonly used methods for the analysis of EBG structures are plane-wave-expansion [19][20], multiple scattering theory [21]-[23], transfer matrix method [24], finite difference method [25][26], finite difference time domain method (FD-TD) [27][28], finite element method (FEM) [29]-[31] and method of moments (MoM) [32]-[35].

Plane wave expansion method starts with the Maxwell's equations in a generalized eigenvalue form:

$$\overline{\nabla}x\left(\frac{1}{\varepsilon(r)}\overline{\nabla}x\overline{H}\right) = \frac{\omega^2}{c^2}\overline{H} \qquad (1.1)$$

Thereafter the magnetic field is written in terms of plane wave basis functions using the periodicity of the crystal and Bloch theorem. The resulting

eigenvalue problem is solved with an appropriate method to obtain eigenvalues and eigenvectors. This method has found widespread use because it is a simple and computationally efficient method. To obtain good convergence, large number of plane waves should be used and this makes the analysis of complex structures difficult. A good explanation of the method is given by Johannopoulos [19].

Multiple scattering theory is an analytical method used to obtain transmission characteristics in 2D arrays of rigid cylinders. The basic idea behind the multiple scattering theory is as follows: In response to the incident field from the source and scattered waves from the other objects, each object scatters waves repeatedly. These scattered waves can be expressed in terms of modal series of partial waves. Considering these scattered waves as an incident wave to other scatterers, a set of equations can be obtained and computed. The total wave at any spatial point is the summation of direct waves from the source and scattered waves from the other scatterers [23]. It is generally used to model 2-D photonic crystals and Negative Refraction Index Materials (NRIM). Analytical formulation of scatterings in 3-D complex structures is difficult and the method is not suitable to analyze such structures.

In the transfer matrix method firstly Maxwell's equations are solved for a single unit of the structure. The field is then transferred throughout the structure by applying Maxwell's equations to obtain the scattering matrix of the structure. Using the method, transmission and reflection coefficients can be obtained [24].

In the finite difference method (FD), discretized Maxwell's equations are solved in frequency domain. The derivatives are calculated through difference formulas. Due to numerical calculation of derivatives the accuracy of the method is not sufficient for structures with sharp resonances. To increase the accuracy, number of discretizations should be increased but this increases the computation time also.

In the finite-difference time-domain (FD-TD) method, Maxwell's equations are solved in time domain by using the marching-on-in-time procedure. The derivatives involved in Maxwell's equations are calculated via finite differencing. With a single run it characterizes broadband response of the structure so it can be

computationally efficient when the broadband response is required. The application of the method to EBG structures is similar to the conventional structures. To increase the computational efficiency, the method is applied to unit cell of the EBG structure using periodic boundary conditions.[28]. It has been demonstrated that the method is useful for the prediction of the bandgap characteristics. However according to Maagt [24], it is not sufficiently accurate compared to others methods. Due to this reason the analysis of resonance structures can take relatively long time.

MoM and FEM are two well known numerical techniques used in electromagnetic theory. The FEM procedure starts with dividing the entire volume into sub-volumes. The unknown functions are represented by interpolation functions. Thereafter, the weak formulation of the Helmholtz equation that includes the boundary conditions is solved in spatial domain following the Rayleigh-Ritz approach. To increase the computational efficiency in the analysis of electromagnetic bandgap structures, the periodicity of the structure can be utilized and the problem can be reduced to a unit cell.

The FD, FD-TD and FEM methods are versatile methods that could be easily applied in the analysis of arbitrary 3-D geometries . Therefore, they received much attention in the development of commercial simulation packages. For instance the Ansoft Corporation announced that starting from version seven; HFSS with Optimetrics engine is capable to solve EBG structures [36]. The program uses FEM technique and linked boundary conditions to solve periodic structures. Complex structures involving arbitrarily shaped inhomogeneous regions could be easily analyzed by using finite methods. However, since these methods require discretization of whole volume of interest, the number of unknowns might be quite large for such complex structures. Although the storage of the resulting large matrix does not cause a severe memory problem due to the sparse nature of the matrix, matrix solution time could be rather long for complex structures with large number of unknowns. Moreover, these finite methods are applicable to only closed structures with predefined boundary conditions on the surface that enclose the solution space. Therefore, in the analysis of open radiating

structures like microstrip antennas, the solution space should be limited by introducing artificial boundaries like perfectly matched layers. The inclusion of such boundaries adds some approximation errors to the analysis. These errors could be minimized by placing the artificial boundaries far from the radiating elements. But this would result in a larger solution space which increases the number of unknowns.

Method of moments (MoM) is the most frequently used technique for the analysis of open field problems, especially printed geometries in planar stratified media [37]. In this method the integral equation is transformed into a matrix equation by approximating the unknown function in terms of basis functions and then by applying the weighted residual technique. The unknown functions are generally the equivalent surface and/or volume currents. Therefore, only the surface currents on electric or magnetic conductors and the equivalent volume currents that replace an inhomogeneous region are discretized in MoM whereas the whole solution space is discretized in finite methods. Consequently MoM results in a smaller matrix equation compared to finite methods. However, MoM matrix is a dense matrix as opposed to the sparse matrices obtained in finite methods. Moreover, MoM procedure requires the evaluation of the Green's functions associated with the problem under investigation. In spite of these drawbacks, when the analysis of open structures is considered, MoM turns out to be computationally more efficient compared to finite methods due to the smaller matrix size. The method enables the analysis of aperiodic microwave structures on periodic substrates, such as microstrip lines on EBG substrates [38]. As far as the author's knowledge currently, there is no other appropriate computational scheme for the field solution of printed structures build on artificial periodic materials. There are some approximation techniques that replace the periodic structures with an effective medium. However, the approximate formulas used to calculate the constitutive parameters of the effective medium are accurate only for lower frequencies [35].

1.3 Summary of the present work

This study has two purposes. The first purpose is to develop an efficient method of moment procedure to analyze EBG materials that are used as a substrate for microwave structures. The multilayered structures with periodically implanted blocks are an example to those structures and considered throughout the thesis. The structures can be manufactured by drilling holes into a multilayered slab and they are used to design efficient microstrip antennas, resonators etc. The second purpose of the study is to propose a method for the analysis of microstrip structures those are aperiodically positioned on periodic EBG substrates.

As a starting point of the thesis firstly 2-D planar structures in stratified media is analyzed using efficient MoM procedure proposed by Aksun et. al [39]. Such geometries can be used in the design of superlenses, leaky wave antennas, frequency selective surfaces. Using the method the geometries are optimized to increase or decrease electric field in a predefined region. This is a previously started study by M.I. Aksun and M. Küçükgöz. It has been completed and extended to analyze TE mode electromagnetic fields. The optimization of 2-D structures is the first contribution of the thesis, that is made in cooperation with M. I. Aksun and M. Küçükgöz. The second chapter is devoted to this study. In this chapter the method is briefly explained and then several optimization examples are presented.

In Chapter 3 the theory and implementation of MoM procedure to analyze 3-D EBG structures is given. The method is originally proposed by Yang [33]. In this method, the embedded dielectric materials are replaced by equivalent currents through volume equivalence theorem. The coefficients of these currents in one unit cell are obtained following the regular MoM technique. The dispersion and reflection parameters are calculated and the implementation is verified by comparing the results to those results found in the literature.

The method given in Chapter 3 is computationally slow and not suitable in obtaining dispersion diagrams and spectral response of reflection coefficients. To increase the computational efficiency of the method the asymptotic waveform

evaluation technique (AWE) is applied. The difficulty in the application of AWE technique to stratified media lies behind the calculation of high order derivatives of the complex Green's functions. In this study the required derivatives are calculated through automatic differentiation theory (AUTODIFF). The automatic differentiation is a relatively new concept and it has been applied to complex mechanical problems in recent years. The theory and application of AWE technique to the present problem is given in Chapter 4.

In Chapter 5 a method is proposed to analyze microstrip lines on EBG substrates. Previously a two step procedure called Double Vector Integral Equation (DOVIE) method was proposed by Yang to analyze aperiodic structures build on periodic substrates [38]. In the first step of DOVIE method, 2D array of electric dipoles are placed on a substrate with material gratings. The periodicity of the array is chosen to be same as the periodicity of material gratings. Then the equivalent volume currents within the material gratings are calculated by using 3D MoM procedure. In the second step, the numerical solution found in the first step is used in conjunction with the array scanning method to obtain the Green's function of a single dipole placed on the PBG structure. Finally, the current distribution on the printed structure is solved by using this Green's function in traditional MoM procedure. The main drawback of this method is the long computation time due to the numerical evaluation of the Green's function for every scan angle considered in the array scanning method. Therefore in this thesis, an alternative method to DOVIE method is proposed. In the proposed method an approximate Green's function for the EBG substrate is obtained by replacing the generalized Fresnel reflection coefficient expressions appearing in the spectral domain Green's function of a multilayered structure, with the numerical reflection coefficient values of the EBG substrate computed via the 3D MoM solution explained in Chapter 3. Once the approximate Green's function for the periodically implanted substrate is obtained, the dispersion characteristics of microstrip lines, build on such substrates, are calculated through the use of spectral domain MoM procedure and compared with the literature. The results are discussed at the end of the chapter.

The thesis ends with the conclusion part that includes the planned study as a future work.

CHAPTER 2

OPTIMIZATION OF 2-D GEOMETRIES USING THE EFFICIENT MOM TECHNIQUE

2.1 Introduction

It was recently demonstrated that 2-D geometries in stratified media could be analyzed efficiently using generalized pencil-of-functions (GPOF) [40] method in conjunction with the spectral domain MoM technique [39]. This makes the method suitable to be used in the optimization of 2-D geometries. In this study we extend the previous work and use it to optimize reflected and transmitted electric fields from 2-D slab geometries. In the considered problems, the optimization goal is to accurately define the electric fields anywhere above or below the slab geometry. Such an optimization could be useful in the design of frequency selective surfaces, antenna arrays, superlenses in photonics, increasing the electric field strengths in corridors of a building etc. Although there is no inherent preference of the method towards any type of optimization algorithms, a genetic optimization algorithm is employed in conjunction with the method. This chapter starts with the brief overview of the spectral-domain MoM using GPOF given in Section 2.2. The optimization algorithms and procedures are presented in Section 2.3. In Section 2.4 three examples are given and the results are demonstrated.

2.2 Brief Overview of the Efficient MoM

Application of the MoM to 2-D planar multilayer geometries results into a matrix equation whose entries are double integrals over finite domains in the spatial domain formulation, and single integrals over infinite domain in the

spectral domain formulation. Hence, the matrix fill time in the application of MoM is mainly determined by the evaluation of the integrals. However the integration in the later process can be eliminated with the use of generalized pencil-of-functions (GPOF) method and matrix entries can be written in terms of finite summation of Hankel functions. This significant improvement in the computational efficiency makes the method a good candidate to be used in the optimization of 2-D geometries. The details of the method are given in [39], for the sake of completeness the method will be explained briefly.
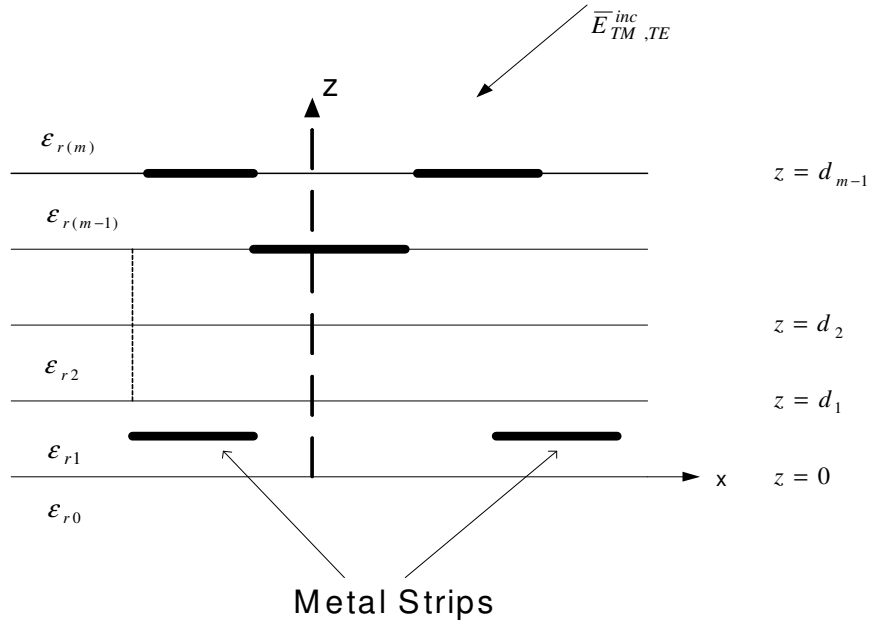
Fig. 2.1 2-D conductors embedded in multilayer medium.

Consider the sample 2.5D multilayer geometry shown in Fig. 2.1, where it is assumed that the layers extend to infinity in the transverse directions($\hat{x}$ and $\hat{y}$). An electromagnetic wave that is transverse electric (TE) or transverse magnetic (TM) to $\hat{y}$ is incident upon the structure. Each layer is considered to have different electric and magnetic properties *(ε_{ri}, μ_{ri})* and thickness *(d_i)*. Finite extend

perfect electric conductors that are infinite in $\hat{y}$ direction are embedded in the structure.

The spectral domain representations of the scattered fields are given as:

$$\tilde{E}_x^s = -j\omega\tilde{G}_{xx}^E\tilde{J}_x(k_x) \qquad TE\ excitation \qquad (2.1.a)$$

$$\tilde{E}_y^s = -j\omega\tilde{G}_{yy}^A\tilde{J}_y(k_x) \qquad TM\ excitation \qquad (2.1.b)$$

where ~ denotes the spectral-domain representation, $\tilde{G}_{xx}^E$ and $\tilde{G}_{yy}^A$ represent Green's functions for the electric field and vector potential, respectively, and $\tilde{J}_x$ and $\tilde{J}_y$ are the unknown current densities on the conductors. To find the current densities on the conductors, first total tangential electric field on the plane of conductors are written and then boundary conditions are implemented as:

$$\tilde{E}_x^i + \tilde{E}_x^s = \tilde{E}_x^i - j\omega\tilde{G}_{xx}^E\tilde{J}_x(k_x) = 0 \qquad TE\ excitation \qquad (2.2.a)$$

$$\tilde{E}_y^i + \tilde{E}_y^s = \tilde{E}_y^i - j\omega\tilde{G}_{yy}^A\tilde{J}_y(k_x) = 0 \qquad TM\ excitation \qquad (2.2.b)$$

The incident plane wave in layer-i is written in the spatial domain as:

$$\overline{E}_{TE}^i = \frac{1}{\omega\varepsilon_i}H_i e^{jk_x x}\left((-\hat{x}k_z + \hat{z}k_x)e^{jk_{zi}z} + (\hat{x}k_z + \hat{z}k_x)\tilde{R}_{TM}^{i,i-1}e^{-jk_{zi}z}\right) \qquad (2.3.a)$$

$$\overline{E}_{TM}^i = \hat{y}E_i e^{jk_x x}\left(e^{jk_{zi}z} + \tilde{R}_{TE}^{i,i-1}e^{-jk_{zi}z}\right) \qquad (2.3.b)$$

The tangential components of the incident plane wave in the spectral domain are as follows:

$$\tilde{E}_x^i = -\frac{k_i\cos\theta H_i}{\omega\varepsilon_i}2\pi\delta(k_x + k_i\sin\theta)\left(e^{jk_i\cos\theta z} - \tilde{R}_{TM}^{i,i-1}e^{-jk_i\cos\theta z}\right) \qquad (2.4.a)$$

$$\tilde{E}_y^i = E_i 2\pi\delta(k_x + k_i\sin\theta)\left(e^{jk_i\cos\theta z} + \tilde{R}_{TE}^{i,i-1}e^{-jk_i\cos\theta z}\right) \qquad (2.4.b)$$

where $k_i = \sqrt{k_x^2 + k_{zi}^2}$, $k_x = k_i\sin\theta$, $k_{zi} = k_i\cos\theta$, and the angle of incidence θ is defined with respect to the direction of normal at $z=0$ plane. $\tilde{R}_{TE}$, $\tilde{R}_{TM}$ are generalized TE and TM mode reflection coefficients respectively [41]. It should be noted that the generalized reflection coefficients are defined with respect to $\hat{z}$. On the other hand in the formulations above TE and TM electric fields are defined with respect to $\hat{y}$ because of the 2-D nature of the structure. Therefore, the TE

15

fields are obtained in terms of TM reflection coefficients and TM field are obtained in terms of TE reflection coefficients.

To find the unknown current density $\tilde{J}_x, \tilde{J}_y$ on the conductors due to a line source or incident plane wave excitation, a well-known approach, the method of moments (MoM) in the spectral domain, is employed. The main step in the application of MoM is to write the unknown function in terms of known expansion (basis) functions with unknown coefficients.

$$J_x(x) = \sum_{n=1}^{N} I_{xn} B_{xn}(x) \qquad (2.5.a)$$

$$J_y(x) = \sum_{n=1}^{N} I_{yn} B_{yn}(x) \qquad (2.5.b)$$

where $B_n(x)$ is the basis function, and I_n is the unknown coefficient.
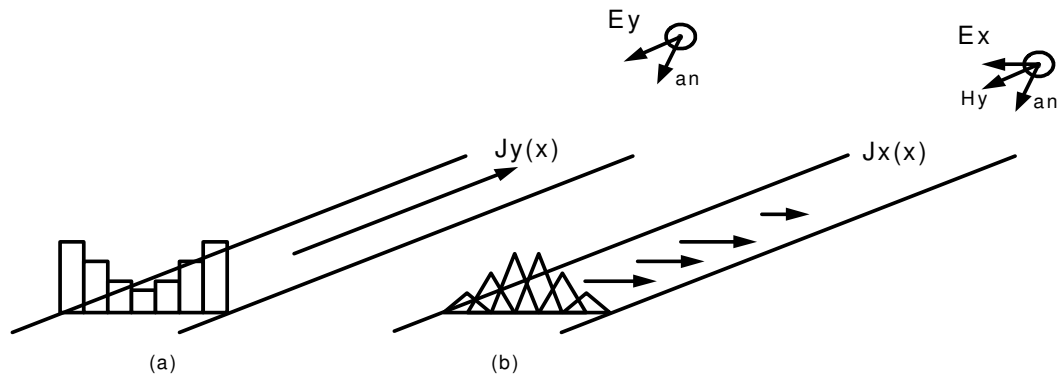
Fig. 2.2 Basis functions used in the analysis of 2-D strips. (a) Pulse type basis functions used for TM excitation (b) Triangular basis functions used for TE excitation.

For TE excitation the current density is zero at the edges of the conductor (transverse currents) whereas, it goes to infinity when the conductor is excited by a TM mode field (longitudinal currents). To accurately model the behavior of the current densities at the edges of the conductor triangular and pulse type functions are chosen as the basis functions for J_x and J_y respectively. (Fig. 2.2)

16

$$B_{xn}(x) = \begin{cases} 1 - \dfrac{|x - nh_x|}{h_x} & \text{if } (n-1)h_x \le x \le (n+1)h_x \\ 0 & \text{otherwise} \end{cases} \tag{2.6.a}$$

$$B_{yn}(x) = \begin{cases} 1 & \text{if } (n-1/2)h_x \le x \le (n+1/2)h_x \\ 0 & \text{otherwise} \end{cases} \tag{2.6.b}$$

The Fourier transform of the basis functions are as follows:

$$\tilde{B}_{xn}(k_x) = h_x e^{jk_x n h_x} \text{sinc}^2\left(\frac{k_x h_x}{2}\right) \tag{2.7.a}$$

$$\tilde{B}_{yn}(k_x) = h_x e^{jk_x n h_x} \text{sinc}\left(\frac{k_x h_x}{2}\right) \tag{2.7.b}$$

Substituting the Fourier transform of (2.5) into (2.2), and implementing the boundary condition on the conductors in integral sense via taking the inner product of the resulting equation with testing functions (chosen to be same as the basis functions, the Galerkin's method), the following set of linear equations are obtained:

$$-j\omega \sum_{n=1}^{N} I_{yn} \left\langle \tilde{T}_{ym}^*, \tilde{G}_{yy}^A \tilde{B}_{yn} \right\rangle = -\left\langle \tilde{T}_{ym}^*, \tilde{E}_y^i \right\rangle \quad \text{for } m = 1, \ldots, N \tag{2.8}$$

$$\left\langle \tilde{T}_{ym}^*, \tilde{G}_{yy}^A \tilde{B}_{yn} \right\rangle = \int_{-\infty}^{\infty} dk_x e^{-jk_x h_x (m-n)} h_x^2 \, \text{sinc}^2\left(\frac{k_x h_x}{2}\right) \tilde{G}_{yy}^A \tag{2.9}$$

$$\left\langle \tilde{T}_{ym}^*, \tilde{E}_y^i \right\rangle = E_i \, 2\pi e^{j(k_i \sin\theta)mh_x} \left(e^{jk_i \cos\theta z} + \tilde{R}_{TE}^{i,i-1} e^{-jk_i \cos\theta z}\right) \times h_x \, \text{sinc}\left(\frac{k_i \sin\theta h_x}{2}\right) \tag{2.10}$$

for TM excitation and

$$-j\omega \sum_{n=1}^{N} I_{xn} \left\langle \tilde{T}_{xm}^*, \tilde{G}_{xx}^E \tilde{B}_{xn} \right\rangle = -\left\langle \tilde{T}_{xm}^*, \tilde{E}_x^i \right\rangle \quad \text{for } m = 1, \ldots, N \tag{2.11}$$

$$\left\langle \tilde{T}_{xm}^*, \tilde{G}_{xx}^E \tilde{B}_{xn} \right\rangle = \int_{-\infty}^{\infty} dk_x e^{-jk_x h_x (m-n)} h_x^2 \, \text{sinc}^4\left(\frac{k_x h_x}{2}\right) \tilde{G}_{xx}^E \tag{2.12}$$

17

$$\left\langle \tilde{T}^*_{xm}, \tilde{E}^i_x \right\rangle = -\frac{k_i \cos\theta \, H_i}{\omega\varepsilon_i} 2\pi e^{j(k_i \sin\theta)mh_x} \left(e^{jk_i \cos\theta z} - \tilde{R}^{i,i-1}_{TM} e^{-jk_i \cos\theta z} \right) \times h_x \, \mathrm{sinc}^2\left(\frac{k_i \sin\theta \, h_x}{2} \right)$$
(2.13)

for TE excitation.

The Fourier-transform like integral in (2.9) and (2.12) can be evaluated analytically by implementing the GPOF method. To be more specific, the integrand except for the first term (the exponential kernel of the Fourier transform) is approximated in terms of complex exponentials divided by k_{zi}. This approximated expression enables the use of the following integral identity.

$$H_0^{(2)}(k_\rho\rho) = \frac{1}{\pi} \int_{-\infty}^{\infty} \frac{e^{-jk_x x - jk_z|z|}}{k_z} dk_x$$
(2.14)

Hence, the matrix entries are written as a finite summations of Hankel functions with the explicit terms of the indices of basis and testing functions *n* and *m*, and the observation and source planes *z* and *z′* , respectively. For the case of TE excitation a general matrix entry is obtained as:

$$-j\omega\left\langle \tilde{T}^*_{xm}, \tilde{G}^E_{xx} \tilde{B}_{xn} \right\rangle = -\frac{\omega\pi\mu_i h_x^2}{2} \left\{ \sum_{p_{xx}=1}^{P_{xx}} C_{p_{xx}} H_0^{(2)}(k_i \rho_{p_{xx}}) + \sum_{p_{1xx}=1}^{P_{1xx}} C_{p_{1xx}} H_0^{(2)}(k_i \rho_{p_{1xx}}) + \right.$$

$$\left. \sum_{p_{2xx}=1}^{P_{2xx}} C_{p_{2xx}} H_0^{(2)}(k_i \rho^{(1)}_{p_{2xx}}) + \sum_{p_{3xx}=1}^{P_{3xx}} C_{p_{3xx}} H_0^{(2)}(k_i \rho_{p_{3xx}}) + \sum_{p_{2xx}=1}^{P_{2xx}} C_{p_{2xx}} H_0^{(2)}(k_i \rho^{(2)}_{p_{2xx}}) \right\}$$
(2.15)

where,

$$\rho_{p_{xx}} = \sqrt{[(m-n)h_x]^2 + (|z-z'| - j\alpha_{p_{xx}})^2}$$
(2.16.a)

$$\rho_{p_{1xx}} = \sqrt{[(m-n)h_x]^2 + (z+z' + j\alpha_{p_{1xx}})^2}$$
(2.16.b)

$$\rho^{(1)}_{p_{2xx}} = \sqrt{[(m-n)h_x]^2 + (z-z' + j\alpha_{p_{2xx}})^2}$$
(2.16.c)

$$\rho^{(2)}_{p_{2xx}} = \sqrt{[(m-n)h_x]^2 + (z-z' - j\alpha_{p_{2xx}})^2}$$
(2.16.d)

$$\rho_{p_{3xx}} = \sqrt{[(m-n)h_x]^2 + (z+z' - j\alpha_{p_{3xx}})^2} \, ,$$
(2.16.e)

C_p's and α_p's are obtained from the GPOF method as the coefficients and exponents of the complex exponentials used to approximate the parts of the integrand of (2.9) and (2.12). It is worth emphasizing that having *m, n, z,* and *z′*

explicitly in the end result (2.15) provides the one and only one closed-form expression for the entire entries of the linear equations given in (2.8) and (2.11). In other words, (2.15) represents all of the interactions between the conductors in a 2D geometry. In addition, if some additional conductors are needed to satisfy the design criteria, one does not need to re-formulate or re-derive (2.15), just to evaluate the same expression with proper choices of z, z', m and n for each additional conductor. Therefore, with just one expression, (2.15), one can analyze and optimize any 2D structure very efficiently.

2.3   Optimization Problems and Algorithms

When an efficient EM simulation algorithm is developed it is important to demonstrate its use in design problems, to verify its efficiency and ease to use in conjunction with optimization algorithms. For this purpose the developed method is combined with an optimization algorithm to use in design problems. Although there is no inherent preference of the method towards any type of optimization algorithms, a genetic optimization algorithm (GA) is employed in conjunction with the method. GA's solve problems by emulating the natural evolution process. In a genetic algorithm the parameters to be optimized are encoded into binary string called as genes or individuals. A set of individuals constitutes a population and it evolves from generation to generation as in the natural evolution process, through predefined genetic operations like reproduction, crossover, selection, mutation [42]. Since GA's are well documented in the literature details of the algorithms will not be discussed. The further details of the genetic algorithms are covered in [43].

The first problem discussed in this study is optimization of conductor positions in a 2-D geometry to obtain desired field strengths at specified points. Consider the structure in Fig. 2.1. For this geometry the field strengths over user-defined points could be optimized by placing fixed width conductors at proper locations. In this problem it is assumed that conductor locations are permitted over a range such that no conductors can be located outside the range. The excitation for such a geometry could be linesource or TE, TM mode plane wave. Such a

design problem could be useful in synthesizing transmission or reflection characteristics of single or multiple slab geometries.

The optimization process starts with the calculation of C_p and α_p coefficients via GPOF method for the discrete points over the permitted conductor locations. Using these coefficients the matrix entries are calculated. Since the matrix entries contains only summation of Hankel function terms matrix filling is performed in an efficient manner. As it is emphasized before, the coefficients and matrix entries are explicit terms of *m, n, z,* and z' so it is sufficient to compute them at the beginning of the process to increase computational efficiency. Thereafter, individual chromosomes are generated as random binary strings that represent the conductor positions. The conductor positions are encoded into binary strings as follows:

$$\underbrace{00000011}_{\substack{x\ position \\ of\ 1st\ cond.}} \quad \underbrace{000000111}_{\substack{x\ position \\ of\ 2nd\ cond}} \quad \cdots\cdots\cdots \quad \underbrace{00010101}_{\substack{x\ position \\ of\ N\ th\ cond}}$$

The number of conductors and conductor widths are specified by the user initially but the optimization algorithm is implemented such that they are changed during the optimization process if there is an overlapping between the conductors. For example, consider two conductors have a width of 3 *cm*. If the first conductor position is 8.8 *cm*, second conductor position is 11.2 *cm* is obtained, these two conductors are merged into one conductor have a width of 5.4 *cm* located at *x*=8.8 *cm*. The electric field strengths for each individual are obtained via the MoM procedure described in the previous section. Least square norm of the electric field strengths over the goal positions are used to calculate fitness values. Following the conventional GA process selection, crossover and mutation operations are performed to generate fittest individuals until the convergence is reached. As a selection strategy tournament selection is used. In tournament selection a subpopulation of N individuals, where N is the tournament size, are selected from

20

the population randomly. Among these individuals the one with the highest fitness value is the winner of the tournament and it is selected for the next generation.

2.4 Results and Discussions

In this section to illustrate the efficiency of the method combined with an optimization algorithm some results are presented.
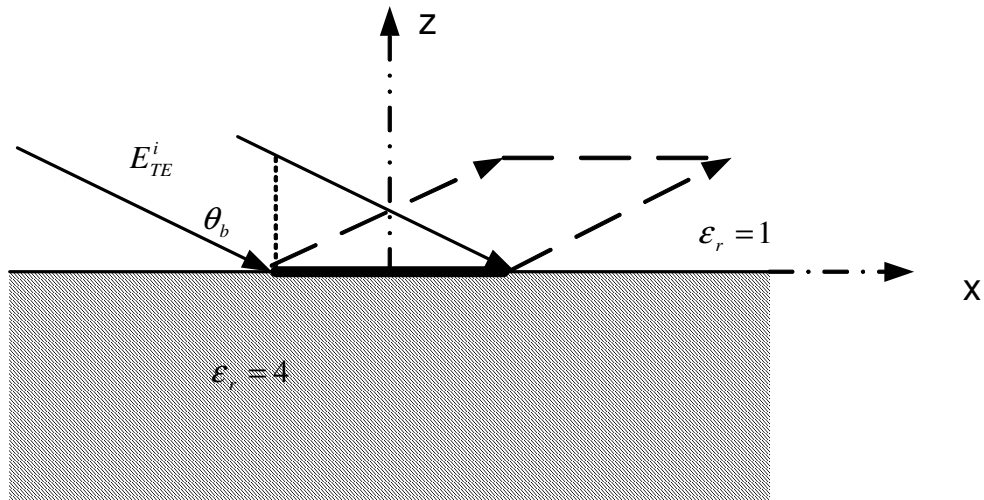
Fig. 2.3 The conductor located at the dielectric interface illuminated by a TE mode incident field.

First a simple example is chosen to demonstrate the accuracy in the calculation of electric field intensity by making intuitive discussions based on the physical nature of the problem. Consider the geometry shown in Fig. 2.3. In the figure a conductor is located at the interface between dielectric with $\varepsilon_r = 4$ and free space. A TE field is incident upon the conductor with a Brewster angle, $\theta_b = 63.43^o$, so no transmission occurs at the dielectric interface. The frequency of operation is 30 Ghz so $\lambda = 1\,cm$. The conductor is located between $x=12$-$18\,cm$ has a width of 6 cm which is electrically large in the frequency of operation. The

scattered field is calculated at $z=3$ *cm* which is the near field of the conductor. For this case it is expected that the conductor reflects the incident field and scattered field is observed at the other side of the conductor with a maximum between $x=18$-24 *cm* range. The calculated electric field magnitude agrees with this expectation as shown in Fig. 2.4. In Fig. 2.4 magnitude of the scattered field is plotted versus x position. As shown in the figure magnitude of the scattered electric field have an increased magnitude at $x=18$-24 *cm* range with a maximum at $x=21$ *cm*.
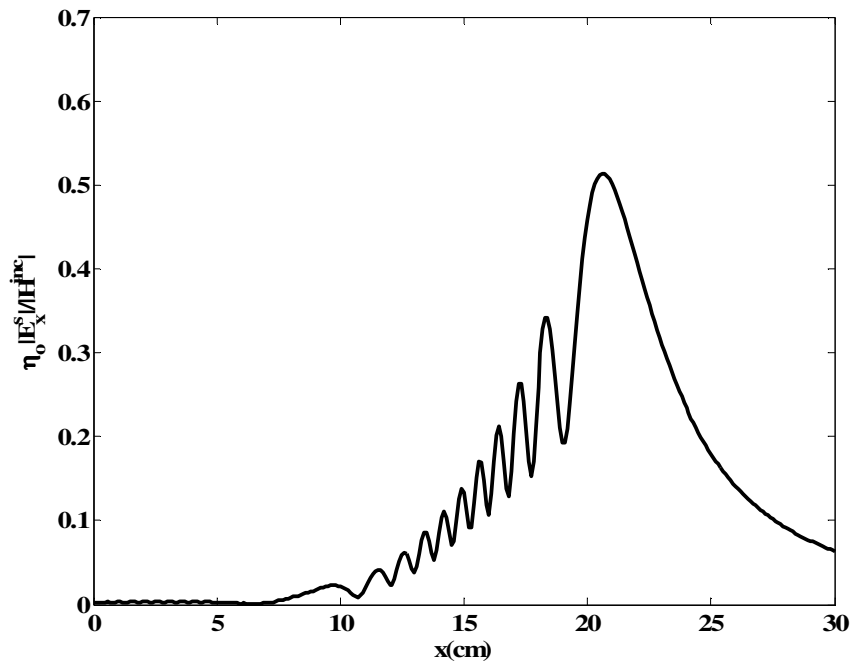
Fig. 2.4 Normalized magnitude of the transmitted electric field for geometry shown in Fig 2.3, at $z=3$ *cm*, $\theta_i=-63.43^o$.

Next the optimization capability of the developed software is demonstrated by the following experiment. From the previous example it is known that when a strip is located at $x=12$-18 *cm* range, a scattered electric field is observed *at $z=3$ cm* with a maximum value between $x=18$-24 *cm* range. If we reverse the process

and start with an initial position of the conductor anywhere on the slab and optimize the conductor position to obtain a maximum scattered electric field in the *x=18-24* cm range the program should give the conductor position at *x=12-18 cm* range. We perform such an optimization and after the optimization the program gives the conductor position at *x=11.75-17.75 cm* range which assesses the correct implementation of the optimization process.

As a second example consider the dielectric slab with ε_r = 4.0, *d* = 3 *cm* located in free space as shown in Fig. 2.5.

$$E^{inc}_{TE,TM}$$

$$\varepsilon_r = 1$$

$$z = 0.1\lambda$$

$$\varepsilon_r = 4$$

$$z = 0$$

$$x = 0 \qquad \varepsilon_r = 1 \qquad x = \lambda$$
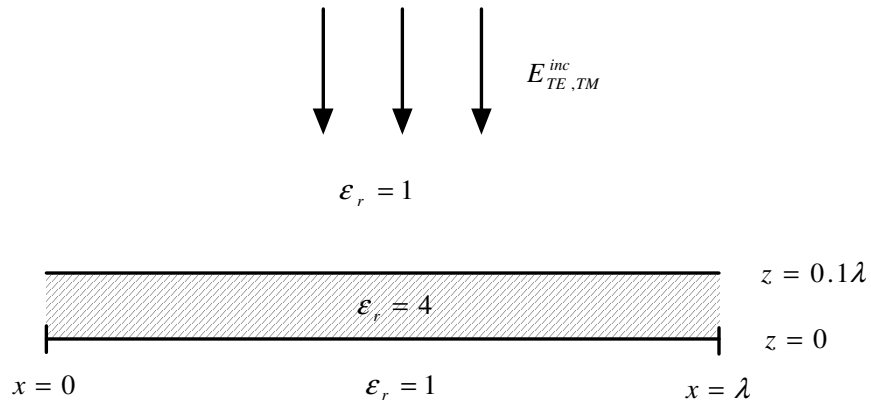
Fig. 2.5 The one slab geometry

The slab is illuminated by an incident field at incidence angle $\theta=0^o$. The frequency of operation is *f=1 GHz*. In this example the goal is to maximize the field strength over user-defined coordinates with the help of eight conductors with an initial width of 3 cm, positioned anywhere over the ranges of *x* = 0-30 *cm* at *z=0 cm* and *z* = 3 *cm* planes. The user-defined coordinates for the field strengths are chosen at *x* = 20-21 *cm* range at 30 cm below the slab. The main parameters of the genetic algorithm are chromosome length, population size, and tournament size. They are chosen as 80, 100 and 16, respectively. The discretization size in MoM algorithm is set to 0.2 cm so 15 basis functions are used on each conductor.

23

Fig. 2.6 and Fig. 2.7 show the normalized magnitude of the total electric field strengths after the optimization for TE and TM incident plane waves respectively. Fig. 2.8 and Fig. 2.9 show optimized electric field strengths for the incidence angle $\theta = -45^o$ for the same goal ranges. As seen from the figures there is a significant improvement in the electric field strengths over the goal positions.

Table 2.1 shows the optimized conductor positions. It should be noted that the number of conductors and the widths were set to 8 cm and 3 cm respectively at the beginning of the process. After the optimization it is observed that some conductors are merged and the widths are changed by the algorithm due to the reasons explained in Section 2.3. Starting from the initial conductor positions it took thirteen generations to converge, each generation requires 130-140 s CPU time on a PC with Pentium- III 733 MHz.

The optimization process is completed approximately in 25 minutes which is considerably a short time. CPU times for the evaluation of matrix entries, solution of matrix equations are given in Table 2.2.

Fig. 2.6 Normalized magnitude of the transmitted electric field with (solid line) and without (dashed line) conductors for TM mode incidence, $\theta_i=0^o$.
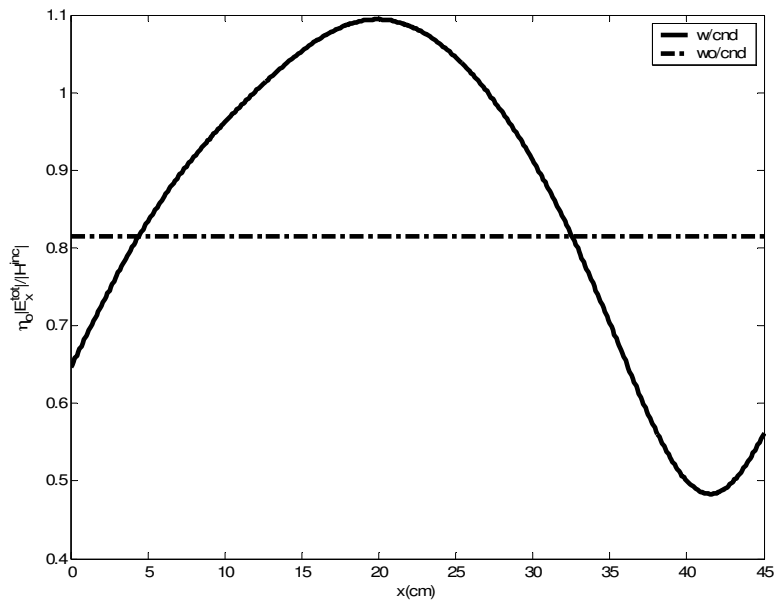
Fig. 2.7 Normalized magnitude of the transmitted electric field with (solid line) and without (dashed line) conductors for TE mode incidence, $\theta_i=0^o$.

25
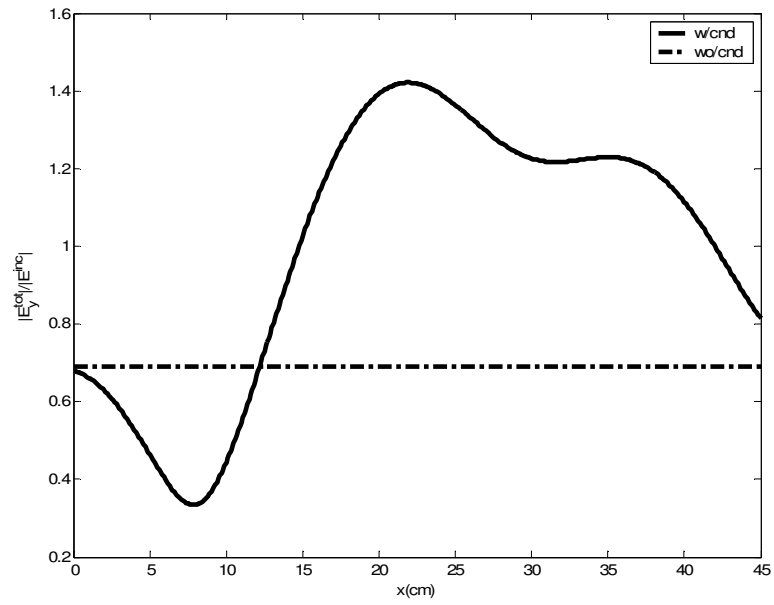
Fig. 2.8 Normalized magnitude of the transmitted electric field with (solid line) and without (dashed line) conductors for TM mode incidence, θ_i=-45°
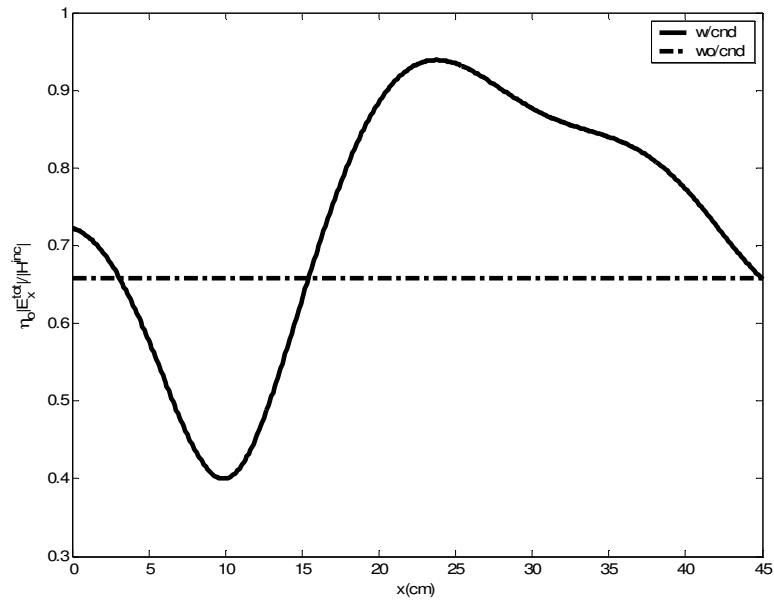
Fig. 2.9 Normalized magnitude of the transmitted electric field with (solid line) and without (dashed line) conductors for TE mode incidence, θ_i=-45°

Table 2.1 Conductor positions for one slab geometry after optimization. The conductor positions are optimized for maximum transmission between *x=20-21 cm* at *z=-30 cm* plane.

θ	TE			TM		
	z (cm)	x (cm)	width (cm)	z (cm)	x (cm)	width (cm)
0°	0	10.2	5.8	0	8.8	5.4
	0	16.4	4.8	0	23.2	3
	3	13.8	3	0	28	2
	3	17	6.6	3	12	3
				3	18.2	3
				3	23.6	3.6
-45°	0	24.6	5	0	8.6	3
	3	22	7.6	0	18.2	6
	3	2.4	5.2	3	19	3.6
				3	24.2	3.4

Table 2.2 CPU times

Process	CPU Time (sec)
Approximation of Green's function via GPOF	1.462
Calculation of matrix entries	0.791
Matrix fill time	<0.01
Matrix solution time	8.111

To check the optimization results intuitively, the optimized conductor positions obtained for TM field incident upon the structure in the normal direction is illustrated in Fig. 2.10. There are two main components that contribute to the electric field at the optimization points. The first component is due to the radiation of conductors in the lower half space (*z<0*) when they are excited by the incident field. The second contribution comes from the radiation of conductors at *z=0 cm*

27

plane in the positive $\hat{z}$ direction. The waves radiated from these conductors in the positive $\hat{z}$ direction reflect from the conductors in $z=3$ *cm* plane, that results an increase in the electric field strengths at the optimization points.
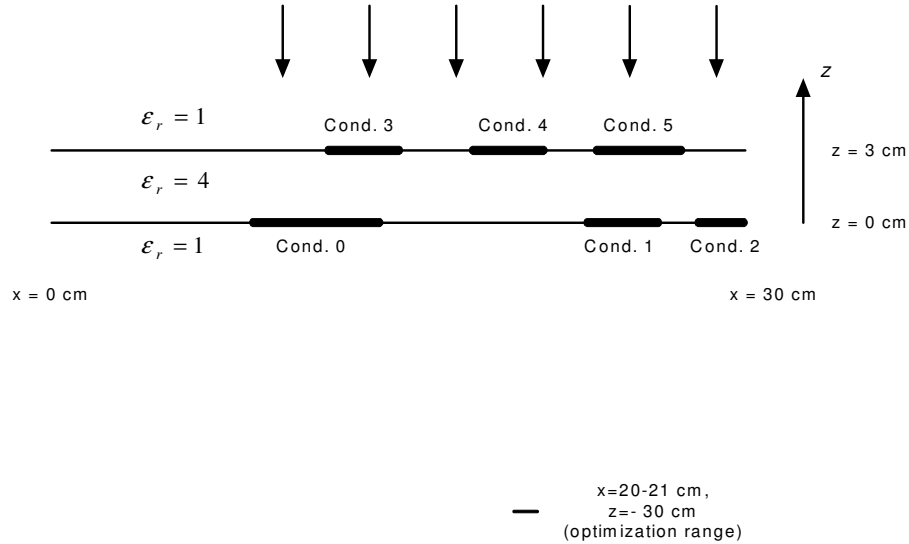
Fig. 2.10 The illustration of optimized conductor positions for TM incidence , $\theta_i=0^o$.

As a third example, consider the optimization of reflected field from the one slab geometry. In this example the magnitude of the reflected field from the one slab geometry is tried to be minimized with the help of conductors having an initial width of 3 cm. The conductors are permitted to be within $x=0$-30 *cm* range at $z=0$ *cm* and $z=3$ *cm* planes. The optimization range to minimize the electric field is $x=0$-30 *cm* at a plane 30 cm above the slab. The angle of incidence is $\theta=0^o$. The Fig. 2.11 and Fig. 2.12 show the magnitude of the electric field strengths after the optimization for TM and TE cases respectively. As seen from the figures, using conductors, the reflected electric field is reduced nearly two-three times over the specified goal positions. Table 2.3 shows the conductor positions obtained from the optimization. Such a design problem could be useful in the elimination of unwanted radiation from the dielectric interfaces.

28
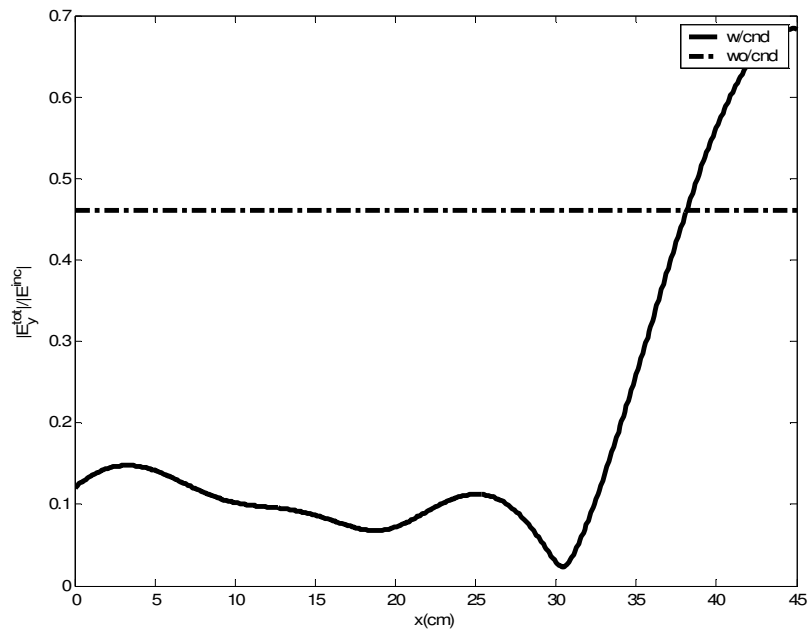
Fig. 2.11 Normalized magnitude of the reflected electric field with (solid line) and without (dashed line) conductors for TM mode incidence, $\theta_i=0^o$.
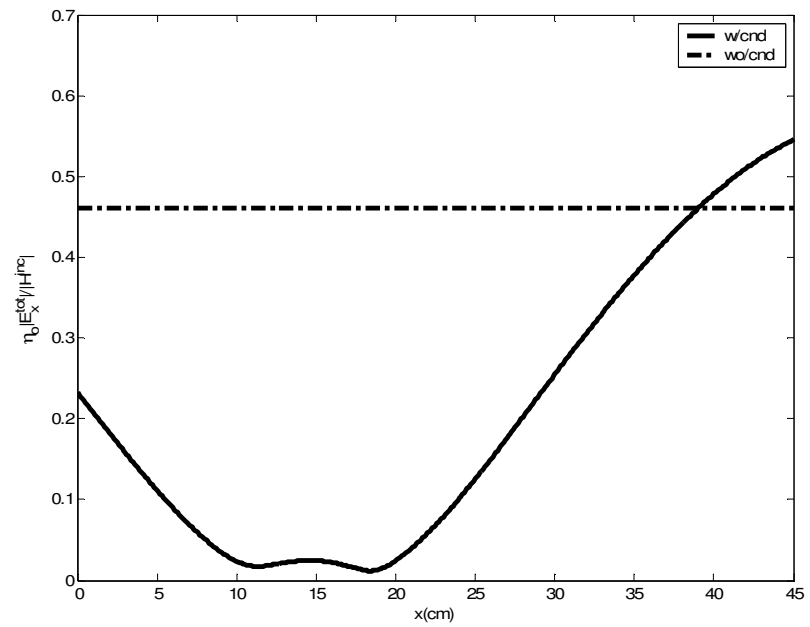
Fig. 2.12 Normalized magnitude of the reflected electric field with (solid line) and without (dashed line) conductors for TE mode incidence, $\theta_i=0^o$

29

Table 2.3 Conductor positions for one slab geometry after optimization. The conductor are positions optimized for minimum reflection between *x=0-30 cm* at *z=30 cm* plane.

TM			TE		
z (cm)	x (cm)	width (cm)	z (cm)	x (cm)	width (cm)
0	0.4	4.2	3	0.2	3
0	7.2	5.6	3	6.4	3.8
0	16.4	5.8	3	19.6	3
0	23.6	4	3	25.4	3.8
			0	29.4	0.6
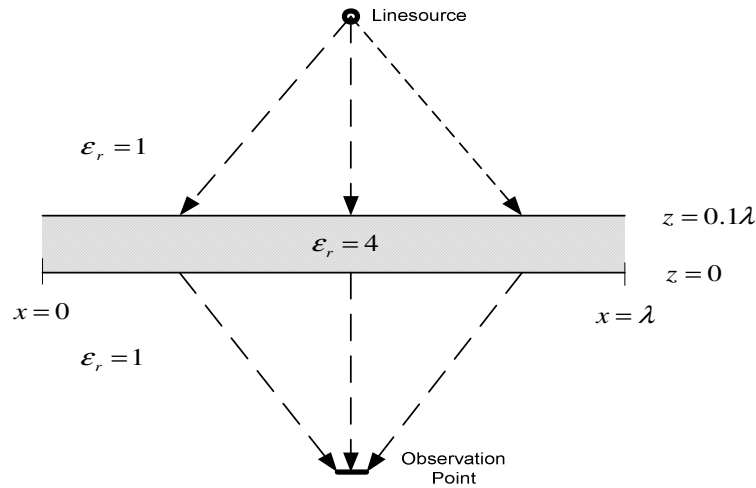
Fig. 2.13 The slab illuminated by a linesource.

As a last example consider the one slab geometry as shown in the Fig. 2.13. For this case the slab is illuminated by a line source infinite in the y direction and located at 30 cm above the slab. The magnitude of the transmitted field is maximized over *x=14-16 cm* ranges, 30 cm below the slab with the aid of five conductors having a width of 3 cm. As in the previous example the conductors are permitted to be positioned within *x=0-30 cm* range at *z=0 cm* and *z=3 cm* planes. The frequency of operation is 1GHz. Table 2.4 shows the conductor positions

30

after the optimization. Fig. 2.14 plots the magnitude of the transmitted electric fields over the optimization range with and without conductors. As shown in the figure, using conductors the magnitude of the electric field is increased about five times compared to the case without conductors.

Table 2.4 Conductor positions for one slab geometry after optimization. The slab is illuminated by a line source located at 30 cm above the slab. The conductor positions are optimized for maximum transmission between *x*=14-16 *cm* below the slab .

Linesource		
z (cm)	x (cm)	width (cm)
0	0	3
0	26	3
3	0.1	3
3	14.6	3
3	27.2	2.8

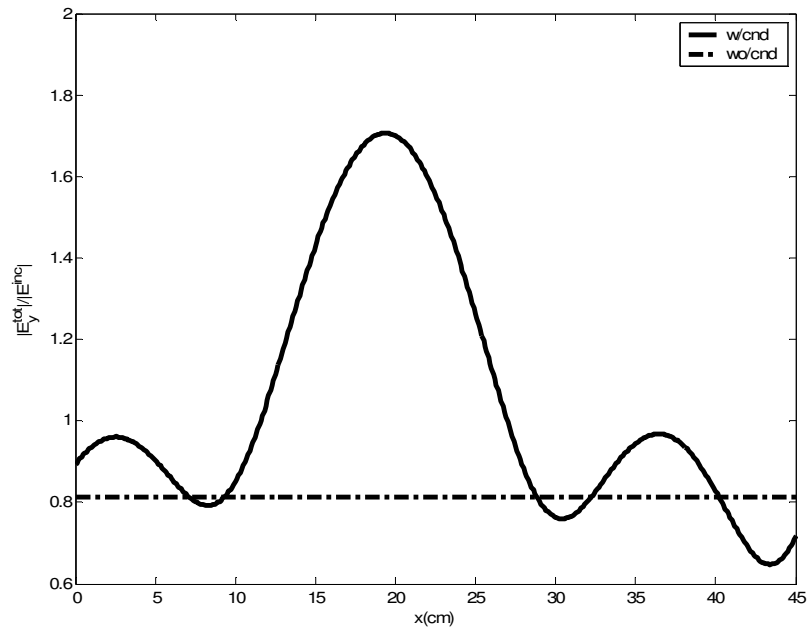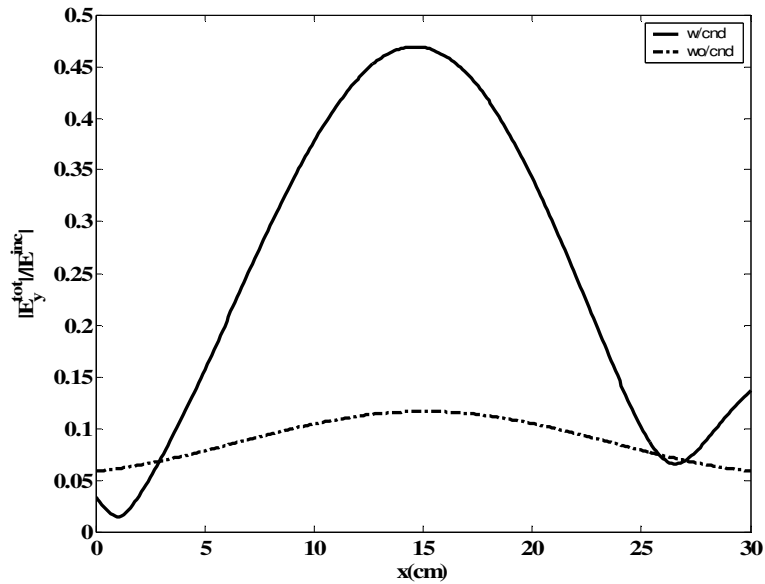**Fig. 2.14 Normalized magnitude of the transmitted electric field with (solid line) and without (dashed line) conductors for linesource illumination**

CHAPTER 3

THE ANALYSIS OF MULTILAYERED STRUCTURES WITH IMPLANTED PERIODIC MATERIAL BLOCKS USING METHOD OF MOMENT TECHNIQUE

3.1   Introduction

The thin film structures with periodically implanted material blocks have found wide applications including filters, leaky wave antennas, frequency selective layers, absorbing materials etc. [2]. They are also used as microstrip antenna substrates to eliminate unwanted surface waves penetrating into the structure [10]. Such structures are formed by periodically implanting dielectric blocks into a slab with a dielectric constant different than the slab. The periodic implants can be in one or two directions depending on the application. If such structures are used as microstrip antenna substrate the backside is a ground plane. The analysis of 3-D doubly periodic structures is important in the design of microstrip structures on EBG substrates.

In this chapter a three dimensional formulation in conjunction with method of moment is applied to the multilayered structures with periodically implanted material blocks. Such a structure is seen in Fig. 3.1 where a, b are unit cell sizes, L ,W are dimensions of implanted dielectric blocks, h is the thickness of the slab. The formulation is based on the paper by Yang [33], [34]. In the formulation implanted materials are replaced by volume equivalent currents through volume equivalence theorem. The method of moment formulation is applied to obtain equivalent currents. The full set of dyadic electric field Green's functions is used in the analysis.
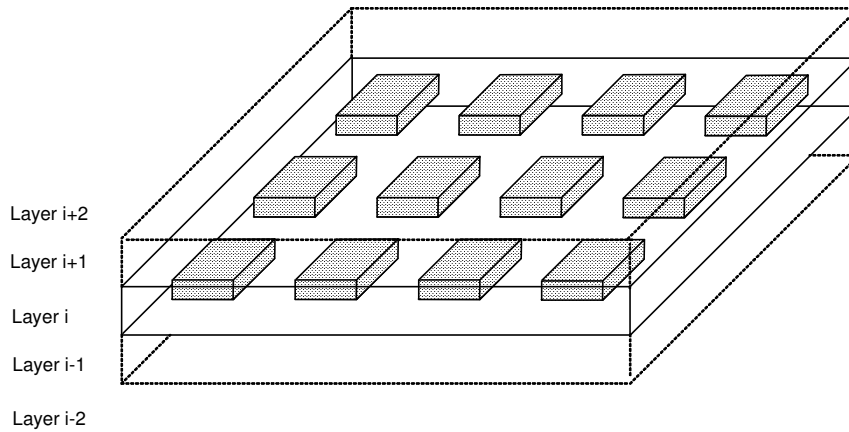
Fig. 3.1 The 3-D structure with periodically implanted dielectric blocks

3.2 The 3-D MoM Procedure

Due to the implanted dielectric blocks the electromagnetic analysis of the structure is difficult without converting it to the equivalent problem. However volume equivalence theorem enables us to replace implanted dielectric materials with equivalent volume currents as shown in Fig. 3.2. The detailed derivation of the volume equivalence theorem is given in Appendix-A
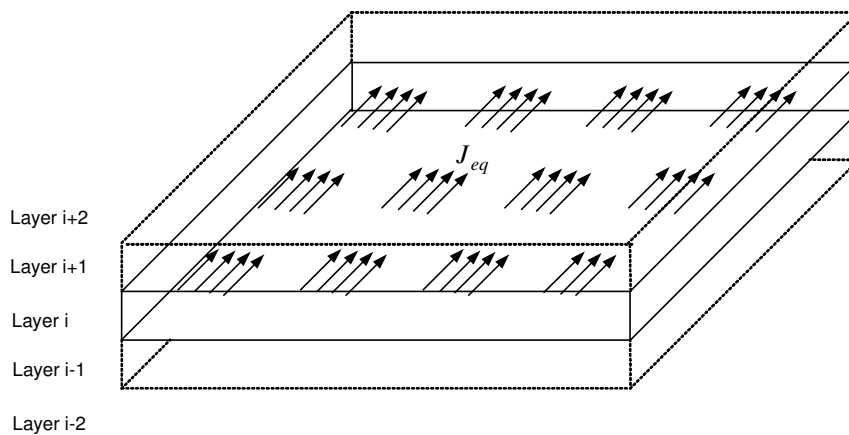
Fig. 3.2 The volume equivalent problem

33

The theorem says that if the electric source $\bar{J}$ and magnetic source $\bar{M}$ radiate into a medium represented by (ε_m, μ_m) in the presence of embedded scattering object represented by (ε_e, μ_e). The scattering object can be replaced by equivalent sources given by:

$$\bar{J}_{eq} = j\omega(\varepsilon_e - \varepsilon_m)\bar{E}$$
$$\bar{M}_{eq} = j\omega(\mu_e - \mu_m)\bar{H}$$

(3.1)

where, E, H are the total fields in the medium.

For the equivalent problem, the electric field in the structure is given by the volume integral equation as:

$$\bar{E}(\bar{r}) = \iiint_v [G(\bar{r},\bar{r}')]\bar{J}_{eq}(\bar{r}')dv' + \bar{E}^{(i)}(\bar{r}')$$

(3.2)

where, $\bar{E}^{(i)}$ is the incident field, [G] is the full set of dyadic electric field Green's functions for homogenous substrate and given by:

$$[G] = \begin{bmatrix} G_{xx}^E & G_{xy}^E & G_{xz}^E \\ G_{yx}^E & G_{yy}^E & G_{yz}^E \\ G_{zx}^E & G_{zy}^E & G_{zz}^E \end{bmatrix}$$

(3.3)

Since the structure is periodic the Floquet's (or Bloch's) theorem [44] can be utilized and the problem can be simplified by expressing the whole structure in terms of unit cells as shown in Fig. 3.3. Floquet theorem states that, for periodic structures from one unit cell to another, the solution differs only by a phase variation $\beta_0 a$, where β_0 is the propagation constant and a is the period of the structure. Using the theorem one can write the equivalent currents as:

$$\bar{J}_{eq}(x + ma, y + nb, z) = \bar{J}_{eq}(x, y, z).e^{-jma\beta_x}e^{-jnb\beta_y}$$

(3.4)

The use of Floquet's theorem has two implications. Firstly, it determines the electromagnetic boundary conditions by stating that the solution is periodic through the structure. Secondly, there is no need to search the solution through the entire structure, the solution in one unit cell is sufficient to characterize overall structure.

34
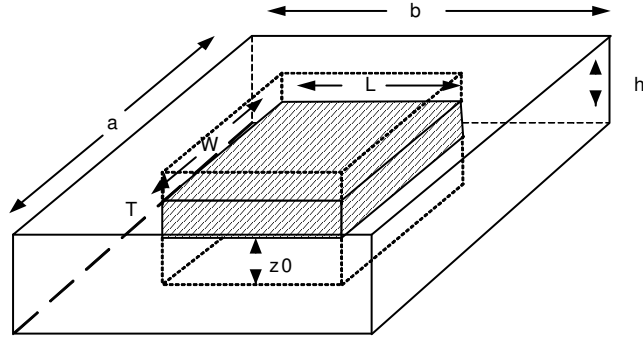
Fig. 3.3 The unit cell

Using Floquet's theorem and Poisson's summation formula the Green's function for doubly periodic structure is derived as [45]:

$$G_{uv}(\bar{r},\bar{r}') = \frac{1}{ab} \sum_{m=-\infty}^{\infty} \sum_{n=-\infty}^{\infty} \tilde{G}_{uv}(k_x,k_y,z,z')e^{-jk_x(x-x')}e^{-jk_y(y-y')} \quad (3.5)$$

where, $k_x = 2\pi n/a + \beta_x$, $k_y = 2\pi n/b + \beta_y$, $\tilde{G}_{uv}$ is the $\hat{u}$ component of the spectral domain electric field Green's function in terms of k_x, k_y, z, z', for a $\hat{v}$ directed electric dipole. The expressions for the spectral domain Green's functions are given in Section 3.3. The derivation of (3.5) is given in Appendix-B.

To calculate the electric field in the structure the unknown equivalent current densities should be obtained. These currents could be calculated through volume integral equation and 3-D MoM procedure. Following the MoM procedure the implanted material volumes are discretized into small cells and equivalent current densities are expanded in terms of 3-D basis functions and unknown coefficients as:

$$\bar{J}_{eq} = j\omega\varepsilon_0(\varepsilon_s - \varepsilon_e) \sum_{m_x=1}^{M_x} \sum_{m_y=1}^{M_y} \sum_{m_z=1}^{M_z} \bar{J}_{m_x m_y m_z} f_{m_x m_y m_z}(x,y,z) \quad (3.6)$$

where, J_{m_x,m_y,m_z} is the vector of unknown coefficients, M_x, M_y, M_z are number of subdomains inside the implanted material blocks in $\hat{x}, \hat{y}, \hat{z}$ directions respectively, $f_{m_x m_y m_z}(x,y,z)$ is the basis function. The basis function should be selected such

35

that it should satisfy the boundary conditions and represent the current variation accurately. For the considered problem, current is periodic through the structure, therefore the basis function should not vanish at the end points. On the other hand because of the complexity of the problem the basis functions should be selected as simple as possible. By considering these issues, as a basis function 3-D pulse basis function is chosen. The pulse type basis function is given by:

$$f_{m_x m_y m_z}(x,y,z) = \begin{cases} 1 & (m_x-1)\Delta_x \le x < m_x\Delta_x, (m_y-1)\Delta_y \le y < m_y\Delta_y, (m_z-1)\Delta_z \le z < m_z\Delta_z \\ 0 & else \end{cases}$$

(3.7)

where, Δ_x, Δ_y, Δ_z are discretization sizes in respective directions.

If we substitute (3.5) and (3.6) into the volume integral equation given in (3.2) we obtain:

$$\sum_{m_x=1}^{M_x}\sum_{m_y=1}^{M_y}\sum_{m_z=1}^{M_z}\overline{J}_{m_x m_y m_x} f_{m_x m_y m_z}(x,y,z)$$

$$= \frac{j\omega\varepsilon_0(\varepsilon_s-\varepsilon_e)}{ab}$$

$$\cdot \iiint_v \left(\sum_{m=-\infty}^{\infty}\sum_{n=-\infty}^{\infty}[\tilde{G}]e^{-jk_x(x-x')-jk_y(y-y')}\right)\left(\sum_{m_x=1}^{M_x}\sum_{m_y=1}^{M_y}\sum_{m_z=1}^{M_z}\overline{J}_{m_x m_y m_x} f_{m_x m_y m_z}(x',y',z')\right)dx'dy'dz'$$

$$+ \overline{E}^i$$

(3.8)

Following the Galerkin's procedure, the following equation is obtained after taking the inner product integral of both sides of (3.8) with the testing functions.

$$\overline{J}_{n_x n_y n_z} = \sum_{m_x=1}^{M_x}\sum_{m_y=1}^{M_y}\sum_{m_z=1}^{M_z}\sum_{m=-\infty}^{\infty}\sum_{n=-\infty}^{\infty}\left[g_{n_x n_y n_z,m_x m_y m_z}(m,n)\right]\overline{J}_{m_x m_y m_z}(\varepsilon_s-\varepsilon_e) + \frac{1}{\Delta v}\overline{e}_n^i \qquad (3.9)$$

where,

$$\left[g_{n_x n_y n_z,m_x m_y m_z}(m,n)\right] = \frac{j\omega\varepsilon_0\Delta_x\Delta_y}{ab\Delta_z}e^{-jk_x(x_{m_x}-x_{n_x})}e^{-jk_y(y_{m_y}-y_{n_y})}\frac{\sin^2(\frac{k_x\Delta_x}{2})}{\left(\frac{k_x\Delta_x}{2}\right)^2}\frac{\sin^2(\frac{k_y\Delta_y}{2})^2}{\left(\frac{k_y\Delta_y}{2}\right)^2}$$

$$\int_{z_{n_z}-\Delta_z/2}^{z_{n_z}+\Delta_z/2}\int_{z_{m_z}-\Delta_z/2}^{z_{m_z}+\Delta_z/2}\left[\tilde{G}(k_x,k_y,z,z')\right]dz'dz$$

(3.10)

36

$$\overline{e}_n^i = \langle T_n, \overline{E}_i \rangle, \ \Delta v = \Delta_x \Delta_y \Delta_z.$$

(3.10) can be written in matrix form as:

$$[J] = [g][J] + [E^i] \qquad (3.11)$$

where, the dimension of J matrix is *3xMₓxMᵧxMᵤ*. This is the characteristic equation of the structure. From this equation the coefficients of the current densities can be calculated as:

$$. [J] = [I - g]^{-1}[E^i] \qquad (3.12)$$

where *[I]* represents the identity matrix.

In the next two sections first spectral domain Green's functions for multilayer structures will be presented, then the numerical problems associated with the solution of the characteristic equation will be discussed.

3.3   Formulations of Spectral Domain Green's Functions
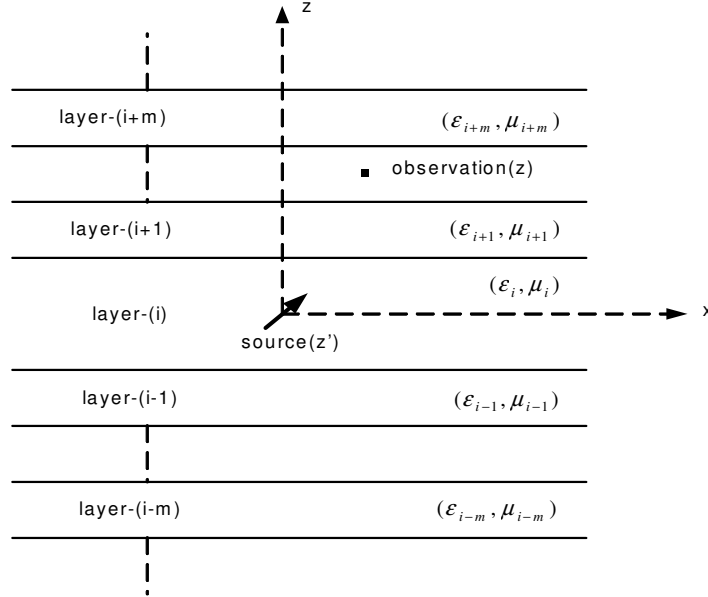
Fig. 3.4 Line source embedded in a multilayer geometry

The solution of (3.11) requires extensive use of full set of dyadic electric field Green's functions. These functions are derived by using plane wave representation of sources and boundary conditions. For the multilayered geometry shown in Fig. 3.4, explicit expressions of these functions are given as [37]:

For horizontal electric dipole (HED):

$$
\tilde{G}_{xx}^{E} = \frac{-1}{2\omega\varepsilon k_{\rho}^2 k_{zi}}
\begin{bmatrix}
(k_x^2 k_{zi}^2 + k_y^2 k_i^2)e^{-jk_{zi}|z-z'|} \\
+ (k_y^2 k_i^2 \tilde{R}_{TE}^{i,i+1} M_i^{TE} - k_{zi}^2 k_x^2 \tilde{R}_{TM}^{i,i+1} M_i^{TM})e^{jk_{zi}(z+z'-2d_i)} \\
+ (k_y^2 k_i^2 \tilde{R}_{TE}^{i,i+1} \tilde{R}_{TE}^{i,i-1} M_i^{TE} + k_{zi}^2 k_x^2 \tilde{R}_{TM}^{i,i+1} \tilde{R}_{TM}^{i,i-1} M_i^{TM})e^{jk_{zi}(z-z'-2d_i)} \\
+ (k_y^2 k_i^2 \tilde{R}_{TE}^{i,i-1} M_i^{TE} - k_{zi}^2 k_x^2 \tilde{R}_{TM}^{i,i-1} M_i^{TM})e^{-jk_{zi}(z+z')} \\
+ (k_y^2 k_i^2 \tilde{R}_{TE}^{i,i+1} \tilde{R}_{TE}^{i,i-1} M_i^{TE} + k_{zi}^2 k_x^2 \tilde{R}_{TM}^{i,i+1} \tilde{R}_{TM}^{i,i-1} M_i^{TM})e^{-jk_{zi}(z-z'+2d_i)}
\end{bmatrix}
$$

(3.13)

$$
\tilde{G}_{xy}^{E} = \frac{k_x k_y}{2\omega\varepsilon k_{\rho}^2 k_{zi}}
\begin{bmatrix}
k_{\rho}^2 e^{-jk_{zi}|z-z'|} \\
+ (k_i^2 \tilde{R}_{TE}^{i,i+1} M_i^{TE} + k_{zi}^2 \tilde{R}_{TM}^{i,i+1} M_i^{TM})e^{jk_{zi}(z+z'-2d_i)} \\
+ (k_i^2 \tilde{R}_{TE}^{i,i+1} \tilde{R}_{TE}^{i,i-1} M_i^{TE} - k_{zi}^2 \tilde{R}_{TM}^{i,i+1} \tilde{R}_{TM}^{i,i-1} M_i^{TM})e^{jk_{zi}(z-z'-2d_i)} \\
+ (k_i^2 \tilde{R}_{TE}^{i,i-1} M_i^{TE} + k_{zi}^2 \tilde{R}_{TM}^{i,i-1} M_i^{TM})e^{-jk_{zi}(z+z')} \\
+ (k_i^2 \tilde{R}_{TE}^{i,i+1} \tilde{R}_{TE}^{i,i-1} M_i^{TE} - k_{zi}^2 \tilde{R}_{TM}^{i,i+1} \tilde{R}_{TM}^{i,i-1} M_i^{TM})e^{-jk_{zi}(z-z'+2d_i)}
\end{bmatrix}
$$

(3.14)

$$
\tilde{G}_{yy}^{E} = \frac{-1}{2\omega\varepsilon k_{\rho}^2 k_{zi}}
\begin{bmatrix}
(k_y^2 k_{zi}^2 + k_x^2 k_i^2)e^{-jk_{zi}|z-z'|} \\
+ (k_x^2 k_i^2 \tilde{R}_{TE}^{i,i+1} M_i^{TE} - k_{zi}^2 k_y^2 \tilde{R}_{TM}^{i,i+1} M_i^{TM})e^{jk_{zi}(z+z'-2d_i)} \\
+ (k_x^2 k_i^2 \tilde{R}_{TE}^{i,i+1} \tilde{R}_{TE}^{i,i-1} M_i^{TE} + k_{zi}^2 k_y^2 \tilde{R}_{TM}^{i,i+1} \tilde{R}_{TM}^{i,i-1} M_i^{TM})e^{jk_{zi}(z-z'-2d_i)} \\
+ (k_x^2 k_i^2 \tilde{R}_{TE}^{i,i-1} M_i^{TE} - k_{zi}^2 k_y^2 \tilde{R}_{TM}^{i,i-1} M_i^{TM})e^{-jk_{zi}(z+z')} \\
+ (k_x^2 k_i^2 \tilde{R}_{TE}^{i,i+1} \tilde{R}_{TE}^{i,i-1} M_i^{TE} + k_{zi}^2 k_y^2 \tilde{R}_{TM}^{i,i+1} \tilde{R}_{TM}^{i,i-1} M_i^{TM})e^{-jk_{zi}(z-z'+2d_i)}
\end{bmatrix}
$$

(3.15)

$$
\tilde{G}_{zx}^{E} = \frac{k_x}{2\omega\varepsilon_i}
\begin{bmatrix}
\pm e^{-jk_{zi}|z-z'|} \\
+ \tilde{R}_{TM}^{i,i+1} M_i^{TM} e^{jk_{zi}(z+z'-2d_i)} \\
- \tilde{R}_{TM}^{i,i+1} \tilde{R}_{TM}^{i,i-1} M_i^{TM} e^{jk_{zi}(z-z'-2d_i)} \\
- \tilde{R}_{TM}^{i,i-1} M_i^{TM} e^{-jk_{zi}(z+z')} \\
+ \tilde{R}_{TM}^{i,i+1} \tilde{R}_{TM}^{i,i-1} M_i^{TM} e^{-jk_{zi}(z-z'+2d_i)}
\end{bmatrix}
$$

(3.16)

For vertical electric dipole (VED):

$$\tilde{G}_{zz}^{E} = \frac{-1}{2\omega\varepsilon_{i}k_{zi}}k_{\rho}^{2}\begin{bmatrix} e^{-jk_{zi}|z-z'|} \\ + \tilde{R}_{TM}^{i,i+1}M_{i}^{TM}e^{jk_{zi}(z+z'-2d_{i})} \\ + \tilde{R}_{TM}^{i,i+1}\tilde{R}_{TM}^{i,i-1}M_{i}^{TM}e^{jk_{zi}(z-z'-2d_{i})} \\ + \tilde{R}_{TM}^{i,i-1}M_{i}^{TM}e^{-jk_{zi}(z+z')} \\ + \tilde{R}_{TM}^{i,i+1}\tilde{R}_{TM}^{i,i-1}M_{i}^{TM}e^{-jk_{zi}(z-z'+2d_{i})} \end{bmatrix} + \frac{j}{\omega\varepsilon_{i}}\delta(z-z')e^{-jk_{z}|z-z'|} \quad (3.17)$$

$$\tilde{G}_{xz}^{E} = \frac{k_{x}}{2\omega\varepsilon_{i}}\begin{bmatrix} \pm e^{-jk_{zi}|z-z'|} \\ - \tilde{R}_{TM}^{i,i+1}M_{i}^{TM}e^{jk_{zi}(z+z'-2d_{i})} \\ - \tilde{R}_{TM}^{i,i+1}\tilde{R}_{TM}^{i,i-1}M_{i}^{TM}e^{jk_{zi}(z-z'-2d_{i})} \\ + \tilde{R}_{TM}^{i,i-1}M_{i}^{TM}e^{-jk_{zi}(z+z')} \\ + \tilde{R}_{TM}^{i,i+1}\tilde{R}_{TM}^{i,i-1}M_{i}^{TM}e^{-jk_{zi}(z-z'+2d_{i})} \end{bmatrix} \quad (3.18)$$

where,

$$\tilde{R}_{TE,TM}^{j+1,j} = \frac{R_{TE,TM}^{j+1,j} + \tilde{R}_{TE,TM}^{j,j-1}e^{-jk_{zj}2d_{j}}}{1 - R_{TE,TM}^{j,j+1}\tilde{R}_{TE,TM}^{j,j-1}e^{-jk_{zj}2d_{j}}} \quad (3.19)$$

$$M_{j}^{TE,TM} = [1 - \tilde{R}_{TE,TM}^{j,j+1}\tilde{R}_{TE,TM}^{j,j-1}e^{-jk_{zj}2d_{j}}]^{-1} \quad (3.20)$$

$$R_{TM}^{j,j-1} = \frac{\varepsilon_{i-1}k_{zi} - \varepsilon_{i-1}k_{z(i-1)}}{\varepsilon_{i-1}k_{zi} + \varepsilon_{i-1}k_{z(i-1)}} \quad (3.21)$$

$$R_{TE}^{j,j-1} = \frac{\mu_{i-1}k_{zi} - \mu_{i-1}k_{z(i-1)}}{\mu_{i-1}k_{zi} + \mu_{i-1}k_{z(i-1)}} \quad (3.22)$$

and R and $\tilde{R}$ are Fresnel and generalized reflection coefficients, respectively, for which the subscripts TE and TM represent the polarization of the wave with respect to z axis, and superscripts *(i,i-1)* and *(i,i+1)* show the layer numbers. The expressions for generalized reflection coefficients are recursive relations and calculated starting from the bottom layer to the top layer, recursively.

Note that,

$$\tilde{G}_{yx}^{E} = \tilde{G}_{xy}^{E},$$
$$\tilde{G}_{zy}^{E} = (k_{y}/k_{x})\tilde{G}_{zx}^{E}.$$
$$\tilde{G}_{yz}^{E} = (k_{y}/k_{x})\tilde{G}_{xz}^{E}$$

The derivations of the electric field Green's functions are given in references [37], [46]. However, the derivation of $\tilde{G}_{zz}^E$ requires special attention due to discontinuity term, the second term of (3.17). The z component of the electric field Green's function for vertical dipole has a singularity at $z = z'$ due to double derivative of E_z with respect to $\hat{z}$ and this should be examined carefully in the calculation of this Green's function. If the singularity term is not included in the formulation, erroneous results will be produced [35], [47]. Therefore derivation of $\tilde{G}_{zz}^E$ will be presented in this part.

Starting from the Maxwell's equations the electric field for a vertical dipole can be derived as [37]:

$$E_z = \frac{-1}{4\pi^2 2\omega\epsilon k_z}(k_i^2 + \frac{\partial^2}{\partial z^2})\int_{-\infty}^{\infty}\int_{-\infty}^{\infty} dk_x dk_y e^{-jk_x(x-x')}e^{-jk_y(y-y')}F_{TM}(z,z') \qquad (3.23)$$

where,

$$F_{TM}(z,z') = e^{-jk_z|z-z'|} + A_v^e e^{-jk_z(z-z')} + B_v^e e^{jk_z(z-z')} \qquad (3.24)$$

The first term in (3.24) represents the direct wave, second and third terms represent up-going and down-going waves respectively. A_v^e and B_v^e are the coefficients of down-going and up-going waves due to reflections and can be obtained by matching up-going and down going waves at the interfaces. These coefficients can be found as:

$$A_v^e = \frac{\tilde{R}_{TM}^{j,j-1}e^{-j2k_{zi}z'} + \tilde{R}_{TM}^{j,j-1}\tilde{R}_{TM}^{j,j+1}e^{-j2k_{zi}d_i}}{1 - \tilde{R}_{TM}^{j,j-1}\tilde{R}_{TM}^{j,j+1}e^{-j2k_{zi}d_i}} \qquad (3.25)$$

$$B_v^e = \frac{\tilde{R}_{TM}^{j,j+1}e^{-j2k_{zi}(d_i-z')} + \tilde{R}_{TM}^{j,j-1}\tilde{R}_{TM}^{j,j+1}e^{-j2k_{zi}d_i}}{1 - \tilde{R}_{TM}^{j,j-1}\tilde{R}_{TM}^{j,j+1}e^{-j2k_{zi}d_i}} \qquad (3.26)$$

Equation (3.23) is a Fourier transform like integral and from this equation the spectral domain Green's function due to VED can be written as: ,

$$\tilde{G}_{zz}(k_x,k_y,z,z') = \frac{-1}{2\omega\epsilon k_z}\left(k_i^2 + \frac{\partial^2}{\partial z^2}\right)F_{TM}(z,z') \qquad (3.27)$$

At this point it should be noticed that

$$\frac{\partial^2}{\partial z^2}\left(e^{-jk_z|z-z'|}\right) \neq -k_z^2 e^{-jk_z|z-z'|}$$

Using the distribution theory [48]:

$$\frac{\partial^2}{\partial z^2}\left(e^{-jk_z|z-z'|}\right) = -k_z^2 e^{-jk_z|z-z'|} - 2jk_z\delta(z-z')e^{-jk_z|z-z'|} \tag{3.28}$$

Therefore using (3.27) and (3.28), $\tilde{G}_{zz}^E$ is written as:

$$\tilde{G}_{zz}^E = \frac{-1}{2\omega\varepsilon abk_z}\left(k_\rho^2 F_{TM}(z,z') - 2jk_z\delta(z-z')e^{-jk_z|z-z'|}\right) \tag{3.29}$$

where, the last term accounts for the singularity. If coefficients given in (3.25) and (3.26) are substituted into (3.29), (3.17) can be easily obtained.

A special attention should also be given when calculating the integrals on the Green's functions. The characteristic matrix that is obtained through the solution of volume integral equation contains a convolution integral on the basis functions and an inner product integral on the testing function. These integrals should be carefully examined; otherwise they may cause erroneous results. The following integral should be splitted into two parts by considering the absolute value on the direct wave terms:

$$\int_{z_n-\Delta/2}^{z_n+\Delta/2}\int_{z_m-\Delta/2}^{z_m+\Delta/2} e^{-jk_z|z-z'|}dz'dz = \int_{z_n-\Delta/2}^{z_n+\Delta/2}\int_{z_m-\Delta/2}^{z} e^{-jk_z(z-z')}dz'dz + \int_{z_n-\Delta/2}^{z_n+\Delta/2}\int_{z}^{z_m+\Delta/2} e^{jk_z(z-z')}dz'dz$$

$$\tag{3.30}$$

3.4   Determination of Dispersion Relations

Dispersion relations determine the phase velocity and number of modes propagating in the structure. By determining the propagation constant for various frequencies dispersion diagrams can be obtained. Dispersion diagrams are especially important for periodic structures because by inspecting them it is possible to observe the bandgaps in the structure.

3.4.1   Numerical Considerations

Recall that the matrix equation (3.11) represents the relation between the coefficient of the unknown equivalent currents and the incident field. If there is no incident field term on the right hand side, an eigenvalue equation which determines the dispersion characteristics of the structure is obtained. That is:

$$[J]\underbrace{[I - g]}_{C} = 0 \qquad (3.31)$$

where, C is the characteristic matrix of the structure. The propagation constant of the structure can be obtained by setting the determinant of the characteristic matrix to zero as:

$$\det[C] = 0 \qquad (3.32)$$

If the determinant of the matrix was a smoothly changing function it would be easy to find the point where it reaches to zero by using a proper root finding algorithm. However this is not the case for this problem. In Fig. 3.5 the real part of the determinant calculated for the sample geometry is plotted versus β_x/k_0. As seen from the figure the determinant contains singularities and steep gradients. Also it is a very small number and the search is sensitive to round off errors. In general, without human intervention it is not easy to find the propagation constant by looking at only the determinant value.

The singularities are related to the poles in the formulation and causes fluctuations in the determinant. This problem is extensively discussed in the literature [49]-[52]. In [49] a pole free formulation is suggested to obtain dispersion characteristics of the strip lines. In [50] firstly eigenvalue decomposition is applied to the characteristic matrix as:

$$[C] = [V_a^T]^*[\Lambda_a][V_a] \qquad (3.33)$$

where, Λ_a, V_a are the eigenvalues and eigenvectors respectively. The point at which one of the eigenvalue crosses the origin is searched by scanning the spectrum. At this point the determinant is equal to zero therefore it gives the

propagation constant. The method is implemented but satisfactory results could not be obtained.
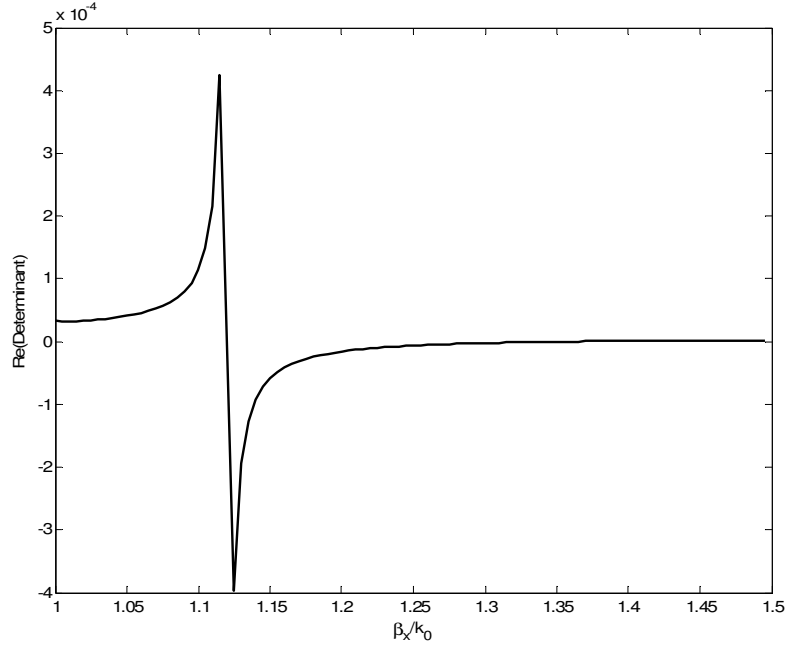
Fig. 3.5 The real part of the determinant versus β_x/k_0 calculated for the grounded slab with implanted periodic material blocks, ε_s=10, ε_e=1, a=b=5 mm, h=2 mm, W=3 mm, L=2.5 mm, z_0=1.5 mm, T=0.5 mm, f=20.0 GHz.

Alternatively minimum singular value can be used to find the points where the determinant is zero [51]. The singular value decomposition of the matrix is given by [53]:

$$[C] = [W][S][V]^T \tag{3.34}$$

where, S is a diagonal matrix formed by singular values in decreasing order, the columns W and V are left and right singular vectors of A. Notice that because S is a diagonal matrix, the determinant is zero when the minimum singular value is zero. The calculation of minimum singular value is insensitive to round off errors. In Fig. 3.6 the minimum singular value calculated for the sample geometry is plotted versus β_x/k_0. As seen from the figure, the variation of the minimum

43

singular value with respect to phase constant contains no singularities and has sharp peaks which can easily be detected.
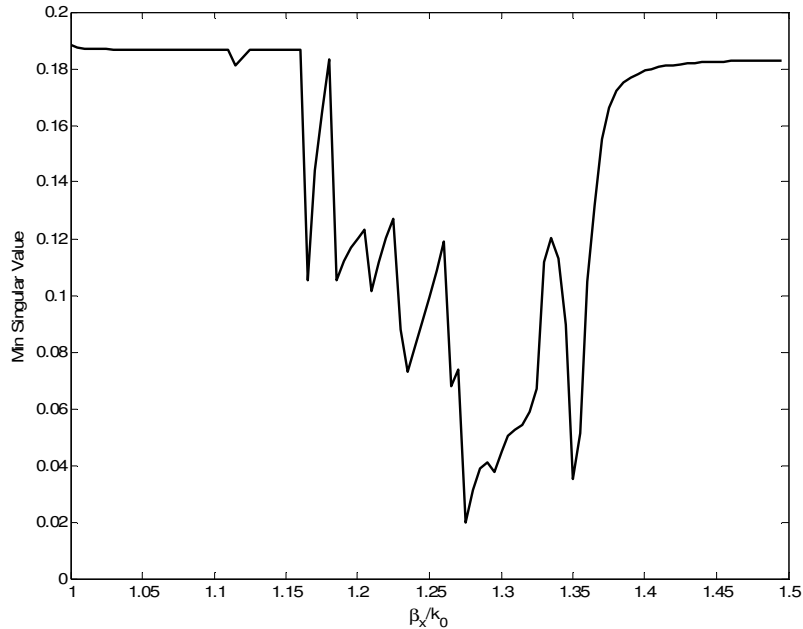
Fig. 3.6 The minimum singular value versus β_x/k_0 calculated for the grounded slab with implanted periodic material blocks, ε_s=10, ε_e=1, a=b=5 mm, h=2 mm, W=3 mm, L=2.5 mm, z_0=1.5 mm, T=0.5 mm, f=20.0 GHz.

Using the singular value of the determinant the propagation constant can be determined using a line search algorithm; however still two questions remain to be answered. The first question is: "How many roots exist in the interested range?". The second question is: "What should be the starting point for the line search algorithm?". Because, line search algorithms require an initial point to find local minima. The roots can be obtained by directly scanning the spectrum step by step. This technique does not need an initial point and all roots can easily be extracted. However to extract closely spaced roots accurately, very fine scanning is required and this increases the computation time. For these reasons a hybrid method is applied. Firstly, the spectrum is scanned with coarse steps and possible root

44

locations, below a threshold level are determined. Then those possible root locations are given to the optimization algorithm as an initial point to find the exact locations of the roots.

It was found that for this problem direct search method by Hooke-Jeeves [54] is suitable to use as an optimization algorithm. It can extract the optimum point of a function that has "sharp valleys" and fast fluctuations. This method can solve the optimization problems where the classical methods do not work. With the Hooke's words "The optimization approach that we called direct search was born because of a problem that didn't respond to classical methods."

The method is an unconstrained minimization method. In our case we are looking for roots in a predetermined range and the limit of the optimization should be determined. To give such constraints to the problem the penalty and barrier methods are used.

The basic algorithm is as follows [55]:

Let $d_1.........d_n$ be the coordinate directions. Choose a scalar $\varepsilon > 0$ to be used for terminating the algorithm. Furthermore choose an initial step size $\Delta \geq \varepsilon$ and an acceleration factor $\alpha > 0$. Choose a starting point x_1, let $y_1 = x_1$, let $k = j = 1$ and go to the main step.

The Algorithm:

1. *If $f(y_j + \Delta d_j) < f(y_j)$, the trial is termed a success; let $y_{j+1} = y_j + \Delta d_j$ and go to step2. If however, $f(y_j + \Delta d_j) \geq f(y_j)$, the trial is termed as a failure. In this case, if $f(y_j - \Delta d_j) < f(y_j)$, let $y_{j+1} = y_j - \Delta d_j$, and go to step2; if $f(y_j - \Delta d_j) \geq f(y_j)$, let $y_{j+1} = y_j$, and go to step2.*

2. *if $j < n$ replace j by $j+1$, and repeat step 1. Otherwise, go to step 3 if $f(y_{n+1}) < f(x_k)$, and go to step 4 if $f(y_{n+1}) \geq f(x_k)$.*

3. *Let $x_{k+1} = y_{n+1}$, and let $y_1 = x_{k+1} + \alpha(x_{k+1} - x_k)$. Replace k by $k+1$, let $j=1$, and go to step1.*

4. *$\Delta \leq \varepsilon$, stop; x_k is the solution. Otherwise, replace Δ by $\Delta/2$. Let $y_1 = x_{k+1}$, $x_{k+1} = x_k$, replace k by $k+1$, let $j=1$, and repeat step1.*

The direct search algorithm performs two types of search. The first is called as exploratory search and second is called as pattern search. The exploratory search performed in steps 1-2 is a trial search and aims to obtain the information on another trial point. The pattern search aims to find the minimum on the next trial point. It is called as pattern search because for multidimensional search it searches minimum by following a pattern but for a one dimensional system, it is simply a one dimensional search. The algorithm could be best understood by the diagram given by Hooke as follows:
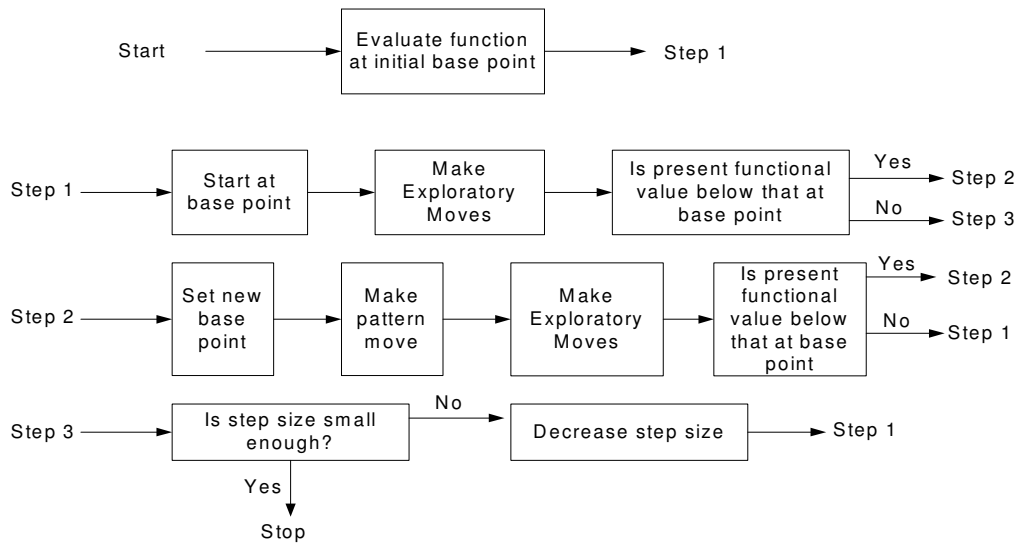
Fig. 3.7 Flow diagram of the pattern search [54].

3.4.2   Results and Discussions

To illustrate some results the phase constants of the structure are calculated at different frequencies. The parameters of the structure are $a = 3\,mm$, $b = 3\,mm$, $h = 3\,mm$, $\varepsilon_s = 10$, $\varepsilon_e = 1$, $L = W = 1\,mm$, $T = 3\,mm$, $z_0 = 0\,mm$. The direction of propagation is $\hat{x}$. To calculate propagation constant in this direction β_y is set

to zero and β_x is calculated using the procedure explained above. The results are compared with the ones calculated by Yang using MoM and theory of effective medium [33]. To observe the effects of material gratings on the waveguiding characteristics of the dielectric substrate, the propagation constants of the surface wave contributions of the grounded slab without the implants are given in the fifth column of the Table 3.1. It is seen that the results are in a good agreement. Moreover, it is observed that at lower frequencies the periodic materials gratings has no significant effect on the propagation modes of the grounded dielectric slab. Therefore the propagation constant of the periodic structure and the surface wave modes of the homogenous structure are very close to each other. But when the frequency is increased, the size of the periodic elements becomes comparable with the wavelength that results in a considerable variation in the propagation modes of the guiding structure. It is also observed that effective medium theory gives more accurate results at lower frequencies as expected.

Table 3.1 Phase Constant Comparison ($M_x=M_y=M_z=3$, *No. of Floq.=529*)

Frequency (GHz)	$\beta(k_0)$	$\beta(k_0)$ (Yang.)	$\beta(k_0)$ (eff. medium)	$\beta(k_0)$ (surf. wave)	Calc. Time (s)
2	1.00668	1.007	1.007	1.00699	215.059
4	1.03425	1.035	1.035	1.03800	212.65
6	1.12478	1.124	1.123	1.161433	179.368
8	1.43459	1.430	1.422	1.62779	168.933
10	1.065 1.914	1.061 1.910	1.050 1.896	1.25192 2.16062	198.33

To understand the effect of the grid size the propagation constant for the structure is calculated using different number of cells, as listed in Table 3.2. The

computational error with respect to the reference result obtained by the smallest mesh size ($M_x=3$, $M_y=3$, $M_z=3$) is also shown in the table. As it is expected, as the number of basis functions, that are used in the construction of the system matrix, increases the accuracy also increases. It is deduced from the table that the number of cells in the vertical direction is more crucial. Discretization in $\hat{x}$ and $\hat{y}$ directions does not change accuracy effectively but increases computation time. This condition is clearly seen if the first and fifth rows are compared.

Table 3.2 Effect of mesh size on the calculation of phase constant (*f=8 GHz, No. of. Floq=529*)

M_x,M_y,M_z	$\beta(k_0)$	Rel. err	Calc. Time (s)
1,1,1	1.4621	1.92%	12.287
2,2,1	1.4658	2.18%	14.621
1,1,2	1.4426	0.56%	43.903
2,2,2	1.4407	0.43%	52.765
1,1,3	1.4377	0.22%	97.35
2,2,3	1.4356	0.08%	116.757
3,3,3	1.4345	-	196.052

The effect of the number of Floquet modes used in the calculation is shown in Table 3.3. In the table the relative error obtained when different number of Floquet modes used in the calculation is given as the reference solution $45x45$ Floquet modes are considered. It is observed from the table that the first five summation terms are dominant. The other modes have a minor effect and $21x21= 441(n=10, m=10)$ number of Floquet terms are sufficient for most of the calculations.

Table 3.3 Effect of number of Floquet modes in the calculation of phase constant (*f*=8 *GHz*, M_x=M_y=M_z=3)

Number of Floq. Modes	$\beta(k_0)$	Rel. err	Calc. Time (s)
n=m=2	1.4835	3.64%	1.201
n=m=3	1.4439	0.87%	13.719
n=m=5	1.4408	0.66%	43.001
n=m=10	1.4345	0.22%	168.933
n=m=22	1.4314	-	838.385

In the theory of EBGs/PBGs the dispersion relation is represented in terms of dispersion diagrams. These diagrams give valuable information about the electromagnetic bandgaps. By looking at the dispersion diagrams it is possible to see the bandgaps where the propagation of the wave is prohibited. In dispersion diagrams, variation of frequency with respect to the variations in the wave vector is plotted versus in the first "**Brillouin zone**" which is also called "**reduced Brillouin zone**" [44].

One of the important conclusions of the Floquet's (Bloch's) theorem is that a mode with a wave vector $\bar{\beta}$ and a mode with a wave vector $\bar{\beta} + \bar{k}$ give rise to same field solution if $\bar{k}$ is a corresponding lattice vector in spectral domain such that $\bar{k}.\bar{a} = m2\pi$, where $\bar{a}$ is the lattice vector, so, incrementing $\bar{\beta}$ by $\bar{k}$ results in the same field solution. This means that wave vectors that differ by a multiple of $2\pi/a$ should be regarded as same wave vectors since they give rise to same solution. Therefore, for complete set of wave vectors, different solutions are obtained if these vectors are limited to a zone, called as the Brillouin zone. The location of a zone with $2\pi/a$ range can be selected freely. However, due to symmetry considerations first Brillouin zone is defined as $[-\pi/a, \pi/a]$ range. The smallest region within the Brillouin zone for which the *β* directions are not related by symmetry is called the *irreducible* Brillouin zone. As a result of this, in

dispersion diagrams frequency is plotted with respect to the phase constants (or wave vectors) only in the first Brillouin zone.

In Fig. 3.8 dispersion diagram of a sample dielectric slab with periodic implants are plotted. In the Fig. 3.8.a frequency is plotted with respect to the propagation in x direction in the first reduced Brillouin zone. To obtain the diagram β_y is set to zero and β_x is calculated. In the figure the points at which surface waves turn into leaky waves are indicated as "**light line**" and above this line, propagation of surface waves in the structure are not allowed. As it can be remembered from the solution of the homogenous dielectric slab [56], the surface waves become leaky waves when

$$\beta = k_0 = \frac{2\pi f}{c} \tag{3.35}$$

The bandgap in the propagation direction is clearly visible in the figure between frequencies ≈18.2-19.8 GHz.

To observe the surface and leaky wave characteristics Fig. 3.8.b shows the variation of the normalized propagation constant with frequency of operation, where the normalization is done with respect to k_0. As seen from the figure up to 18 GHz only surface wave modes exist in the structure. After this point the surface waves turns into leaky waves and radiates into space. Using the structure it is possible to design a leaky wave antenna. The beam of the antenna is simply given by:

$$k_0 \sin\theta = \beta_x \Rightarrow \theta = \sin^{-1}\frac{\beta_x}{k_0} \tag{3.36}$$
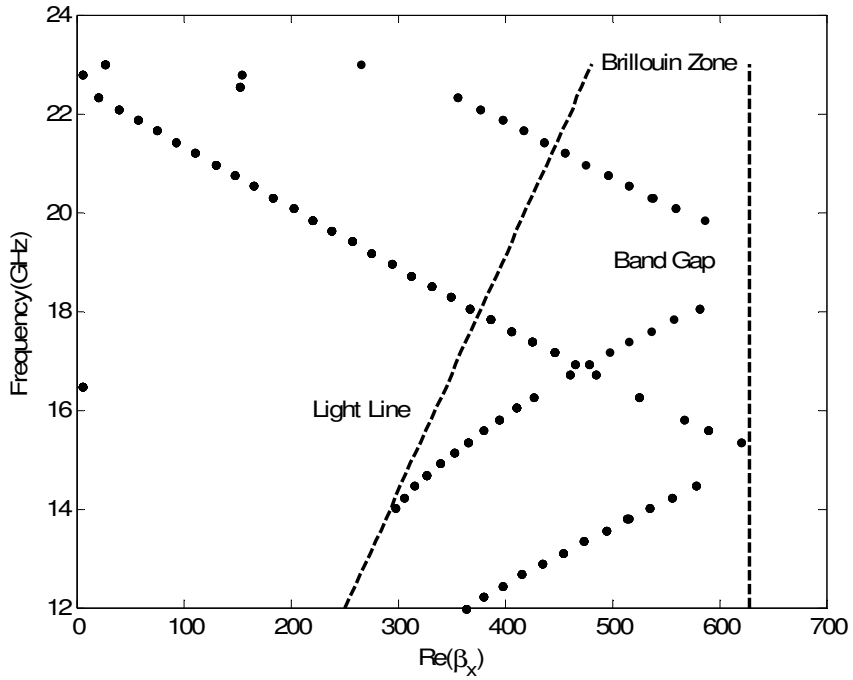
(a)
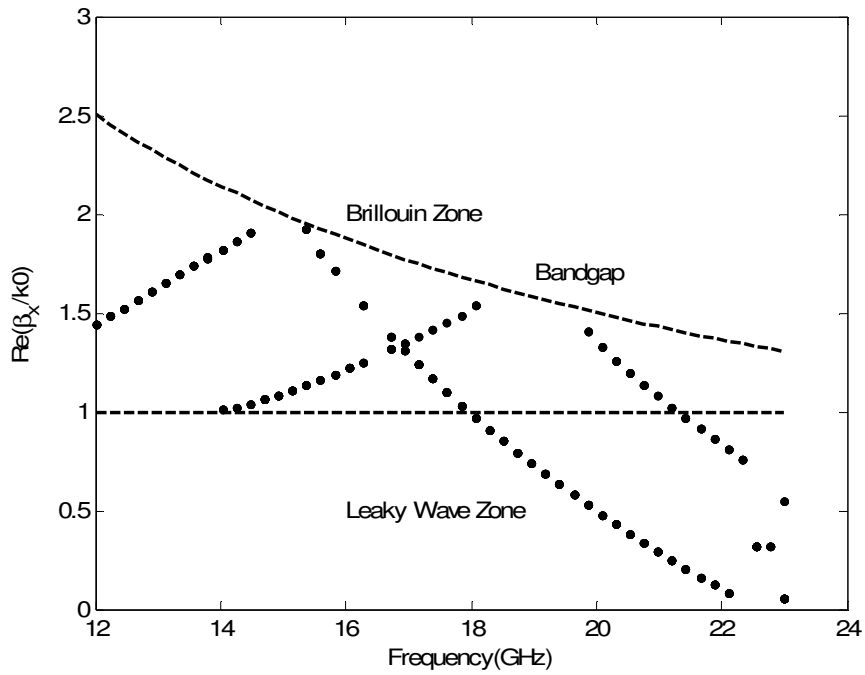
(b)

Fig. 3.8 Dispersion diagrams for modes in the grounded slab with implanted periodic material blocks, ε_s=10, ε_e=1, a=b=5 mm, h=2 mm, W=3 mm, L=2.5 mm, T=0.5 mm, z_0=1.5 mm.

3.5 Reflection properties of the EBG Structure

At some frequencies, electromagnetic bandgap materials prohibit the propagation of waves through the structure. At these frequencies such materials reflect all waves incident to the structure and because of this property they are used as "frequency selective layers (FSL)". In the design of FSL's accurate determination of reflection coefficient is important to characterize stop band regions. In this section the calculation of reflection coefficients from the structure is explained.

3.5.1 Calculation of the Reflection Coefficient

When an EBG structure is illuminated with a plane wave, due to the discontinuity of dielectric constants in the structure, volume equivalent currents occur, which results in an additional reflected field component. The scattered field has two components. One is due to Fresnel reflection principle and the other is due to the volume equivalent currents.
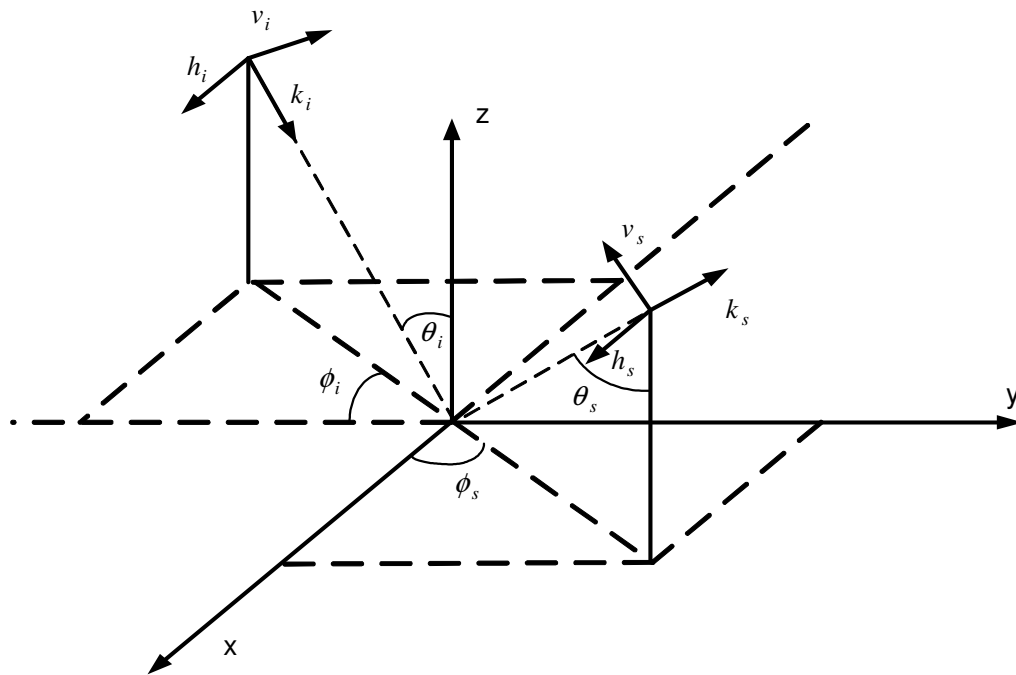
Fig. 3.9 Incident plane wave in kDB coordinate system

52

Let's assume that a dielectric slab with implanted material block is excited by a time harmonic plane wave. The plane is defined by:

$$\overline{E}^i = \overline{P}_i e^{-j\overline{k}_i \overline{r}} = (e_h \hat{h}_i + e_v \hat{v}_i) e^{-j\overline{k}_i \overline{r}} \tag{3.37}$$

where P_i is the polarization of incident wave, k_i is the wavenumber in the direction of propagation. As shown in Fig. 3.9. The unit vectors are defined in terms of spherical angles (θ, ϕ) as:

$$\hat{k}_i = \hat{x} \cos \phi_i \sin \theta_i + \hat{y} \sin \phi_i \sin \theta_i - \hat{z} \cos \theta_i$$

$$\hat{h}_i = \frac{\hat{k}_i x \hat{z}}{|k_i x \hat{z}|} = \hat{x} \sin \phi_i - \hat{y} \cos \phi_i \tag{3.38}$$

$$\hat{v}_i = \hat{x} \cos \phi_i \cos \theta_i + \hat{y} \sin \phi_i \cos \theta_i + \hat{z} \sin \theta_i$$

For reflected wave these unit vectors are given as:

$$\hat{k}_s = \hat{x} \cos \phi_s \sin \theta_s + \hat{y} \sin \phi_s \sin \theta_s + \hat{z} \cos \theta_s$$

$$\hat{h}_s = \frac{\hat{k}_s x \hat{z}}{|k_s x \hat{z}|} = \hat{x} \sin \phi_s - \hat{y} \cos \phi_s \tag{3.39}$$

$$\hat{v}_s = -\hat{x} \cos \phi_s \cos \theta_s - \hat{y} \sin \phi_s \cos \theta_s + \hat{z} \sin \theta_s$$

This coordinate systems is called as kDB coordinate system and composed of wave vector, $\hat{k}$, electric and flux density vectors , D, B [35]

Let's assume that the polarization of the incident electric field is horizontal. For this case there is no electric field component in the $\hat{z}$ direction and the TE incident fields with respect to $\hat{z}$ direction are given by:

$$\overline{E}^i_{TE} = \hat{h}_i E_{i0} e^{-j\overline{k}_i \overline{r}} \tag{3.40}$$

$$\overline{H}^i_{TE} = \hat{v}_i \frac{1}{\eta_i} E_{i0} e^{-j\overline{k}_i \overline{r}} \tag{3.41}$$

If the structure is illuminated by a plane wave magnetic field with horizontal polarization, TM incident fields with respect to $\hat{z}$ direction are given by:

$$\overline{H}^i_{TM} = \hat{h}_i H_{i0} e^{-j\overline{k}_i \overline{r}} \tag{3.42}$$

$$\overline{E}^i_{TM} = \hat{v}_i \eta_i H_{i0} e^{-j\overline{k}_i \overline{r}} \tag{3.43}$$

The electric fields reflected from the slab due to Fresnel reflection principle are given by:

$$\overline{E}_{TE}^r = \hat{h}_s \tilde{R}_{TE}^{i,i-1} E_{i0} e^{-j\bar{k}_s \bar{r}} \tag{3.44}$$

$$\overline{E}_{TM}^r = \hat{v}_s \eta_i \, \tilde{R}_{TM}^{i,i-1} H_{i0} e^{-j\bar{k}_s \bar{r}} \tag{3.45}$$

$\tilde{R}_{TE}, \tilde{R}_{TM}$ are generalized TE and TM mode reflection coefficients respectively [41].

The total electric fields incident to implanted dielectrics blocks are the summation of incident and reflected field from the slab and given by:

$$\overline{E}_{TE,TM}^{ti} = \overline{E}_{TE,TM}^i + \overline{E}_{TE,TM}^r \tag{3.46}$$

It should be noted that the electric field expressions are given for air and these fields should be transferred to the observation layer when they are used to calculate the volume equivalent currents. The amplitude coefficients that relate the fields between adjacent layers are given by:

$$A_{j-1}^- = A_j^- \frac{T_{j,j-1,j} e^{-j(k_{z_i} - k_{z_{i-1}})d_{i-1}}}{1 - \tilde{R}_{i-1,i-2}^{TE,TM} R_{i-1,i} e^{-jk_{z_{i-1}} 2(d_{i-1} - d_i)}} \tag{3.47}$$

where A_j^-, A_{j-1}^- are amplitudes of the down-going waves in j and j-1 respectively. Similarly amplitudes of up-going waves can be written as:

$$A_{j+1}^- = A_j^- \frac{T_{j+1,j,j} e^{-j(k_{z_i} - k_{z_{i+1}})d_i}}{1 - \tilde{R}_{i+1,i+2}^{TE,TM} R_{i+1,i} e^{-jk_{z_{i+1}} 2(d_{i+1} - d_i)}} \tag{3.48}$$

In (3.12) a matrix equation that relates the coefficients of the volume equivalent currents to the incident field is derived in Section 3.2. Using this matrix equation and incident field expression with amplitude transfer relations given in (3.47) and (3.48), the volume equivalent current can be obtained. If the volume equivalent currents are substituted into the volume integral equation we obtain:

$$\overline{E}_{TE,TM}^s(\bar{r}) = \iiint_v [G(\bar{r},\bar{r}')] \overline{J}_{eq}(\bar{r}') dv' \tag{3.49}$$

$$\overline{E}_{TE,TM}^s(\bar{r}) = \frac{1}{ab} \sum_{m_z=0}^{M_z-1} \sum_{m_y=0}^{M_y-1} \sum_{m_x=0}^{M_x-1} J_{mx,my,mz} \sum_{n=-\infty}^{\infty} \sum_{m=-\infty}^{\infty} \left[\begin{array}{c} e^{-jk_x(x-x_{mx})} . e^{-jk_y(y-y_{my})} . \dfrac{\sin(\frac{k_x \Delta_x}{2})}{\frac{k_x \Delta_x}{2}} \dfrac{\sin(\frac{k_y \Delta_y}{2})}{\frac{k_y \Delta_y}{2}} \Delta_x \Delta_y \\[2em] \displaystyle\int_{z_{mz} - \Delta_z/2}^{z_{mz} + \Delta_z/2} [G] dz' \end{array} \right]$$

$$\tag{3.50}$$

where, *G* represents the electric field Green's function in the slab, Δ_x, Δ_y represents the mesh size in x, y directions respectively. The total scattered electric field from the slab is the summation of scattered field and reflected field and given by:

$$\overline{E}^{ts}_{TE,TM} = \overline{E}^{s}_{TE,TM} + \overline{E}^{r}_{TE,TM} \tag{3.51}$$

The specular TE, TM reflection coefficients are calculated at the far field by using the following formula:

$$\Gamma_{TE,TM} = \frac{\overline{E}^{ts}_{TE,TM}(\overline{r})}{\overline{E}^{ti}_{TE,TM}(\overline{r})} \tag{3.52}$$

3.6   Results and Discussions

The calculation procedure is verified using, a PBG substrate with fill ratio equal to 1, that is *a/W=b/L=*1. In this case the reflection coefficients should be equal to the generalized Fresnel reflection coefficients because the structure becomes homogenous. Fig. 3.10 shows the real and imaginary part of the TM reflection coefficients calculated for the structure when the fill ratio is 1. The dielectric constants of the slab and implanted blocks are $\varepsilon_s = 4$ and $\varepsilon_e = 10$ respectively. The other parameters are, $a = b = L = W = 1\,cm$, $h = T = 0.2\,cm$, $\theta = 0°$, number of Floquet modes are 23*x*23=569. The number of basis functions for each component of the equivalent current is *3x3x3=27*. The calculation of the reflection coefficient at 100 number of frequency points takes approximately 937 seconds on a PC with a 1.6 Pentium mobile processor. The generalized reflection coefficients are also plotted on the same figure for comparison. As seen from the figure up to 10 GHz the calculated reflection coefficients are almost indistinguishable from the generalized reflection coefficients. After that the error increases and at 14 GHz reaches to 1%. As it is explained in the previous section the mesh size that is used in z direction is a crucial parameter in the calculations. At 14 GHz it corresponds to 30λ. To reduce the errors after that point more basis functions with smaller mesh sizes should be used.
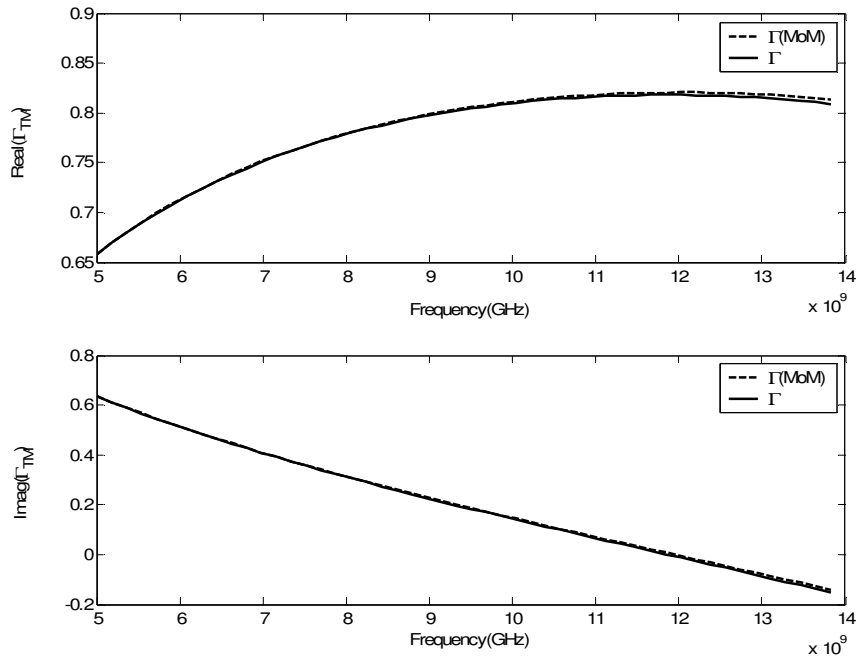
Fig. 3.10 TM reflection coefficient versus frequency when fill ratio is one.
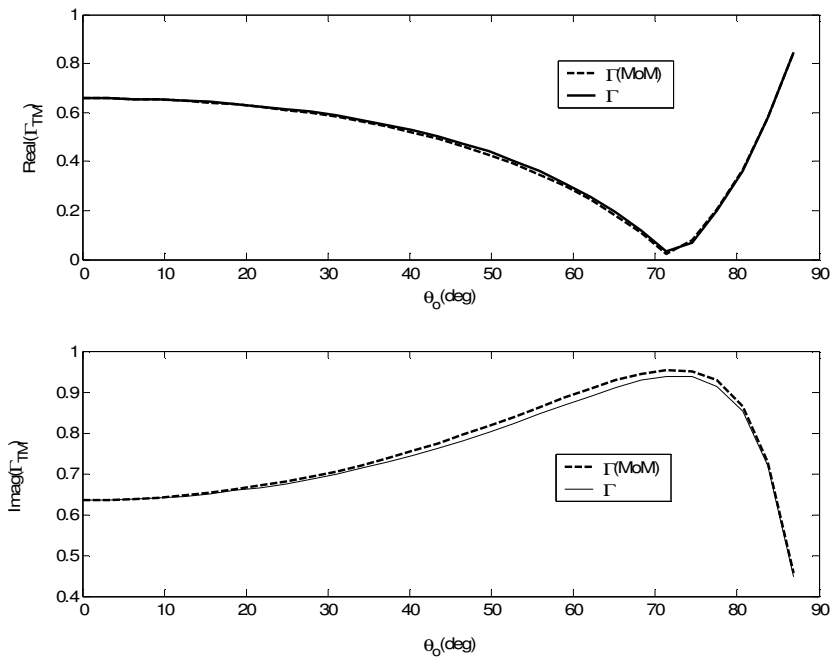
Fig. 3.11 TM reflection coefficient versus incidence angle when the fill ratio is one

56

The variation of the reflection coefficient with the angle of incidence is given in Fig. 3.11. As seen from the figure for incidence angles up to 40° the results are in a good agreement. After that point the error in the calculation increases and reaches to 2%. This condition can be explained insufficient modeling of z-variation of the structure for large incidence angles. To reduce the error the number of cells in the $\hat{z}$ direction should be increased.

To demonstrate the accuracy of the developed software the reflection coefficients for a structure with fill ratio different than one is studied and the results are compared with the ones presented in [34]. The cell dimensions are $a = b = 2\,cm$, $L = W = 1cm$ and other parameters are same with the previous example. Fig. 3.12 plots the reflection coefficient versus frequency for three angles of incidence, $\theta = 0^o, 15^o, 30^o$. As seen from the plot the results are in a good agreement with the results calculated by Yang.
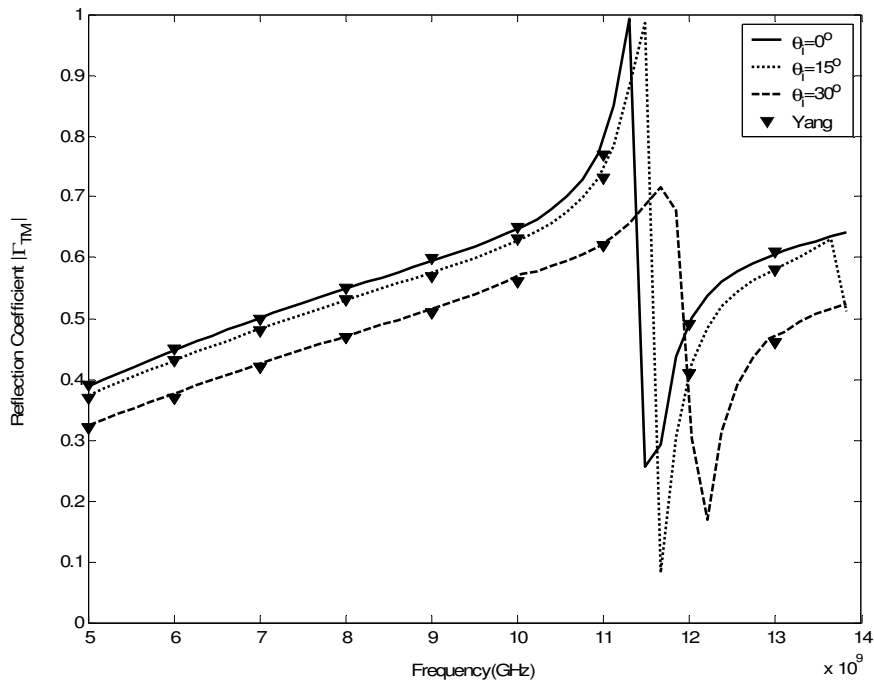
Fig. 3.12 Specular reflection coefficient of a TM plane wave from a dielectric slab with periodically implanted material blocks

57

It should be noted that although the solution procedure is developed for 3-D structures, 2-D structures (infinite in one direction) could be easily analyzed by this program without any modification. Only the fill ratio (*a/W* or *b/L*) in the infinite direction should be set to 1. Therefore with the developed program we can also solve the 2-D PBG slab problems.

3.7 Conclusions

In this chapter a 3-D moment method to analyze multilayered structures with periodically implanted materials has been presented. The method requires extensive use of full dyadic spectral domain Green's function. The full set of spectral domain Green's functions has been formulated for stratified media. Using the method the propagation constants have been calculated. It has been seen that the automatic determination of propagation constants is not an easy task. An hybrid technique, that uses singular value of the characteristic matrix and direct search algorithm is developed to overcome difficulties. The dispersion diagram of the structure has been obtained and seen that the periodic structure has bandgaps in some directions. The reflection properties of the structure are examined using the method. Using the volume equivalent currents the specular reflection coefficient has been calculated. It has been seen that at some frequencies the structure behaves as a frequency selective layer. The results are compared with the literature and a perfect agreement has been observed. In the examples the structures with cubical implants has been examined. The method can be extended to analyze arbitrary geometries but such structures require finer meshes and large number of basis functions that increases the computation time. Modifications in the analysis method are required to analyze complex structures efficiently.

CHAPTER 4

USE OF ASYMPTOTIC WAVEFORM EVALUATION TECHNIQUE IN THE ANALYSIS OF MULTILAYERED STRUCTURES WITH IMPLANTED PERIODIC MATERIAL BLOCKS

4.1   Introduction

In the previous chapter, a dielectric slab with periodically implanted material blocks was analyzed using volume equivalence principle and method of moment technique. The method is robust and applicable to the periodic structures in stratified media. Although the method is relatively slow due to the double summation of Floquet modes it is useful in obtaining the reflection coefficient and the propagation constant of the periodic structure.

The EBG materials are generally used as frequency selective layers in optics and electromagnetics. For such applications, the reflection coefficient is the main parameter of interest. To extract the point where the stop band occurs, the reflection coefficient should be calculated at more than 200 frequency points, around the resonance. The dispersion diagrams are also important in the analysis of EBG materials. To calculate dispersion diagrams, fine frequency scanning is necessary to accurately characterize stop band. For such analyses propagation constant should be calculated at more than 1000 frequency points. When the dispersion diagram or full frequency response of the reflection coefficient is required, the studied method becomes inefficient due to its computational cost. In this chapter asymptotic waveform evaluation (AWE) technique is suggested to be utilized to obtain reflection and band response of EBG materials in a shorter time. This chapter starts with the overview of the AWE technique given in Section 4.2. In Section 4.3 the difficulties in the implementation of AWE technique is

discussed and in Section 4.4 the automatic differentiation technique which is suggested as a solution for these problems is explained. In Section 4.5 the reflection coefficient results obtained through AWE technique is presented. In Section 4.6 the use of AWE technique to obtain dispersion relations are given and some results are presented. This chapter ends with the conclusion section, Section 4.7.

4.2   Asymptotic Waveform Evaluation Technique (AWE)

Asymptotic Waveform Evaluation Technique (AWE) is initially proposed to obtain transient response of the complex circuits from initial conditions [57], later it is extended to numerical solution of electromagnetic problems [58]. Recently, it was shown that the technique can be used successively to obtain radiation properties of microstrip structures in stratified media [59].

One of the disadvantages of the spectral/spatial domain MoM and FEM techniques is that to obtain the full frequency response of the structure the solution has to be repeated at each frequency. For resonant systems, the number of frequency points to capture the resonance can be very large. For such problems, AWE enables to predict the full frequency response from the solution at a single point. The AWE technique is also used to estimate radiation pattern characteristics [60]. Use of AWE in the solution of periodic structures is firstly proposed by Davidovitz [61]. In the formulation of periodic structures, full phase response is necessary to obtain radiation properties, which is a time consuming process. In [61] the technique is used to estimate full phase response, from the single point. By this way the computation time is considerably reduced. The formulation of the AWE is as follows.

In this section, the application of the AWE technique to the MoM solution will be presented. In MoM technique the final impedance matrix equation is obtained in the form of:

$$[J] = [Z]^{-1}[V]$$

where, *[J]* is the column vector for the unknown amplitudes of the basis functions, [V] is the excitation vector and [Z] is the impedance matrix of the structure. The

unknown vector can be expanded in terms of Taylor series around the complex parameter ϕ_o as:

$$J(\phi) = J(\phi_0) + J'(\phi_0)(\phi - \phi_0) + \frac{J''(\phi_0)}{2!}(\phi - \phi_0)^2 + \ldots\ldots = \sum_{n=0}^{\infty} M_n(\phi - \phi_0)^n \quad (4.1)$$

where, M_n is the n th moment vector and is given by

$$M_n = \frac{1}{n!}\frac{\partial^n}{\partial\phi^n}[Z^{-1}(\phi)V]\Big|_{\phi=\phi_0} \quad (4.2)$$

The moment vector includes the derivative of the inverse of the matrix Z, which is difficult to compute. Fortunately the moments can be evaluated by the following recursive relation as [59]:

$$[Z(\phi_0)][M_n] = \sum_{r=1}^{n} \frac{1}{r!}\frac{\partial^r}{\partial\phi^r}[Z(\phi)]\Big|_{\phi=\phi_0} M_{n-r} \quad (4.3)$$

with the initial vector

$$M_0 = [Z(\phi_0)]^{-1}V \quad (4.4)$$

Taylor approximation contains infinite number of summation terms and it is valid only within the radius of convergence around ϕ_0. To approximate the current vector with a finite number of terms and to overcome the radius of convergence problem, the Pade approximation from circuit theory can be utilized. Using Pade approximation, J vector can be expressed as the ratio of two polynomials:

$$J(\phi) \cong \frac{a_0 + a_1(\phi - \phi_0) + \ldots\ldots + a_p(\phi - \phi_0)^p}{1 + b_1(\phi - \phi_0) + \ldots\ldots + b_q(\phi - \phi_0)^q} = M_0 + M_1(\phi - \phi_0) + \ldots + M_{p+q}(\phi - \phi_0)^{p+q}$$

$$(4.5)$$

By matching the two sides of (4.5), the coefficients in the numerator and the denominator of are obtained as:

$$\begin{bmatrix} M_p & M_{p-1} & \cdots & M_{p-q+1} \\ M_{p+1} & M_p & \cdots & M_{p-q+2} \\ \vdots & \vdots & \vdots & \vdots \\ M_{p+q-1} & M_{p+q} & \cdots & M_p \end{bmatrix} \begin{bmatrix} b_1 \\ b_2 \\ \vdots \\ b_q \end{bmatrix} = - \begin{bmatrix} M_{p+1} \\ M_{p+2} \\ \vdots \\ M_{p+q} \end{bmatrix} \quad (4.6)$$

$$a_r = \sum_{j=0}^{r} M_{r-j}b_j \quad (4.7)$$

61

where, $r = 0, 1, \ldots, p$.

In Fig. 4.1 Pade approximation of $\sin(x)$ function is plotted up to fourth order. The function is expanded at $x = 0$. As seen from the Figure, the fourth order Pade approximation exactly approximates one period of the function around the expansion point. As the order of the approximation is increased more information about the behavior of the function is gathered from the higher order derivative values at the expansion point, therefore a better approximation is achieved.
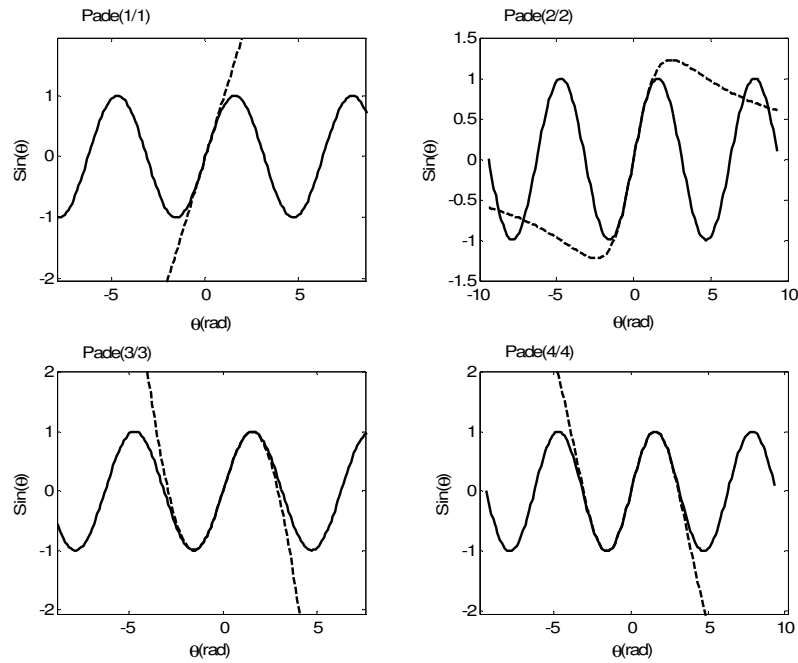
Fig. 4.1 Pade approximation of Sin(x) up to fourth orders

Above, formulation for the one dimensional AWE technique is given. For some cases like the calculation of matrix elements in (4.6), require the use of two dimensional AWE method. The two dimensional AWE technique is firstly proposed in [63] to evaluate the electric field response of a microstrip antenna with respect to frequency and dielectric constant. The formulation procedure is

similar to one dimensional case, the difference lies in the use of two dimensional Taylor approximations on the right hand side of equation (4.5). Following the procedure, the two dimensional approximation for J is obtained as:

$$J(\phi, \beta) = \frac{a_{0,0} + a_{1,0}(\phi - \phi_0) + a_{0,1}(\beta - \beta_0) + ... + a_{p,p}(\phi - \phi_0)^p (\beta - \beta_0)^p}{1 + b_{1,0}(\phi - \phi_0) + b_{0,1}(\beta - \beta_0) + ... + b_{q,q}(\phi - \phi_0)^q (\beta - \beta_0)^q}$$

(4.8)

where, the coefficients of the approximation can be obtained by matching the coefficients as in (4.5).

4.3   Difficulties and Solutions

The AWE method enables to obtain the system response very efficiently, if the higher order derivatives of the solution (Z matrix for this case) are available, if not the derivatives should be calculated by some means. The calculation of derivatives is the major drawback of the method, because for some complex functions it is not easy.

In this study the calculation of the derivatives is the keystone to calculate reflection parameters using AWE. At the first phase of the study, we tried to reduce the complexity of the Green's function by approximating it in terms of complex exponentials by using the Generalized Pencil of Functions Method (GPOF). When the Green's functions are approximated by complex exponentials, the calculation of derivatives would be straightforward.

The periodic electric field Green's functions, those constitute the basis of our kernel equation are given by:

$$G_{uv}(r, r') = \frac{1}{ab} \sum_{m=-\infty}^{\infty} \sum_{n=-\infty}^{\infty} \tilde{G}_{uv}(k_x, k_y, z, z') e^{-jk_x(x-x')} e^{-jk_y(y-y')} \quad (4.9)$$

$$k_x = 2\pi m / a + \beta_x, \, k_y = 2\pi n / b + \beta_y$$

To approximate this expression using GPOF, the spectral domain Green's function should be sampled along the real axis. On the other hand, Green's functions contain singularities around surface wave poles and branch points. When we tried to approximate the Green's functions by using samples along the

real axis, erroneous results are obtained for modes around the surface wave singularities and branch points. Due to this reason, we were not able to approximate the periodic Green's functions correctly and decided to calculate derivatives directly.

There are especially three ways to compute derivatives of expressions with respect to some specific variables with the aid of computers [64].

Approximation by finite differences: This is a well known numerical method, based on the calculation of derivatives by using the value of the function evaluated at discrete points spaced by Δ. This method is applicable if the function is simple and there are no steep gradients in the function. If this is not the case, the results strongly depend on the selection of the step size, Δ, so the solution is not stable numerically. In the electromagnetic theory the kernel formulations have steep gradients around the resonance points therefore the method produces large errors in the solution of such problems.

Symbolic Calculations: This method is essentially "differentiation by hand" method with the exception that the derivatives are calculated symbolically by a computer package like Matlab^{TM}, Maple^{TM}. For simple functions, the method is an effective way to compute derivatives but for high order derivatives of complex functions three problems arises. Firstly the symbolic computation of high order derivatives of complex functions requires generation of long intermediate expressions. During the computation, a large memory space is allocated for each of these variables, which cannot be used until the end of execution. Due to this reason, the program may crash when the available memory on the computer becomes smaller than a predefined level. Our experiences with Matlab^{TM} show that the derivatives of the Green's functions can be calculated up to third or fourth order depending on the computer. The higher order derivatives may cause memory problems. The second problem is the long and cumbersome expressions generated by symbolic compilers. As an example, the fourth order derivative of the Green's function expression with respect to k_x is about 230000 characters long when calculated with Matlab^{TM}. The generated result is huge, illegible and needs a

very good optimizing compiler in order to eliminate all the common sub expressions. Even if we assume that we have a good optimizing compiler another problem occurs related to iterative processes (like the calculation of generalized reflection coefficients) and non-trivial control structures (like the chose of k_z branch). When using symbolic differentiation packages it is not clear how to manage conditional branches and iterative loops symbolically.

Automatic Differentiation: This is the preferred method in this study to calculate derivatives of kernel formulations. The theory of automatic differentiation relies on the chain rule or Taylor's arithmetic depending on the technique that is used. Unlike symbolic calculations the method utilizes standard computer arithmetic. The calculation of derivatives is achieved by using numbers not symbolic expressions. Using the method the higher order derivatives of extremely complicated functions can be calculated exactly.

In automatic differentiation, the calculation of function expression and the derivatives are performed in parallel. Because it uses standard computer arithmetic, iterative expressions and conditional branches can easily be managed. The symbolic packages should unfold the loops to obtain the functional expressions symbolically whereas, this is not the case for automatic differentiation. For complicated expressions with many loops and conditional branches automatic differentiation is an efficient way to compute derivatives.

Versatility of the programs is another key issue that is important in the development of commercial simulation programs. To utilize AWE in a commercial electromagnetic simulation package the code that computes the derivatives should be independent of the kernel function and it should give the possibility to differentiate with respect to different variables with a single change of parameters. Versatility is another advantage of the automatic differentiation over another two methods because both in numerical and symbolic differentiation the computation of derivatives strongly depend on the function to be differentiated and structural changes are required when the function changes.

In the field of mathematical modeling, extensive amount of research has been carried out on the theory of automatic differentiation. The studies of several

workgroups around the world are gathered and published in a web site [65]. In this web site there are also several software packages available through internet in Fortran, Ada, C++ languages. Among these software packages the TADIFF package developed by Claus Bendtsen and Ole Stauning [66] is a fast and easily manageable package which is written in C++ language. Throughout this study, this code is used to calculate derivatives of the functions. The theory of automatic differentiation is explained in details in the following section.

4.4 The Theory of Automatic Differentiation (AUTODIFF)

In the theory of automatic differentiation, basically there are three ways to compute derivatives. These are Forward Automatic Differentiation (FAD), Backward Automatic Differentiation (BAD) and Taylor Automatic Differentiation (TADIFF). All these methods require operator overloading, hence it is easy to implement these methods in languages with operator overloading such as C++, Ada, Pascal. Among these three methods Taylor's method is the most efficient method in terms of computation time. The major drawback of the Taylor's method is that the differentiation with respect to only one variable is possible, which means that the partial derivatives cannot be calculated.

Forward and Backward methods rely on the same principle: **"chain rule".** In forward method the derivatives are calculated from the lowest order to the highest order and in backward method the derivatives are calculated from the highest order to the lowest order using backward substitution. These two methods are well documented in [67] and will not be discussed in here.

The Taylor's differentiation method is completely different from FAD and BAD techniques and it relies on Taylor's arithmetic. The computer package that is used in this study uses Taylor's differentiation and it is explained in detail as follows [66].

The Taylor's expansion of a function is given by:

$$f(t) = \sum_{k=0}^{\infty} (f)_k (t - t_0)^k \qquad (4.10)$$

where,

$$(f)_k = \frac{f^{(k)}(t_0)}{k!} \tag{4.11}$$

The relationship between k^{th} and $k+1^{th}$ coefficients is given as:

$$(f)_{k+1} = \frac{(f)_k}{k+1} \tag{4.12}$$

This relationship can be used to derive following elementary formulas:

$$(u+v)_k = (u)_k + (v)_k \tag{4.13}$$

$$(u-v)_k = (u)_k - (v)_k \tag{4.14}$$

$$(u.v)_k = \sum_{i=0}^{k}(u)_i(v)_{k-i} = \sum_{i=0}^{k}(u)_{k-i}(v)_i \tag{4.15}$$

$$(u/v)_k = \frac{1}{(v)_0}\left((u)_k - \sum_{j=1}^{k}(v)_j(u/v)_{k-j}\right) \quad for \quad (v)_0 \neq 0 \tag{4.16}$$

The above elementary operations constitute the basis for Taylor's arithmetic and other operations are obtained from these rules. The list of rules for other operations, those might arise in the functions are given without the derivation as follows:

$$(u^2)_k = \sum_{i=0}^{k}(u)_i(u)_{k-i} = \begin{cases} 2\sum_{i=0}^{(k-1)/2}(u)_i(u)_{k-i} & k \text{ is odd} \\ 2\sum_{i=0}^{(k-2)/2}(u)_i(u)_{k-i} + (u)_{k/2}^2 & k \text{ is even} \end{cases} \tag{4.17}$$

$$(\sqrt{u})_k = \begin{cases} \dfrac{1}{2(\sqrt{u})_0}(u)_k - 2\sum_{i=1}^{(k-1)/2}(\sqrt{u})_i(\sqrt{u})_{k-i} & k \text{ is odd} \\ \dfrac{1}{2(\sqrt{u})_0}(u)_k - 2\sum_{i=0}^{(k-2)/2}(\sqrt{u})_i(\sqrt{u})_{k-i} + (\sqrt{u})_{k/2}^2 & k \text{ is even} \end{cases} \tag{4.18}$$

$$(u^a)_k = \frac{1}{k(u)_0}\sum_{j=0}^{k-1}(a(k-j)-j)(u^a)_j(u)_{k-j} \quad for\ k \geq 1 \tag{4.19}$$

$$(\exp u)_k = \frac{1}{k}\sum_{j=0}^{k-1}(k-j)(w)_j(u)_{k-j} \quad for\ k \geq 1 \tag{4.20}$$

$$(\cos u)_k = -\frac{1}{k}\sum_{j=0}^{k-1}(k-j)(\sin u)_j(u)_{k-j} \quad for\ k \geq 1 \tag{4.21}$$

$$(\sin u)_k = \frac{1}{k}\sum_{j=0}^{k-1}(k-j)(\cos u)_j(u)_{k-j} \quad for\ k\geq 1 \tag{4.22}$$

$$(\log u)_k = \frac{1}{(u)_0}\left((u)_k - \frac{1}{k}\sum_{j=1}^{k-1}j(\log u)_j(u)_{k-j}\right) \tag{4.23}$$

$$(\tan u)_k = \frac{1}{\cos^2(u)_0}\left((u)_k - \frac{1}{k}\sum_{j=1}^{k-1}j(\tan u)_j(\cos^2 u)_{k-j}\right) \tag{4.24}$$

$$(\sin^{-1} u)_k = \frac{1}{\sqrt{1-(u)_0^2}}\left((u)_k - \frac{1}{k}\sum_{j=1}^{k-1}j(\sin^{-1} u)_j(\sqrt{1-u^2})_{k-j}\right) \tag{4.25}$$

$$(\cos^{-1} u)_k = \frac{-1}{\sqrt{1-(u)_0^2}}\left((u)_k + \frac{1}{k}\sum_{j=1}^{k-1}j(\cos^{-1} u)_j(\sqrt{1-u^2})_{k-j}\right) \tag{4.26}$$

$$(\tan^{-1} u)_k = \frac{1}{1+(u)_0^2}\left((u)_k - \frac{1}{k}\sum_{j=1}^{k-1}j(\tan^{-1} u)_j(1+u^2)_{k-j}\right) \tag{4.27}$$

Above we define the operators that might arise in any function expression. Using these operators and **"operator overloading",** derivatives of an arbitrary function can be calculated. **"Operator overloading",** means calling a function instead of the default operation. For example when computer sees multiplication operator (*) it calls (4.15) instead of default multiplication routine.

To understand the calculation of Taylor's coefficient clearly, let's assume that the function we want to expand is given by $f(t) = \sin(2t)t$. First the function is decomposed as:

$$\begin{aligned}\tau_1(\tau) &= 2.t,\\ \tau_2(\tau) &= \sin(\tau_1),\\ \tau_3(\tau) &= \cos(\tau_1),\\ f(t) &= \tau_2.t\end{aligned} \tag{4.28}$$

To calculate the derivatives, first the zero order coefficients are calculated, then the Taylor's expansion coefficients are obtained recursively as follows:

$$(\tau_1)_k = 2.(t)_k,$$

$$(\tau_2)_k = \frac{1}{k}\sum_{j=0}^{k-1}(k-j)(\tau_3)_j(\tau_1)_{k-j}$$

$$(\tau_3) = -\frac{1}{k}\sum_{j=0}^{k-1}(k-j)(\tau_2)_j(\tau_1)_{k-j}$$

$$(f)_k = \sum_{i=0}^{k}(\tau_2)_i(t)_{k-i} \tag{4.29}$$

Note that using Taylor's differentiation, Taylor expansion coefficients are obtained, not the derivatives. This is an advantage for us to use this technique in Pade approximation, because Pade approximation requires the calculation of Taylor expansion coefficients.
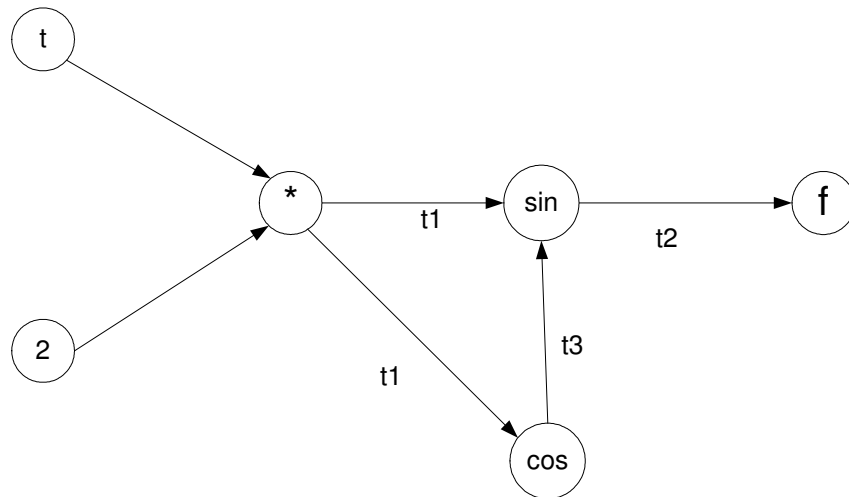
Fig. 4.2 The DAG used to calculate Taylor coefficients of $f(t) = \sin(2t)t$

As seen from the above example, to calculate the derivatives first the function should be written in terms of basic functions. For this purpose a computational graph is composed. This computational graph contains the information of dependent variables in terms of independent variables defined by the user at the initial execution of the program. The composed graph should be an acyclic graph, which means that the variables should depend on the previous values of other variables, therefore the graph is called as *directed acyclic graph*

(DAG). As an example the DAG for the function $f(t) = \sin(2t)t$ is given in Fig. 4.2.

4.5 Results and Discussions

In the previous chapter, a dielectric slab with periodically implanted material blocks was analyzed using the developed software and the specular reflection coefficient of the structure was calculated. The calculated results were compared with the literature and it was seen that they are in good agreement. At this time reflection coefficient of the same structure is calculated using AWE method and compared with the direct calculation results. Fig. 4.3 shows the calculated TM reflection coefficient using AWE and direct methods for a sample geometry. In this case the incidence angle is taken as $\theta = 0^o$ and the equivalent currents are approximated in terms of frequency as:

$$I(f) \cong \frac{a_0 + a_1(f - f_a) + \ldots\ldots + a_p(f - f_a)^p}{1 + b_1(f - f_a) + \ldots\ldots + b_q(f - f_a)^q} \tag{4.30}$$

Direct calculation results correspond to the calculation of the current at each frequency point without making any approximation. On the other hand, AWE method refers to the case that the variation of current with respect to frequency is approximated as in (4.30) by using the moments calculated at the expansion point.

The AWE approximation is calculated at $f_a = 9$ *GHz* which is the midpoint of the interested frequency band. Three different orders, $q=p=1,2,3$ are used to see the effect of the approximation order on the accuracy of the approximation. As seen from the figure when first order approximation is used AWE fails to accurately represent the reflection coefficient around the resonance point. The second order approximation gives somehow good results but still there is no perfect agreement with the results obtained using direct calculation. When the current is approximated with a third order Pade polynomial the agreement is perfect between 5-14.5 GHz band. After 14.5 GHz the deviations are observed.

Fig. 4.3 Specular TM reflection coefficient of the periodically implanted dielectric slab versus frequency $\varepsilon_s=4$, $\varepsilon_e=10$, $a=b=2$ cm, $L=W=1$ cm, $h=T=0.2$ cm, $\theta=0^o$, $f_a=9$ GHz.

In Fig. 4.4 again the reflection coefficient is plotted versus frequency but this time as an expansion point $f_a=5$ *GHz* is used. The first and the second order derivatives at $f_a=5$ *GHz* contains less information on the behavior of the frequency band and higher order derivatives should be used to approximate the currents. From the experiments it is observed that first and second order approximations do not accurately represent the current therefore in Fig. 4.4 AWE results are plotted starting from third order approximation. As seen from the figure third order approximation fails to approximate reflection coefficient around the resonance point, because of the distance between the expansion point and the resonance frequency. The fourth order approximation gives satisfactory results but still there is some error. When the fifth order approximation is used a perfect agreement is obtained.
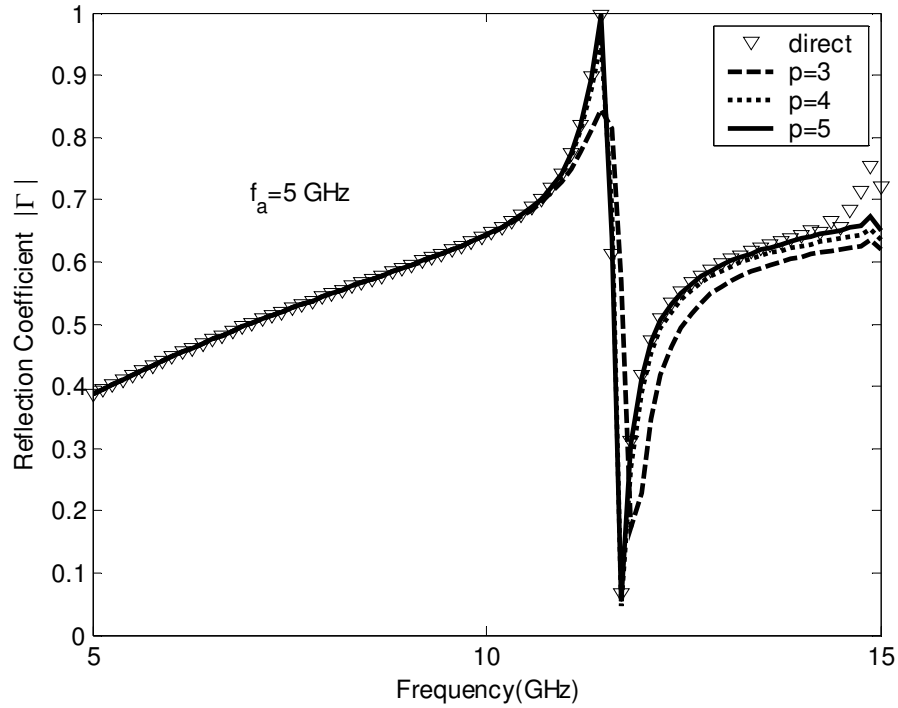
Fig. 4.4 Specular TM reflection coefficient of the periodically implanted dielectric slab versus frequency. The parameters are same as in Fig 4.3. except ,f_a=5 *GHz*.

Up to this point multilayer structures with at most three layers including the ground plane examined. The AWE technique gives accurate results also for more complicated geometries. To demonstrate the versatility of the method five layer geometry shown in Fig. 4.5 is considered. The middle layer of the structure is periodically implanted with dielectric blocks with ε_e=10. Fig. 4.6 shows the reflection coefficient of the structure obtained through AWE method and compared with the direct calculation results. For AWE method, the reflection coefficient is calculated by approximating the current at f=23.9 *GHz*. As seen from the figure a perfect agreement is obtained even with the first order approximation.

72

$$\varepsilon_5 = 1.0$$

$$1.0\,mm \qquad \varepsilon_4 = 2.2$$

$$2.0\,mm \qquad \varepsilon_e = 10.0 \qquad \varepsilon_3 = 6.0$$

$$1.0\,mm \qquad \varepsilon_2 = 4.0$$

$$\varepsilon_1 = 1.0$$

$$a = b = 2\,mm \qquad L = W = 1\,mm$$
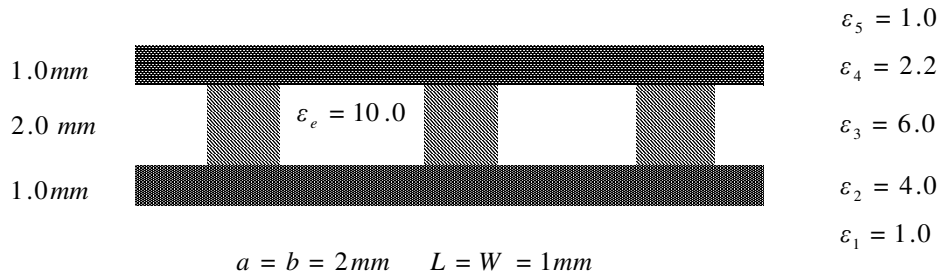
Fig. 4.5 The geometry of five layer dielectric structure
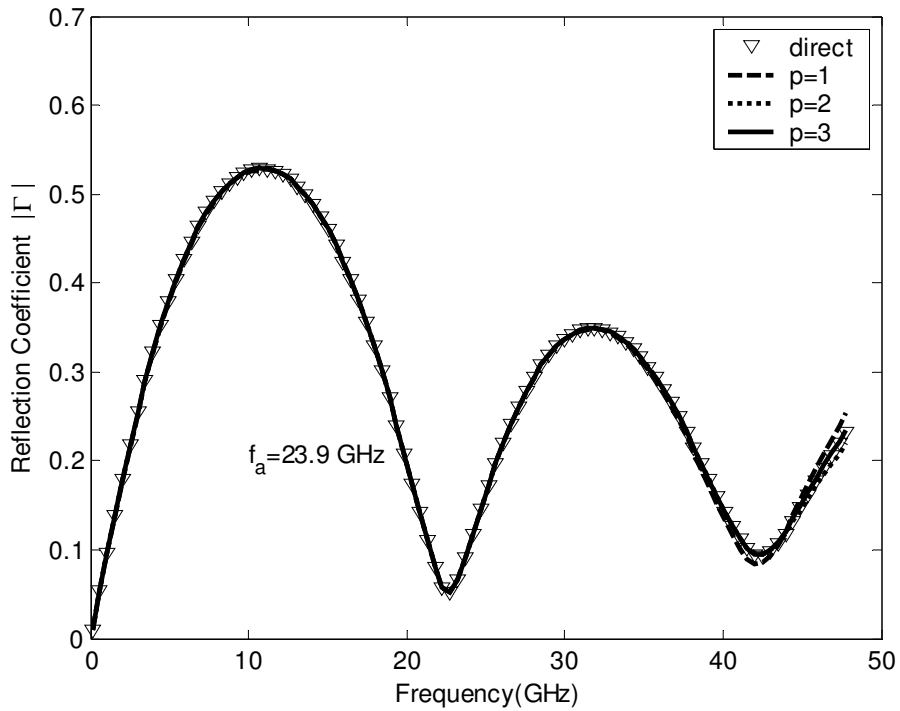
Fig. 4.6 Specular TM reflection coefficient of the periodically implanted five layer dielectric structure. The geometry is given in Fig. 4.5.

The AWE approximation can also be used to calculate angular response of the reflection coefficient. For this purpose the frequency is fixed and equivalent currents are approximated in terms of incidence angle as:

$$I(\theta) \cong \frac{a_0 + a_1(\theta - \theta_a) + \dots + a_p(\theta - \theta_a)^p}{1 + b_1(\theta - \theta_a) + \dots + b_q(\theta - \theta_a)^q} \tag{4.31}$$

73

To calculate the coefficients at this time, the derivatives with respect to incidence angle should be calculated at the expansion point. With the computer package that are used in this study it is an easy task and only thing that should be done is to indicate the differentiation variable.

In Fig. 4.7 the TM reflection coefficient at f=9 *GHz* is plotted versus incidence angle. All parameters of the structure are same as the previous examples. The currents are approximated at θ_a=45° and results are obtained for approximation orders p=1,2,3. As seen from the figure even with first order approximation a good matching is obtained, especially after 45°. However the agreement is not perfect between 0° and 45°. The reason is the fast variation of the reflection coefficient at the expansion point. To obtain a perfect agreement higher order approximations can be used but this slows down the operation of the program. For this reason the expansion point is changed to θ_a=0° and reflection coefficient is calculated again.
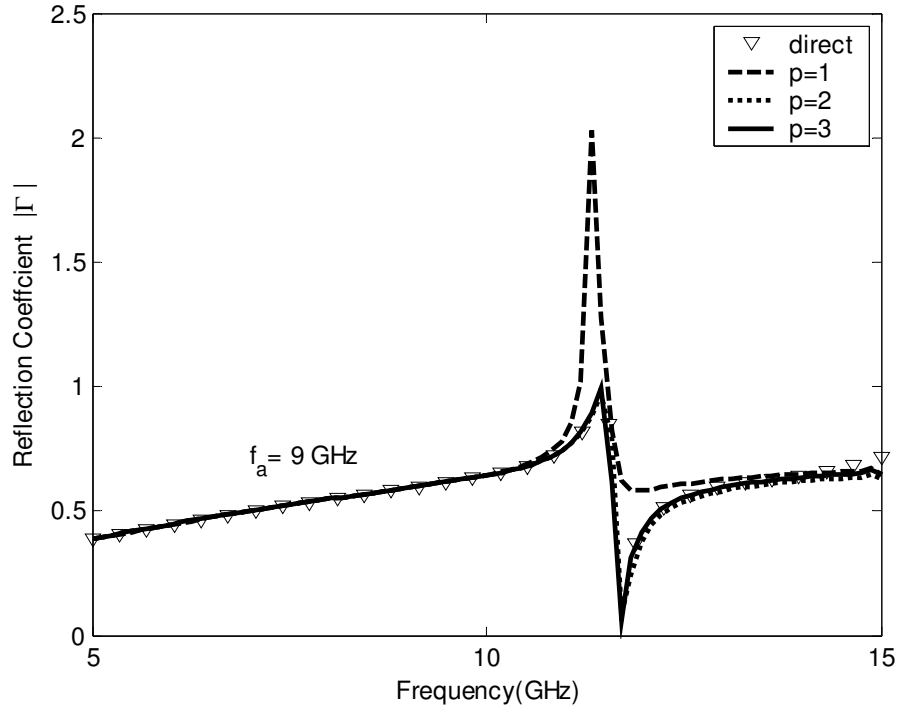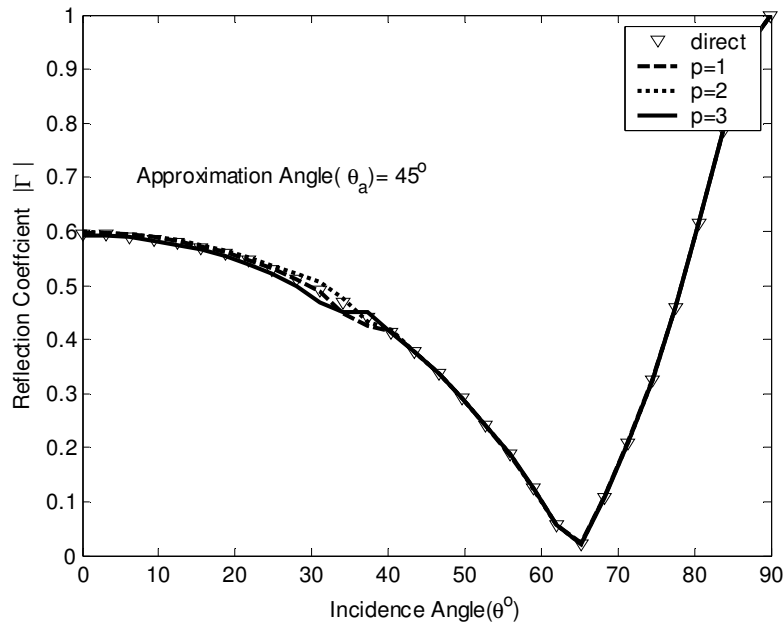

Fig. 4.7 Specular TM reflection coefficient of the periodically implanted dielectric slab versus incident angle, ε_s=4, ε_e=10, a=b=2 *cm*, L=W=1 *cm*, h=T=0.2 *cm*, f=9 *GHz*, θ_a=45°

74

Fig. 4.8 shows the reflection coefficient obtained using $\theta_a=0^o$. As seen from the figure for this case first order approximation is sufficient and perfect agreement is obtained. The structure is symmetric therefore there is no need to calculate results for scan angles -90°-0° range and it can be said that using first order AWE approximation, full angular response of the structure can be obtained. Since full scan angles are between -90^0 and 90^0, 0^0 is the midpoint of the interested range, therefore better results are obtained for this expansion point.
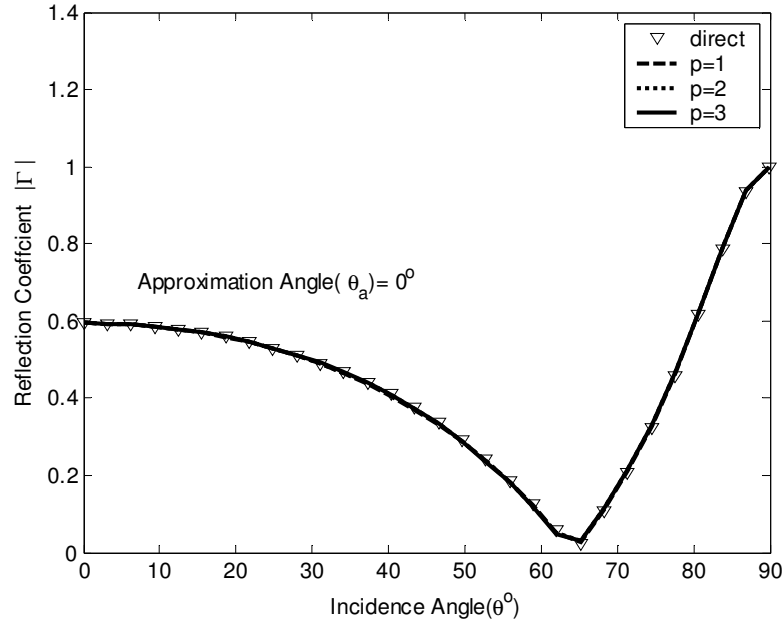
Fig. 4.8 Specular TM reflection coefficient of the periodically implanted dielectric slab versus incident angle. The parameters are same as in Fig 4.7 except, $\theta_a=0^o$.

In this study our motivation in implementing AWE method in the analysis of PBG structures was to reduce the computation time. Table 4.1 shows the computation times for different number of Floquet modes(Nf). As seen from the table the AWE method has a very short current computation time but a long derivative computation time. When the derivatives are obtained, AWE calculates

the reflection parameters very fast, because the computation time of current is almost zero. However long computation times devoted for the computation of derivatives decrease the efficiency of the method. If the reflection coefficient will be calculated for a few number of sample points, the direct method is faster than AWE method. But if the reflection coefficient should be calculated at many points AWE is a more efficient method. For our case if results at more than 1793.99/21.39=84 points are necessary, AWE calculates the reflection coefficient in a shorter time. In general, to accurately characterize the reflection coefficient around resonance, more than 100 points are necessary. Consequently, we can say that AWE is an efficient method for analyzing such structures.

Table 4.1 Computation times for reflection coefficient, $M_x=M_y=M_z=3$

Computation Times(s)	Direct		AWE	
	Nf=529	Nf=2025	Nf=529	Nf=2025
Current Calc. Time	5.09	21.39	~0	0.02
Ref. Coeff. Calc. Time	12.468	51.945	12.448	50.593
Derivative Calc. Time			413.795	1793.99

The efficiency of the AWE method can be increased by decreasing derivative computation times. The alternative techniques will be searched to compute derivatives in a shorter time.

4.6   Determination of Dispersion Relations Using AWE

As it is explained in the previous chapter the MoM solution of the periodic structures results in a matrix equation in the form of:

$$[J][Z] = 0 \qquad\qquad (4.32)$$

The nontrivial solution of this equation exists, if the determinant of the characteristic matrix is zero. Therefore the propagation constant of the structure is obtained by setting the determinant of the characteristic equation to zero.

$$\det\{[Z]\} = 0 \tag{4.33}$$

The propagation constant which gives zero determinant value is obtained using direct search techniques. This is a time consuming process and requires the calculation of characteristic equation at every search points. Typically 200 number of points should be searched to find the points where the determinant is zero.

At this point, the Pade approximation can be used to determine propagation constants. For this purpose firstly, the entries of the Z matrix is approximated in the form of Pade polynomials as:

$$Z_{ij} \cong \frac{a_0 + a_1(\beta - B_a) + \ldots + a_p(\beta - \beta_a)^p}{1 + b_1(\beta - \beta_a) + \ldots + b_q(\beta - \beta_a)^q} \tag{4.34}$$

When the entries of the Z matrix are written as a ratio of two polynomials the searching for zero determinant value can be performed in a second, because of the simplicity of the expression.

It should be noted that to calculate propagation constant this time the characteristic matrix is approximated not the current. To be able to calculate propagation constant accurately, the Pade approximation should accurately represent the determinant of the matrix. To verify, this, the determinant is calculated by using Pade approximation and approximate results are compared to direct calculation results.

In Fig. 4.9 the real part of the determinant is plotted with respect to the phase constant in $\hat{x}$ direction for a grounded slab with implanted air blocks. The approximation is performed at $\beta_x/k_0 = 1.4377$ for orders $p = 1, 2, 3$. As seen from the figure, when the third order approximation is used a perfect agreement is obtained. This figure implies that the characteristic matrix can be approximated through Pade approximation and the zero determinant values can be searched using this approximation to calculate propagation constants. In the figure the determinant is plotted for the range $\beta_x/k_0 = 1 - 1.9377$. Because the lower limit corresponds to k_0 (light line) and upper limit corresponds to Brillouin zone (π/a). After Brillouin zone, due to the periodicity of the structure, same behavior is observed. Below k_0 the surface waves becomes leaky waves.
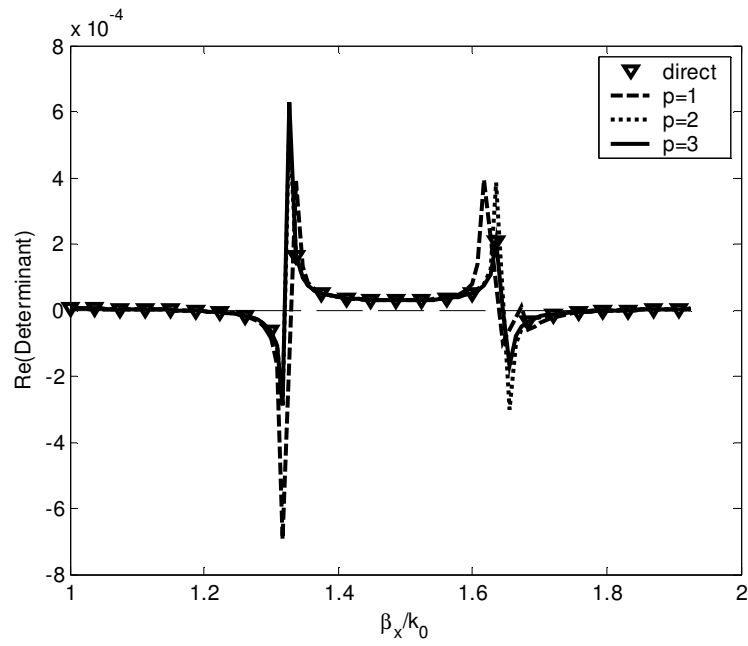
Fig. 4.9 The real part of the determinant versus β_x/k_0 calculated for the grounded slab with implanted periodic material blocks, $\varepsilon_s=10$, $\varepsilon_e=1$, $a=b=5$ mm, $h=2$ mm, $W=3$ mm, $L=2.5$ mm, $T=0.5$ mm, $z_0=1.5$ mm, $f=15.5$ GHz.
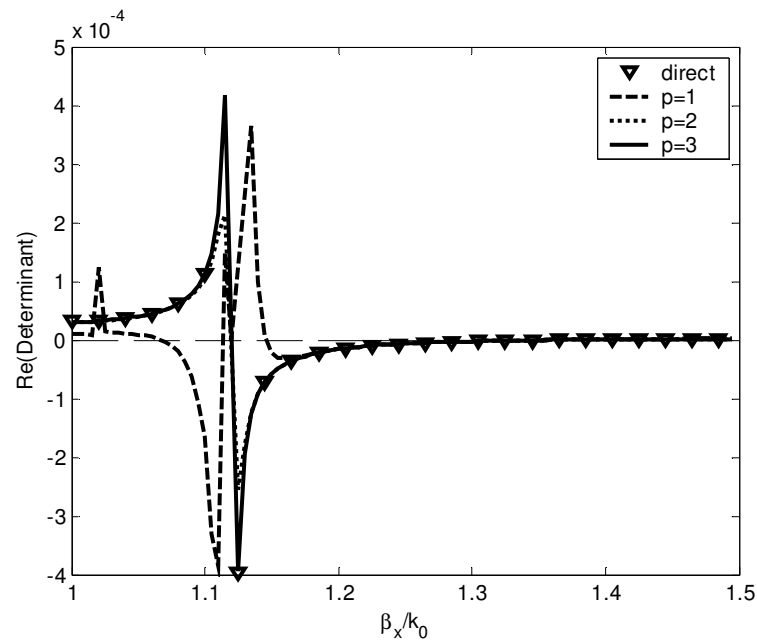
Fig. 4.10 The real part of the determinant versus β_x/k_0 calculated for the grounded slab with implanted periodic material blocks, all parameters are same with the previous figure except, $f=20$ GHz.

78

In the calculation of band diagrams only the propagation constants of the surface waves are important in order to observe the bandgaps so there is no need to calculate propagation constants below k_0. However if the propagation constants below k_0 are needed, another approximation should be performed using an expansion point in this region, because the Green's function has a singularity at k_0 and the function is not analytic. In Fig. 4.10 the real part of the determinant versus phase constant is plotted for $f=20$ *GHz*. As in the previous figure, the determinant is perfectly matched when third approximation is used.

If the Pade approximation is applied directly to the characteristic matrix, the propagation constant in the structure can be obtained by searching the point where minimum singular value of the matrix is zero, using a direct search algorithm. Using Pade approximation very fine scanning is possible because there is no need to calculate characteristic matrix each time. However, the extraction of roots is not easy using a direct search algorithm because the variation of the singular value is not well defined. Especially when the roots are closely spaced it is difficult to decide whether there are two distinct roots or not without human intervention. A more robust method for the extraction of roots is possible by applying Pade approximation to the inverse of the characteristic matrix instead of the matrix itself. From the basic linear algebra the inverse of the matrix is given by:

$$Z^{-1} = \frac{adj(Z)}{\det Z} \tag{4.35}$$

From (4.35) it is seen that when the determinant of the matrix is zero each term in Z^{-1} goes to infinity. This condition is satisfied if the denominator of the Pade approximant of Z^{-1} equal to zero. This means that the propagation constant in the structure can be obtained by extracting the poles of the Pade approximant of Z^{-1}. The Pade approximation of Z^{-1} can be obtained using the same procedure used to obtain the approximation of equivalent currents in the structure. This time there is no incident field and therefore voltage matrix, [V], is set to identity matrix. The poles are extracted by computing the roots of the denominator polynomial. There are robust and well defined polynomial root finding techniques based on the solution of an eigenvalue problem [53]. Therefore extracting the poles of the Pade

approximant is more easy and robust than searching the point that makes the determinant zero.

To demonstrate the accuracy of the method the inverse of the characteristic matrix of sample geometry is approximated and the poles are extracted. Table 4.2 shows the extracted poles for the sample geometry. The frequency of operation is 15.5 GHz. The approximation is performed at the midpoint of the interested range ($\beta_x / k_0 = 1.4377$). In Table 4.2 there are six distinct roots. The imaginary parts of these roots are very close to zero this means that they represent the propagating waves. Among these roots five of them are closely spaced and the distance between these roots are less than 0.004%. As a result we can say that there are two propagating modes in the structure with phase constants are given as $1.8318k_0$ and $1.1652k_0$. The propagation constants that are obtained through direct calculation procedure without making any approximations are $1.8321k_0$ and $1.1654k_0$. If the Pade approximation is directly applied to Z and zero minimum singular value is searched these propagation constants are found as $1.8321k_0$, $1.1652k_0$.

Table 4.2 Poles of the Pade approximant of Z^{-1}. All parameters for the geometry are same as in Fig. 4.9. $M_x=M_y=1$, $M_z=3$. The poles are given in terms of k_0.

0.6968+0.0431i	2.0673-0.0224i	1.8311+0.0020i
0.6983+0.0458i	2.0668-0.0239i	1.8311+0.0020i
0.7003+0.0488i	2.0661-0.0253	1.8312+0.0020i
2.7524+0.0038i	0.6247-0.0031i	1.1652-0.0000i
2.7529+0.0042i	0.6299-0.0035i	1.1652-0.0000i
2.7536+0.0047i	0.6360-0.0039i	1.1652-0.0000i
0.4485+0.0089i	2.1657+0.0466i	1.8364-0.0022i
-5.3428-2.3517i	2.0441-0.0109i	1.8318-0.0005i
0.8214+0.0662i	1.9620-0.0136i	1.8251+0.0043i

In Fig. 4.11 the propagation constant in $\hat{x}$ direction is plotted with respect to frequency using Pade approximation. The structure parameters are same as the previous example. To obtain the results with Pade, two approximation points are used. The propagation constant above light line is calculated by approximating the characteristic matrix at $(\pi/a+k_0)/2$ that is the midpoint of the range between Brillouin zone and dashed line. To calculate the propagation constant below light line the matrix is approximated at $k_0/2$. As seen from the figure Pade approximation gives accurate results.
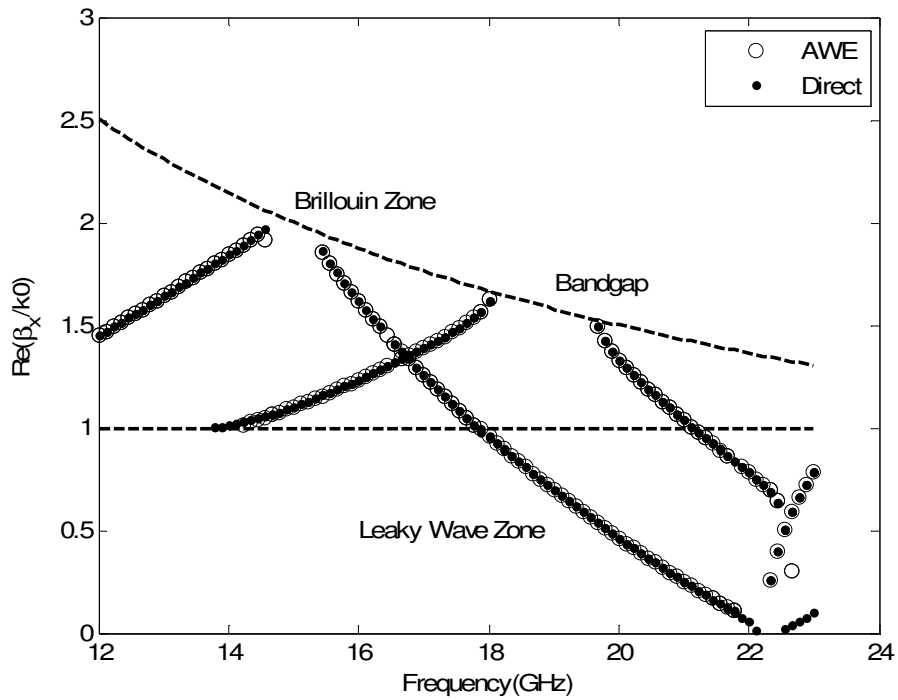
Fig. 4.11 Dispersion diagram for modes in the grounded slab with implanted periodic material blocks, $\varepsilon_s=10$, $\varepsilon_e=1$, $a=b=5$ mm, $h=2$ mm, $W=3$ mm, $L=2.5$ mm, $T=0.5$ mm, $z_0=1.5$ mm.

Table 4.3 shows the computation times required to find all roots at $f=16$ GHz. The computation times are listed for different number of Floquet modes. In AWE method, most of the computation time is devoted to the calculation of derivatives. The computation time for finding the roots are very small, in the order

of 3-5 s. As seen from the table AWE is four times faster than direct calculation method, but this depends on the number of scan points that is necessary to extract all roots. In this case 200 number of points are scanned, but in same cases with closely spaced roots more than 200, about 1000, scan points are required. For such cases, superiority of AWE becomes more clear, because as the number of evaluation points is increased, the computation time required for the direct method increases proportionally whereas the time for AWE does not change.

Table 4.3 Computation times required to calculate propagation constants at f=16 *GHz*. M_x=M_y=M_z=3.

	Direct		AWE	
	Nf=529	Nf=2025	Nf=529	Nf=2025
Computation Times(s)	1878.13	7058.67	433	1368.92

4.7   Conclusions

In this chapter the use of AWE/Pade approximation techniques in the analysis of structures with periodic implants has been presented. It has been shown that using AWE technique the fast parameter sweep is possible without losing the accuracy. The difficulty in the application AWE to such structures lies behind the computation of high order derivatives of the complicated kernel function which includes the expressions of Green's functions for multilayer media. The automatic differentiation theory has been used to compute these derivatives. The theory is an efficient and versatile method for computing high order derivatives exactly. It has been shown that automatic differentiation theory can be confidently used in the solution of advanced electromagnetic problems whenever higher order derivatives of complicated functions with conditional branches are required. In this study one dimensional AWE procedure is used. The automatic differentiation theory enables the computation of partial derivatives

with respect to several variables. Two dimensional AWE procedure can be applied to the periodic structures for fast sweep of two parameters, such as frequency and incidence angle, which is considered as a future work.

CHAPTER 5

MOM ANALYSIS OF MICROSTRIP LINES ON ELECTROMAGNETIC BANDGAP SUBSTRATES

5.1   Introduction

The dimensions and weight are two important parameters that play a leading role in the design of microstrip antennas for mobile communication systems. In order to reduce the weight and dimensions of the antenna, dielectric substrates with high permittivity are preferred. On the other hand when an antenna is placed substrate with high dielectric constant some power may couple into the substrate because of the surface waves resulting in radiation inefficiency. EBG substrates prevent the excitation of surface wave modes and offer a real solution to this problem. When they are used as antenna substrates they increase the radiation efficiency and eliminate the spurious radiation [14]. EBG substrates are also used at the input stage of an antenna to suppress unwanted harmonics and improve return loss. Such a microstrip circuit is formed by placing a microstrip line on an EBG substrate [68].

Traditionally the microstrip structures on EBG substrates are simulated using commercial 3-D electromagnetic simulation packages like HFSS. In such an analysis EBG substrates are modeled with the inclusion of finite number of periodic material blocks into the substrate. Typically 3-5 cells are used to model substrates [10]. The simulation of microstrip structures on EBG substrates that are periodic with infinite number of cells is not possible with such simulation packages because these software packages cannot analyze aperiodic structures on periodic substrates.

The analysis of microstrip structures on periodic substrates is difficult, because the problem cannot be reduced to single unit cell as opposed to analysis of periodic materials. The MoM solution of microstip lines on artificial periodic substrates is firstly proposed by Yang [38]. In this method first the microstrip line is divided into segments. To calculate the interaction between the segments and the dielectric material blocks, the volume equivalent currents in the substrate should be calculated. Due to aperiodic nature of the problem the volume equivalent currents cannot be calculated directly. Instead of solving the problem directly, first the volume equivalent currents in the structure are calculated when the structure is excited by infinite phased array of microstrip segments. For this case the problem is periodic and the MoM solution of volume equivalent currents can be obtained through volume integral equation. After obtaining these equivalent sources, the field due to the array of segments is calculated. To calculate the electric field created by one segment of the microstrip structure, array scanning method (ASM) [69] is used to transform fields. In the second stage, electric field due to each microstrip segment is used to obtain the current distribution on the microstrip line through electric field integral equation and spectral domain MoM technique. To find the propagation constant of the microstrip line the determinant of characteristic matrix that is obtained in the second stage is equated to zero. In this method two integral equations, namely volume integral equation and electric field integral equation are solved simultaneously and therefore it is called as double-vector-integral equation method (DOVIE).

The DOVIE method is computationally expensive and unpractical. The reason is the double infinite Floquet mode summations and Fourier integrals that arise in the formulation. The Fourier integrals that arise in the formulation cannot be calculated analytically due to iterative nature of the method and by this reason they are calculated through a numerical integration procedure resulting in a computationally inefficient procedure. The calculation of Floquet series and Fourier integrals should be repeated for each microstrip segment, which makes the method prohibitively slow.

As an alternative to DOVIE method, if the electric field Green's functions for a dipole on EBG substrate can be obtained by some means, the fast analysis of microstrip line can be achieved as if the substrate is homogenous. At this point the question is: "How can we calculate the Green's functions for EBG substrates?"

In this chapter an alternative method to DOVIE that is developed to analyze microstrip lines on EBG substrates will be explained. The chapter starts with this introduction section. In Section 5.2 the developed analysis technique is formulated. The results and discussions are given in Section 5.4. This chapter ends with the conclusion, Section 5.4.

5.2   The Analysis Technique

The microstrip line on the EBG substrate is shown in the Fig. 5.1. The multilayered dielectric substrate is implanted periodically with material blocks that have dielectric constant different than the dielectric constant of the host substrate. The width of the microstrip line is, w and it is assumed to be narrow, such that only longitudinal currents flow on the line.
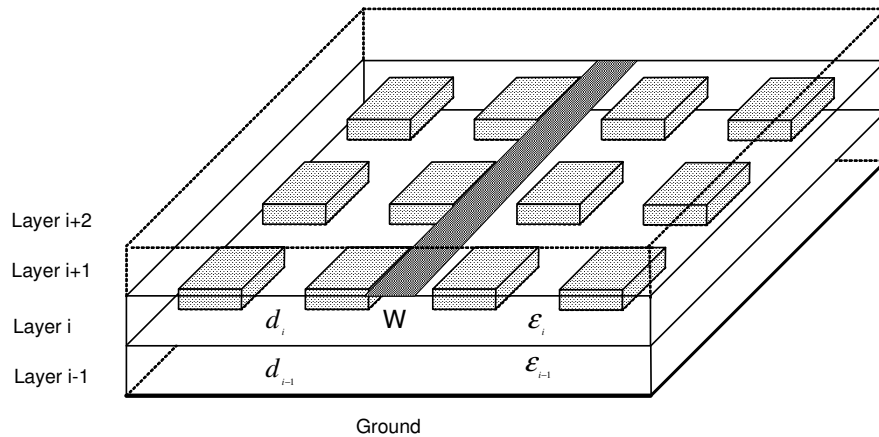
Fig. 5.1 Microstrip line on EBG substrate

The idea to calculate the propagation constant is simple. In the first stage the full set of electric field Green's function for the periodically implanted substrate is

86

calculated. Then using these Green's functions the propagation constant of the microstrip line is calculated as if the substrate is homogenous. To implement the idea first the Green's functions for the periodically implanted substrate should be calculated by some means.

Recall that, the spectral domain expression of the electric field Green's functions are derived using the spectral decomposition technique [37]. In the derivation, first the field radiated from an infinitesimal dipole is decomposed into plane waves through Weyl identity [41] and an equation is formulated that relates the plane waves going in upward direction to plane waves going in downward direction as [37]:

$$E_z = \frac{Il}{8\pi^2 \omega \varepsilon} \int\limits_{-\infty}^{\infty} \int\limits_{-\infty}^{\infty} dk_x dk_y e^{-jk_x(x-x')} e^{-jk_y(y-y')} F_{TM}(z, z') \tag{5.1}$$

where,

$$F_{TM}(z, z') = \pm e^{-jk_z|z-z'|} + B_h^e e^{-jk_z(z-z')} + D_h^e e^{jk_z(z-z')} \tag{5.2}$$

The coefficients of the plane waves going in upward and downward directions are obtained by imposing the boundary conditions. As a result the spectral domain Green's functions are obtained in the form of:

$$\widetilde{G}_{xx}^E = \frac{-1}{2\omega\varepsilon k_\rho^2 k_{zi}} \begin{bmatrix} (k_x^2 k_{zi}^2 + k_y^2 k_i^2) e^{-jk_{zi}|z-z'|} \\ + (k_y^2 k_i^2 \widetilde{R}_{TE}^{i,i+1} M_i^{TE} - k_{zi}^2 k_x^2 \widetilde{R}_{TM}^{i,i+1} M_i^{TM}) e^{jk_{zi}(z+z'-2d_i)} \\ + (k_y^2 k_i^2 \widetilde{R}_{TE}^{i,i+1} \widetilde{R}_{TE}^{i,i-1} M_i^{TE} + k_{zi}^2 k_x^2 \widetilde{R}_{TM}^{i,i+1} \widetilde{R}_{TM}^{i,i-1} M_i^{TM}) e^{jk_{zi}(z-z'-2d_i)} \\ + (k_y^2 k_i^2 \widetilde{R}_{TE}^{i,i-1} M_i^{TE} - k_{zi}^2 k_x^2 \widetilde{R}_{TM}^{i,i-1} M_i^{TM}) e^{-jk_{zi}(z+z')} \\ + (k_y^2 k_i^2 \widetilde{R}_{TE}^{i,i+1} \widetilde{R}_{TE}^{i,i-1} M_i^{TE} + k_{zi}^2 k_x^2 \widetilde{R}_{TM}^{i,i+1} \widetilde{R}_{TM}^{i,i-1} M_i^{TM}) e^{-jk_{zi}(z-z'+2d_i)} \end{bmatrix}$$

$$\tag{5.3}$$

where $\widetilde{R}_{TE,TM}$ are generalized reflection coefficients. Different from the Fresnel reflection coefficients, the generalized reflection coefficients account for the multiple reflections from the multilayered structure.

Let's consider the infinitesimal dipole on EBG substrate. Similar to the previous case, the decomposed plane waves going in downward direction are reflected from the substrate and continue their way in the upward direction. For

87

this case the substrate is not homogenous and there are periodic material gratings. Therefore, the scattered field at the interface will not be a single plane wave. On the contrary, the field at the interface will be composed of infinite number of Floquet modes. However the major contribution comes from the fundamental Floquet mode. With this assumption the fundamental Floquet mode can be used to calculate reflection coefficient at the interface. The assumption is valid when the periodicity of the structure is large and implanted elements are small compared to wavelength. With this assumption the Green's function expression obtained for the EBG substrate is same as the homogenous substrate but for this case the generalized reflection coefficients should be replaced by the reflection coefficients of the EBG substrate. The reflection coefficients can be obtained through 3-D MoM procedure as explained in the previous chapters. The Green's functions are obtained by replacing the generalized reflection coefficients with the calculated reflection coefficients. The resulting Green's function approximates electric field of the infinitesimal dipole on the periodic structure.

Using these Green's functions the propagation constant of the microstrip line could be calculated using the spectral domain MoM procedure as if the substrate is homogenous.

5.3 Calculation of Propagation Constant of Microstrip Line Using Spectral Domain Approach (SDA)

The propagation constant of a microstrip line can be calculated in the spectral domain or the spatial domain. There are several methods in literature proposed to calculate dispersion characteristics of microstrip lines [70]-[73].

An alternative computationally efficient spatial domain approach is proposed during this study and the details of the proposed method are presented in Appendix-C. However the developed procedure requires spatial domain Green's functions that are expressed in terms of complex images through the use of Generalized Pencil of Functions (GPOF) method. Recall that the reflection coefficient of the periodic structure involves some sharp variations at frequencies corresponding to bandgap of the structure. These sharp variations may cause some

numerical problems during the calculation of spatial domain Green's functions in terms of complex images. Consequently, the more robust spectral domain approach presented in [70] is chosen to be implemented in this study. This well-known procedure is summarized here for the sake of completeness.

Consider the microstrip line on uniform substrate as shown in Fig. 5.2. Assume that the width of the line is small so that there is only $\hat{y}$ directed current and the effect of $\hat{x}$ directed current is negligible.
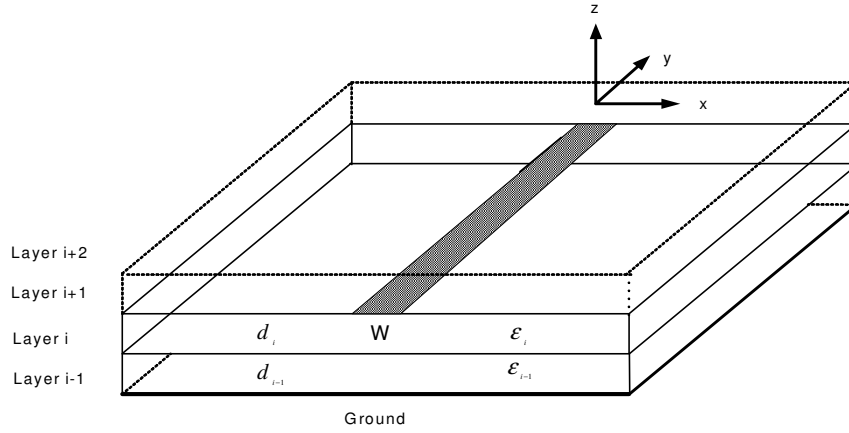
Fig. 5.2 Microstrip line on uniform substrate

The current on the conductor can be written as:

$$J_y(x, y) = \sum_{m=1}^{M} I_{ym} B_m(x) e^{-j\beta_{y0} y} \tag{5.4}$$

where $B_m(x)$ is the basis function. The Fourier transform of the current is given by:

$$\tilde{J}_y(k_x, \beta_y) = \sum_{m=1}^{M} I_{ym} \tilde{B}_x(k_x) e^{-jk_x x_m} \delta(\beta_y - \beta_{y0}) \tag{5.5}$$

The Fourier transform of the electric field is written as:

$$\tilde{E}_y(k_x, \beta_y, z) = \sum_{m=1}^{M} I_{ym} \tilde{B}_x(k_x) e^{-jk_x x_m} \delta(\beta_y - \beta_{y0}) \tilde{G}_y^E(k_x, \beta_y, z, z') \tag{5.6}$$

89

By taking the inner product integral with the Fourier transform of the testing function we obtain:

$$\left\langle \tilde{T}_{xn}^*, \tilde{E}_y \right\rangle = \int\limits_{-\infty}^{\infty} \sum_{m=1}^{M} I_{ym} \tilde{B}_x(k_x) \tilde{T}(k_x) e^{-jk_x(x_m-x_n)} \tilde{G}_y^E(k_x, \beta_{y0}, z, z') dk_x \qquad (5.7)$$

Using the Galerkin's method the matrix entries can be written as:

$$Z_{nm} = \int\limits_{0}^{\infty} \sum_{m=1}^{M} I_{ym} \tilde{B}_x^2(k_x) \tilde{G}_y^E(k_x, \beta_{y0}, z, z') e^{-jk_x(x_m-x_n)} dk_x \qquad (5.8)$$

Using the even symmetry of the imaginary part of the exponential function, (5.8) can also be written as:

$$Z_{nm} = \int\limits_{0}^{\infty} \sum_{m=1}^{M} I_{ym} \tilde{B}_x^2(k_x) \tilde{G}_y^E(k_x, \beta_{y0}, z, z') Cos(k_x(x_n - x_m)) dk_x \qquad (5.9)$$

To calculate the propagation constant, β_y value that makes the determinant of the characteristic matrix zero, is searched using a line search algorithm such as bisection method [53].

The indefinite integral in (5.9) can be calculated numerically using Simpson's rule or Gaussian quadrature method. To avoid the singularities associated with the surface wave poles of the structure the following integration path is used for integration:
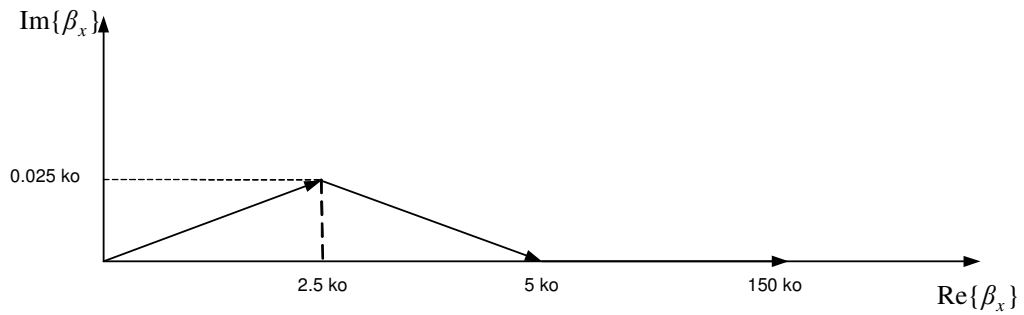
Fig. 5.3 Integration path on k_x

5.4 Calculation of Propagation Constant of Microstrip Line on EBG Substrate

To calculate the propagation constant of a microstrip line on EBG substrate the following algorithm that implement the proposed method is used:

1. Take an initial value for the phase constant as, $\beta_y = \beta_{y0}$ according to line search algorithm. As a line search algorithm bisection method is used.

2. Determine the quadrature points on the integration path in terms of k_x. For each k_x value, calculate the angle of incident wave as follows:

$$\phi = \tan^{-1}(\frac{\beta_y}{k_x})$$

$$\theta = \sin^{-1}(\frac{k_x}{k_0 \cos\phi})$$

   For each incident angle (may be complex as well) TE and TM reflection coefficients are calculated through 3-D MoM procedure. To calculate the reflection coefficients only the fundamental Floquet mode is taken into account.

3. Substitute calculated reflection coefficient values into the Green's function and find the characteristic matrix, Z.

4. Calculate the determinant. If $Det\,|\,Z\,| \ne 0.0$ chose another β_y and repeat the procedure.

5.5 Results and Discussions

The implementation of the SDA method is verified by calculating the propagation constant of a microstrip line on a uniform substrate and comparing the results with the literature. As seen from Table 5.1 the results are in good agreement with literature and error is below 1%. In the calculations only one basis function is used. The accuracy can be increased using more basis functions.

Table 5.1 Calculated propagation constants of a microstrip line with, ε_s=8, (w/h)=1.

h/λ	ε_{eff} (Simpson's Rule)	ε_{eff} (Gauss's Quad.)	ε_{eff} [73]
0.005	5.43808	5.4424	5.467
0.05	6.08747	6.0796	6.122
0.1	6.7029	6.7799	6.75
0.3	7.6535	5.77	7.66

After the verification of the SDA procedure, the behavior of the reflection coefficients is inspected, because the functionality of the proposed method strongly depends on the correct calculation of the reflection coefficients. To verify that the reflection coefficients are calculated correctly for all k_x values a slab with a fill ratio equal to 1 is considered. The reflection coefficients are calculated for a sample slab using 3-D MoM procedure for different k_x values and compared with the generalized reflection coefficients calculated for the homogenous slab. The dielectric constant of the slab is $\varepsilon_s = 10$. The thickness of the slab is $h = 1mm$. The implanted material block sizes are $L = W = 3mm$ with a dielectric constant $\varepsilon_e = 2$. The cell sizes are $a = b = 3mm$. The substrate is actually a uniform substrate with $\varepsilon_s = 2$. The comparison of reflection coefficients are given in Fig. 5.4 and Fig. 5.5 for TM and TE cases, respectively. To obtain these figures the implanted cells are divided into 27 unit boxes and 529 number of Floquet modes is used. As seen from the figures the reflection coefficients are in perfect agreement up to $3k_0$, and after this point the small deviations are observed. The difference increases as k_x increases. However the major contribution to the integral given in (5.8) comes from the lower k_x values and the deviations at high

k_x values do not have considerable effect on the calculation of impedance matrix and propagation constant.

Fig. 5.6 plots the TM reflection coefficients versus k_x for different fill ratios, where the fill ratio is defined as the ratio of the volume of the implanted blocks to the volume of the unit cell. The slab is same with the slab used in the previous example. When the fill ratio is one the effective dielectric constant of the slab is 2. As the fill ratio decreases the effective dielectric constant of the slab increases. The increase in effective dielectric constant increases the reflection coefficient as observed in the magnitude plot.
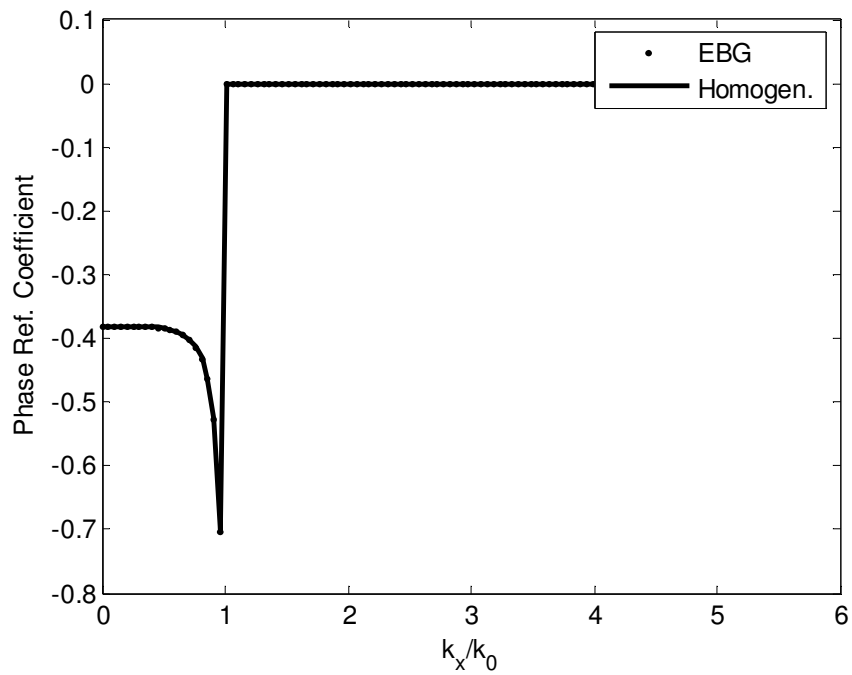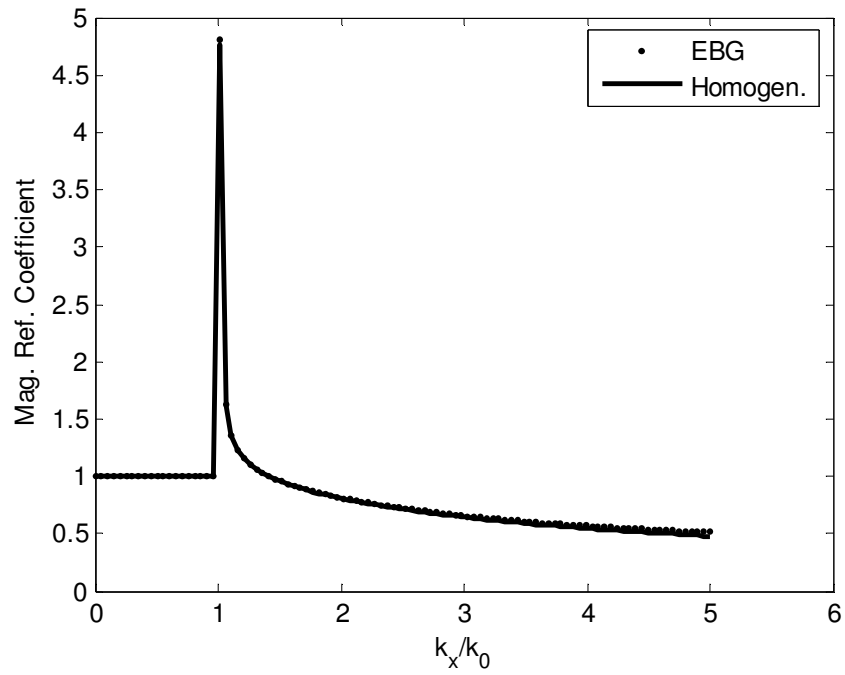
Fig. 5.4 The comparison of TM reflection coefficients calculated for the slab with fill ratio equal to one.
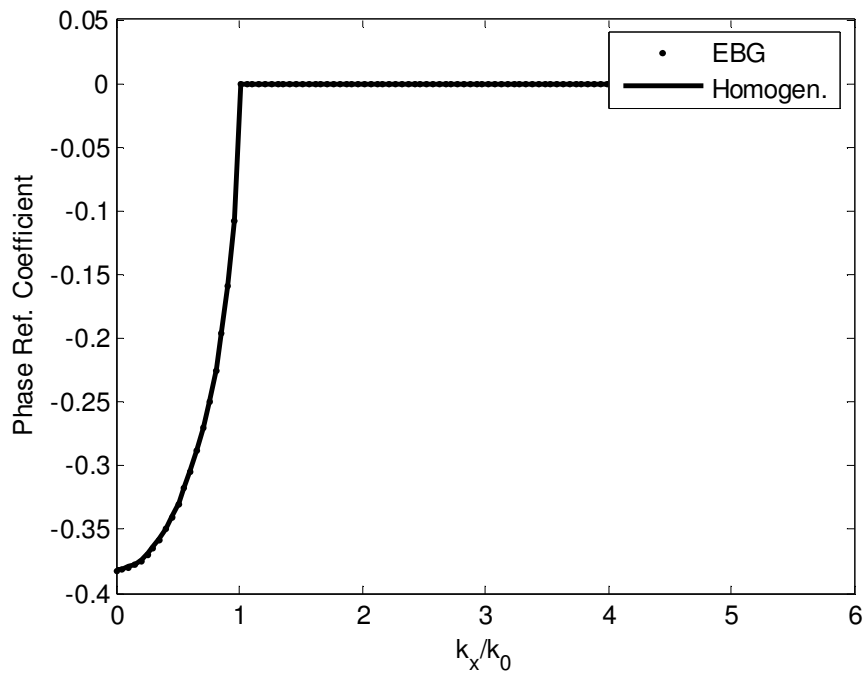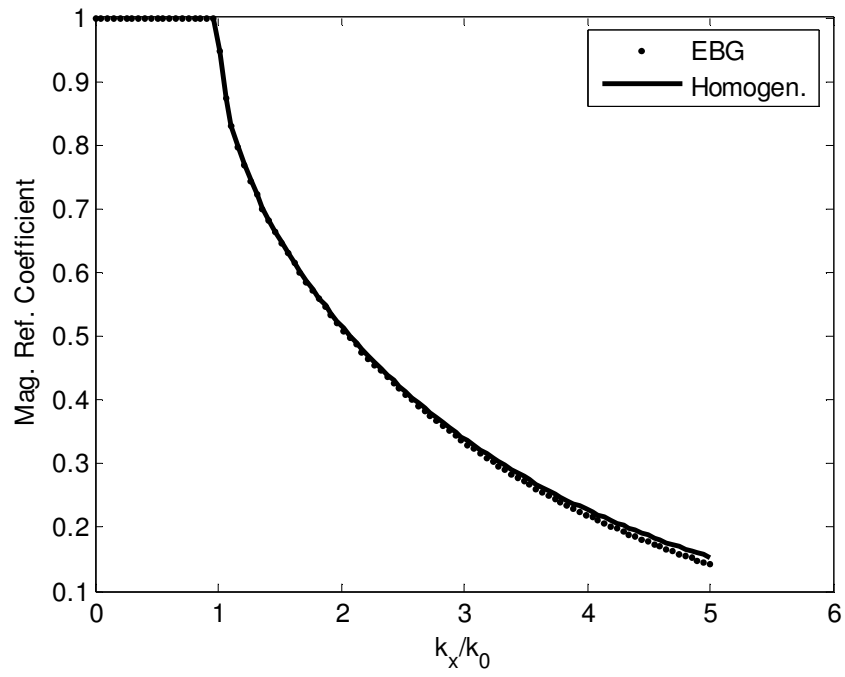
Fig. 5.5 The comparison of TE reflection coefficients calculated for the slab with fill ratio equal to one.
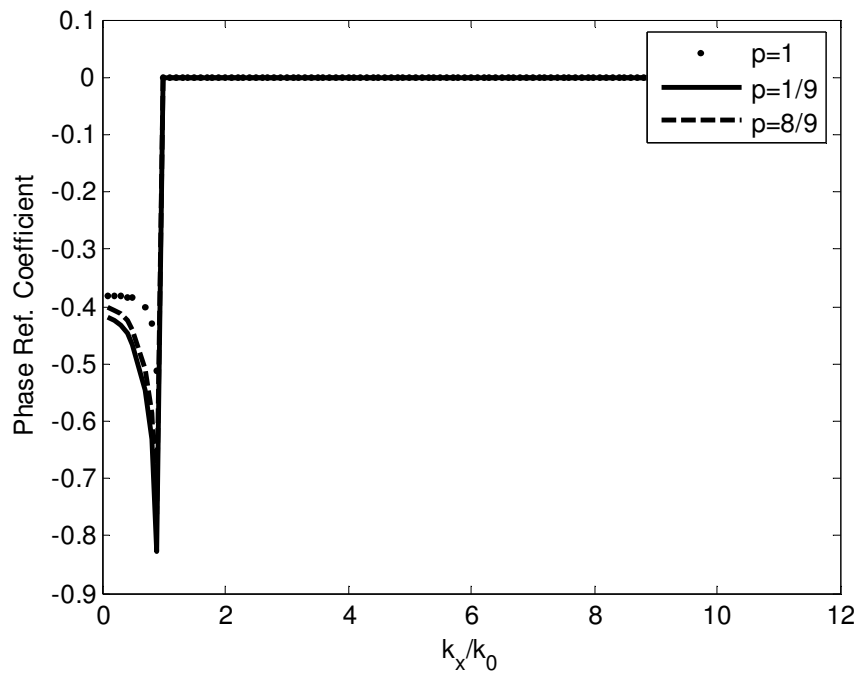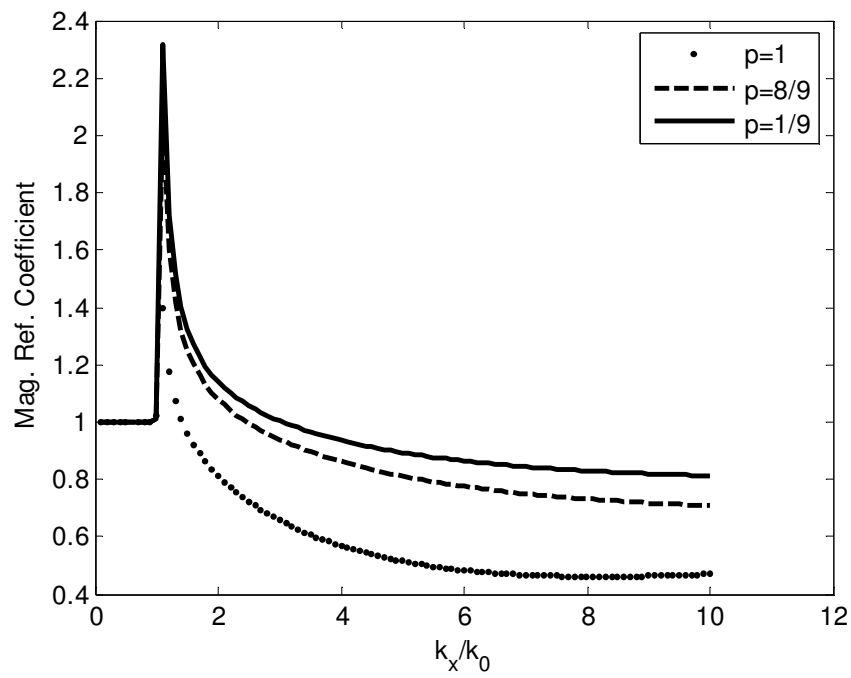
Fig. 5.6 TM reflection coefficients calculated for periodically implanted substrate with different fill ratios (*p*)

After it is seen that the reflection coefficients are calculated correctly, the proposed method is verified using a microstrip line on a periodic substrate. When the fill ratio is 1, the substrate is actually homogenous substrate with dielectric constant equal to the dielectric constant of the implanted cell. This enables the verification of the procedure with the SDA approach. Therefore in the first example, the fill ratio is chosen to be 1. Table 5.2 lists the propagation constant calculated for a sample microstrip line on multilayered EBG substrate with a fill ratio equal to 1. The microstrip line is 1mm wide and the substrate parameters are:

$a=L=3mm$, $b=W=3mm$, $T=0.5mm$, $h=1\ mm$, $z_0=0.0\ mm$, $\varepsilon_s = 4$, $\varepsilon_e = 10$

The substrate is essentially a two layer structure with top layer $\varepsilon = 4$ and bottom layer $\varepsilon = 10$ and each has a thickness of 0.5 mm. The propagation constant calculated using DOVIE method [38] and SDA are also given in the table for comparison. As seen from the table the agreement with the DOVIE method is surprisingly perfect. For lower frequencies the results are in coincidence up to three digits. As the frequency increases slight deviations are observed. This observation can be explained with insufficient modeling of equivalent volume currents at high frequencies. The accuracy of the results can be increased by using more basis functions to model the currents.

Table 5.2 The validity check of the calculated of propagation constant.

Freq. (GHz)	Proposed Method	DOVIE [38]	SDA
4	1.887	1.887	1.895
6	1.900	1.899	1.908
8	1.914	1.914	1.923
10	1.930	1.930	1.939
12	1.946	1.947	1.957
14	1.964	1.965	1.975
16	1.980	1.984	1.994
18	1.996	2.003	2.013
20	2.013	2.023	2.033

Fig. 5.7 shows the calculated propagation constant of a microstrip line on periodically implanted substrate with a fill ratio equal to 0.011. In the figure the results are compared with [38] as well as effective medium theory (EMT). In effective medium theory the effective dielectric constant of the periodic substrate is calculated using the following formula [74]:

$$\varepsilon_{eff} = \varepsilon_s \left[\frac{1 + 2p\left(\dfrac{\varepsilon_e - \varepsilon_s}{\varepsilon_e + 2\varepsilon_s}\right)}{1 - p\left(\dfrac{\varepsilon_e - \varepsilon_s}{\varepsilon_e + 2\varepsilon_s}\right)} \right] \tag{5.10}$$

where, p is the fill ratio.
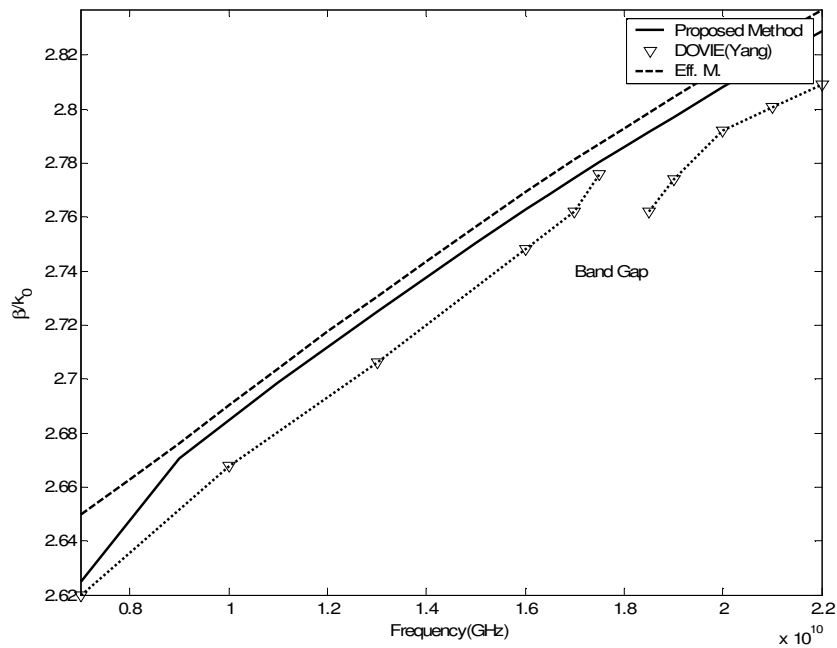
Fig. 5.7 Propagation constant of a microstrip line on periodically implanted substrate. The parameters are ε_s=10, ε_e=2, a=b=3 *mm*, L=W= 0.5 *mm*, h=1 *mm*, T=0.4 *mm*, z_0=0.3 *mm*, w=1 *mm*.

As seen from the figure, propagation constant values obtained by using our procedure are in good agreement with the other results, except the bandgap region. The results that are obtained using our procedure are very close to the results obtained through effective medium theory, which can be attributed to the fact that only the dominant Floquet mode is considered during the calculation of reflection coefficients. Both the proposed method and the effective medium theory assume the single plane wave behavior of the scattered wave at the interface. Therefore similar results are obtained as expected.

The bandgap formation that is observed with the DOVIE method could not be observed with the developed procedure. In the developed procedure to calculate the plane wave reflection coefficients only the fundamental Floquet modes are used. Other Floquet modes are not included in the calculation of reflection coefficients because their k_z values are different than the incident wave. The evanescent waves those are not included in our developed procedure is the reason why bandgap formation is not observed

5.6   Conclusions

Above a MoM procedure has been proposed to analyze a microstrip line on a periodically implanted substrate. The method is based on the idea of calculating the reflection coefficients using 3-D MoM procedure and inserting them into the Green's functions to calculate the dispersion characteristics of microstrip structures. Firstly, the proposed method has been verified using a substrate with a fill ratio equal to 1. Perfect agreement has been observed with the propagation constants calculated using the proposed procedure and SDA. Then a substrate with a fill ratio different than one is considered used and good agreement has been observed with the results found in the literature. The error is smaller than error in the effective medium theory. However the bandgap formation that is reported in the literature has not been observed. On the other hand, the method proposed here is computationally much more efficient than the DOVIE method that accurately predicts the bandgap. As a result it can be said that the proposed calculation

scheme is an alternative to the effective medium theory with more accurate modeling of the periodic substrates

.

CHAPTER 6

CONCLUSIONS

In the first part of the thesis 2-D metal conductors in stratified media has been analyzed using the efficient method of moment technique. Using the method, reflection and transmission characteristics of the structure are calculated in less than 10 s. It has been shown that the method is fast compared to conventional numerical analysis techniques and suitable for optimization. The method has been used to calculate conductor positions to optimize the reflected and transmitted electric fields. The genetic algorithm has been used as an optimization algorithm. As shown in Chapter 2 using 2-D conductors, the reflected and transmitted electric fields at a specified region can be increased or decreased 2-3 times. Such an optimization is useful in the design of backscatterers or leaky wave antennas. Using the method the radar cross section of an object can be reduced by placing 2-D metallic strips on it. The optimization procedure can be easily modified to optimize the radiation pattern and to design directive leaky wave antennas. The method can also be used in the design of superlenses to optimize the electric field at the focal point as shown in the last example of Chapter 2.

In the second part, a 3-D method of moment technique to analyze multilayered structures with embedded dielectric blocks has been presented. Such structures show the electromagnetic bandgap (EBG) material properties and they are used in the design of efficient microstrip antennas, frequency selective layers (FSLs) etc. In the method the volume equivalence theorem has been used to replace dielectric blocks with equivalent currents and method of moment technique has been applied to calculate unknown current coefficients. The full set of dyadic electric field Green's functions for the stratified media are formulated

101

and used. With this form of Green's functions, it is possible to analyze geometries when the dielectric blocks are placed in different layers.

The dispersion characteristics of the structure has been obtained using the method and compared with the literature. It has been shown that the results are in perfect agreement. The determination of the propagation modes in the structure is not an easy task due to odd behavior of determinant of the characteristic matrix. Using minimum singular value of the matrix instead of its determinant, propagation constants can easily be calculated. To obtain the propagation constants in the structure, a hybrid procedure that uses the direct scanning of the spectrum and direct search technique has been developed. Using the procedure the propagation constants has been determined accurately.

The effect of the disretization of the unit cell has been inspected. The discretization in the vertical direction is crucial to reduce the error in the calculation. The discretization in the horizontal plane has not a major role on the accuracy but increases the calculation time. Therefore 3 basis function in vertical direction and 1-2 basis function in horizontal directions are sufficient to calculate dispersion characteristics with an error below 0.5%. The effect of number of Floquet modes used in the calculations has also been inspected. It has been seen that 441 Floquet modes are sufficient to obtain an error below 0.5%. Using the calculated propagation constants the dispersion diagram of the structure is plotted.

The specular reflection coefficient of the structure has also been calculated using the method. The result has been verified by using a sample structure with a fill ratio equal to one. The results are also compared with the literature and it is been seen that they are in perfect agreement. To accurately determine the resonance characteristics, the reflection coefficient should be calculated at more than 200 frequencies.

The 3-D method presented in Chapter 3 is slow to obtain dispersion and reflection characteristics. To extract the characteristics of the structure the parameters should be calculated at many points and this makes the method computationally inefficient. To increase the computational efficiency of the method use of Asymptotic Waveform Evaluation (AWE) method has been

proposed. This is the first application of the AWE method to this problem. AWE method enables to obtain full response of the structure from the calculation at a single point. By this way the dispersion diagrams and spectral/angular response of reflection coefficients can be calculated in a shorter time. The AWE method requires the calculation of high order derivatives of Green's functions. The regular numeric differentiation methods are not suitable to calculate these derivatives. As an alternative, automatic differentiation technique has been used to calculate the derivatives.

Using AWE method frequency response of the reflection coefficient has been obtained. The result has been compared with the result obtained through direct calculation. When the third order AWE method is used the results are in perfect agreement in the interested frequency band. The effect of the expansion point is inspected. It is seen that a better approximation is obtained, when the expansion frequency is close to the midpoint of the interested frequency range. The response of the reflection coefficient with respect to the incidence angle has also been obtained through AWE and compared with the results obtained using the direct calculation. A perfect match has been observed.

AWE method requires the calculation of derivatives of Green's functions at the expansion point. The calculation of these derivatives takes major part of the CPU time. When these derivatives are calculated, the rest of the procedure to evaluate reflection coefficients is fast. To compensate the derivative calculation time, the analysis should be required at many points. The experiments have shown that if the reflection coefficients at more than 84 points are required, AWE method is computationally more efficient than direct calculation.

By comparing the determinant plots of the characteristic matrices, it has been shown that AWE can also be used to obtain dispersion diagrams. The dispersion characteristics have been calculated and band diagram of the structure has been plotted using AWE. It is shown that the dispersion diagram between the light line (the boundary between surface wave modes and leaky waves) and Brillouin zone can be obtained efficiently through the use of Pade approximation

calculated at single point. To approximate the response below leaky wave zone another approximation at a different expansion point is necessary.

When the CPU times required for calculation of band diagrams are compared it has been seen that AWE method is 3 times more efficient than direct calculation procedure. The computational efficiency of AWE can be increased by calculating derivatives in a shorter time. The research is going on to evaluate derivatives in a shorter time.

In Chapter 5 a method is presented to analyze microstrip lines on periodically implanted substrates. In this method firstly the reflection coefficients of the substrate are calculated. Those reflection coefficients are inserted into the Green's function expressions of homogenous substrate to obtain Green's functions of the periodically implanted substrate. Using those Green's functions, the microstrip line has been analyzed as if the substrate is homogenous.

The proposed method is verified using a substrate with a fill ratio equal to one. The propagation constant of a microstrip line on periodically implanted substrate is calculated using the proposed method. The results are compared with the ones that are obtained for the homogenous substrate as well as with the literature. It has been seen that the results are in perfect agreement.

The propagation constants of a microstrip line on a substrate with different fill ratios have also been calculated. The results are compared with the literature and the ones obtained using effective medium theory. It has been seen that using the proposed method a good approximation is obtained. The proposed method gives similar results with effective medium theory. Using the proposed method the bandgap formation that is reported in the literature could not be observed. The reason lies behind the plane wave approximation used in the method. In the method it has been assumed that major contribution of the substrate comes from the fundamental Floquet mode. For this reason only fundamental mode has been used to calculate the reflection coefficients and other modes have been discarded. It has been seen that those discarded Floquet modes plays an important role in the formation of bandgap region.

As a consequence, the proposed method can be used as an alternative to the effective medium theory to model microstrip lines on EBG substrates when the bandgap information has no importance, i.e. to calculate far field radiation.

Future Work

In Chapter 2 a procedure has been developed for the fast analysis and optimization of 2-D metallic structures. In this procedure the electric field at a predefined position is optimized through genetic algorithm. The proposed method can easily be modified to optimize far field pattern of the structure. With this modification the optimization procedure can be used to synthesize 2-D leaky wave antennas.

In Chapter 2 aperiodic microstrip structures has been analyzed and optimized. The periodic 2-D microstrip structures can also be analyzed and optimized with the available computer code. For this purpose the Green's function should be replaced with the periodic Green's functions. With this modification the procedure can be used to design 2-D frequency selective surfaces and EBG structures.

In Chapter 3 a 3-D MoM procedure has been presented. In Chapter 4 the use of AWE method has been suggested to increase the computational efficiency of the procedure. In this work one dimensional AWE procedure has been used to obtain the reduced order model of the structure. This enables obtaining full response of the structure over one sweep parameter. To obtain the model of the structure with respect to two sweep parameters, two dimensional AWE procedure can be applied as in [63]. Using two dimensional AWE procedure, the variation of reflection coefficient with respect to azimuthal and elevation angles can be calculated at the same time. Two dimensional AWE procedure can also be used to obtain a model of the solution with respect to propagation constant and frequency. This will enable fast computation of band diagrams. For this purpose we have to calculate the partial derivatives of the kernel function. Using Taylor's differentiation method (TADIFF) it is not possible because it enables to calculate the derivative of a function can be calculated with respect to one variable.

However, the partial derivatives with respect to. several variables can be calculated through Forward Differentiation (FAD) and Backward Differentiation (BAD) methods [67].

In Chapter 5 a method has been suggested to analyze aperiodic microstrip structures on EBG substrates as an alternative to the effective medium theory. Using the method it is not possible to obtain bandgaps in the structure. For this purpose a new Green's function formulation that includes contribution of all Floquet modes is required. To develop a more accurate procedure the research should go in the direction to formulate such a new Green's function that models the interaction of aperiodic electric dipole with the periodic substrate. If such a Green's function can be formulated, the more accurate analysis of the structure would be possible using the procedure explained in Chapter 5.

The method proposed in Chapter 5 can also be used to obtain scattering characteristics of microstrip lines on EBG substrates. For this purpose the procedure explained in Chapter 2 can be combined with the procedure explained in Chapter 5. The reflection coefficients of the substrate are calculated through 3-D MoM procedure and inserted into Green's functions. The complex exponentials are obtained using GPOF method and currents on the conductors are calculated following the procedure explained in Chapter 2.

REFERENCES

[1] E. Yablonovitch, "Inhibited spontaneous emission in solid state physics and electronics," *Phys. Rev. Lett.*, vol.58, pp. 2059-2062, May 1987.

[2] Y. Rahmat-Samii, "The marvels of electromagnetic bandgap (EBG) structures: Novel microwave and optical applications," in *Microwave and Optoelectronics Conference, 2003*, vol. 1, pp.265–275.

[3] G. Eleftheriades, Y, Vardaxoglou, "Editorial note," *IET Microwave Antennas Propagat. : Special Issue on Metamaterials LHM*, vol. 1, no.1, pp. 1-3, February 2007.

[4] V. G. Veselago, "The electrodynamics of substances with simultaneously negative values of ε and μ," Sov. *Phys. Uspekhi,* vol. 10, no. 4, pp. 509-514, January 1968.

[5] D. R. Smith, W.J. Padilla, D.C. Vier, S.C. Nemat-Nasser and S, Schultz, "Composite medium with simultaneously negative permeability and permittivity," *Phys. Rev. Lett.,* vol. 84, pp. 4184-4187, May 2000.

[6] M. Lapine, S. Tertyakov, "Contemporary notes on metamaterials," *IET Microwave. Antennas Propagat. : Special Issue on Metamaterials LHM*, vol. 1, no.1, pp. 1-3, February 2007.

[7] E. Shamonina, L. Solymar, "Metamaterials: How the subject started," *Metamaterials 1*, pp.2-11, February 2007.

[8] Ari Sihvola, "Metamaterials in electromagnetics," *Metamaterials 1*, pp.2-11, February 2007.

[9] M. J. Vaughan, K. Y. Hur, R. C. Compton, "Improvement of microstrip patch antenna radiation patterns," *IEEE Trans. Antennas Propagat.,* vol. 42, pp. 882-885, June 1994.

[10] R. Gonzalo, P. de Maagt, M. Sorolla, "Enhanced patch-antenna performance by suppressing surface waves using photonic-bandgap substrates,*" IEEE Trans. Microwave Theory Tech.,* vol. 47, pp. 2131-2138, November 1999.

[11] P. Salonen, M. Keskillami, L. Sydanheimo, "A Low-cost 2.45Ghz photonic bandgap patch antenna for wearable systems," *in IEE 11th International Conference on Antennas and Propagat., 2001*, no. 480, pp. 719-723.

107

[12] C. Cheype, M. Thevenot, R. T. Monodiere, A. Reineix, B. Jecko, "An electromagnetic bandgap resonator antenna," *IEEE Trans. Antennas Propagat.,* vol. 50, pp.1285-1290, September 2002.

[13] M. Thevenot, C. Cheype, A. Reineix, B. Jecko, "Directive photonic-bandgap antennas," *IEEE Trans. Microwave Theory Tech.,* vol. 47, pp. 2115-2121, November 1999.

[14] R. Gonzalo, I. Ederra, C. M. Mann, P. de Maagt, "Radiation properties of terahertz dipole antenna mounted on photonic crystal," *Electronic Lett.,* vol. 37, pp. 613-614, May 2001.

[15] V. Radisic, Y. Qian, R. Coccioli, T. Itoh, "Novel 2-D photonic bandgap structure for microstrip lines,*" IEEE Microwave and Guided Wave Lett.,* vol. 8, pp. 69-71, February 1998.

[16] T. Y. Yun, K. Chang, "Uniplanar one-dimensional photonic-bandgap structures and resonators," *IEEE Trans. Microwave Theory Tech.,* vol. 49, pp.549-553, November 2001.

[17] W. J. Chappel, X. Gong, "Wide bandgap composite EBG substrates," *IEEE Trans. Antennas Propagat.,* vol. 51, pp.2744-2750, October 2003.

[18] T. Euler, J. Papapolymerou, "Silicon micromachined EBG resonator and two-pole filter with improved performance characteristics," *IEEE Microwave and Wireless Components Lett.,* vol. 13, pp.373-375, September 2003.

[19] S. G. Johnson, J. D. Joannopoulos, *Photonic Crystals: The Road from Theory to Practice*, chap. 8., Boston: Kluwer Academic Publishers,2002.

[20] K. M. Ho, C. T. Chan, C. M. Soukoulis, "Existence of a photonic gap in periodic dielectric structures," *Phys. Rev. Lett.*, vol. 65, pp.3152-3155, December 1990.

[21] V. Twersky, "Multiple scattering of electromagnetic waves by arbitrary configurations," *Journal of Mathematical Phys.*, vol. 8, pp. 589-610, 1967.

[22] Y.-Y. Chen, Z. Ye, "Acoustic attenuation by two-dimensional arrays of rigid cylinders," *Phys. Rev. Lett.,* vol. 87, pp. 3011-3015 , October 2001.

[23] C.-H Kuo, Z. Ye, "Optical transmission of photonic crystal structures formed by dielectric cylinders: Evidence for non-negative refraction," *Phys. Rev. E.*, vol. 70, pp. 6081-6084, 2004.

[24] P. de Maagt, R. Gonzalo, J. Vardaxooglou, J. M. Baracco, "Review of electromagnetic-bandgap technology and applications," *Radio Science Bulletin*, no. 309, pp. 11-25, June 2004.

108

[25] H. Y.D. Yang, "Finite difference analysis of 2-D photonic crystals," *IEEE Trans. Microwave Theory Tech.,* vol. 44, no.12, pp.2688-2695, 1996.

[26] W. Sun, K. Liu, and C. Balanis, "Analysis of singly and doubly periodic absorbers by frequency-domain finite difference method," *IEEE Trans. Antennas Propagat.,* vol. 44, pp. 798-805, June 1996.

[27] J. A. Roden, S. D. Gedney, M. P. Kesler, J. G. Maloney, P. H. Harms, "Time-domain analysis of periodic structures at oblique incidence: orthogonal and nonorthogonal FDTD implementations," *IEEE Trans. Microwave Theory Tech.,* vol. 46, pp.420-426, April 1998.

[28] P. Harms, R. Mittra, W. Ko, "Implementation of periodic boundary condition in the finite-difference time-domain algorithm for FSS structures," *IEEE Trans. Antennas Propagat.,* vol. 42, no.9, pp. 1317-1324, June 1994.

[29] Z. Lou, J-M. Jin, "Analysis of 3-D frequency selective structures using a higher order finite element method," *Microwave and Optical Technology Lett.*, vol. 38, no.4, pp. 259-263, 2003.

[30] L. Zhang, N. G. Alexopoulos, D. Sievenpiper, E. Yablonovitch, "An efficient finite element method for the analysis of photonic bandgap materials," *IEEE M.T.T. Symposium Digest*, 1999, pp. 1703-1706,.

[31] T. F. Eibert, J. L. Volakis, D. R. Wilton, D. R. Jackson, "Hybrid FE/BI modeling of 3-D doubly periodic structures utilizing triangular prismatic elements and MPIE formulation accelerated by the Ewald transformation," *IEEE Trans. Antennas Propagat.,* vol. 47, no. 5, pp. 843-850, May 1999.

[32] C.F. Yang, W.D. Burnside, R.C. Rudduck, "A double periodic moment method solution for the analysis and design of an absorber covered wall,", *IEEE Trans. Antennas Propagat.,* vol. 41, pp. 600-601, May 1993

[33] H.Y. Yang, "Characteristics of guided and leaky waves on multilayer thin-film structures with planar material gratings," *IEEE Trans. Microwave Theory Tech.,* vol. 45, no. 3, pp. 428-435, March 1997.

[34] H. Y. Yang, "Reflection and transmission of waves from multilayer structures with planar-implanted periodic material blocks," *Journal of Optical Society of America,* vol. 14, no. 10, pp. 2513-2521, October 1997.

[35] J. D. Shumpert, "Modeling of Periodic Dielectric Structures," Ph. D. Thesis, University of Michigan, Michigan, U.S.A, 2001.

[36] I. Bardi, Z. Cendes, "New directions in HFSS for designing microwave devices," *Microwave Journal*, vol. 41, no. 8, pp. 22-36, 1998.

[37] N. Kinayman, M. I. Aksun, *Modern Microwave Circuits*, Boston: Artech House, 2005.

[38] H. Y. Yang, "Theory of microstrip lines on artificial periodic substrates," *IEEE Trans. Microwave Theory Tech.,* vol. 47, no. 5, pp. 629-635, May 1999.

[39] M. I. Aksun, F. Çalıskan, and Levent Gürel, "An efficient method for electromagnetic characterization of 2-D geometries in stratified media," *IEEE Trans. Microwave Theory Tech.*, vol. 50, pp. 1264-1274, May 2002.

[40] Y. Hua, T. K. Sarkar, "Generalized pencil-of-function method for extracting poles of an EM system from its transient response," *IEEE Trans. Antennas Propagat.*, vol. 37, pp.229-234, Feb.1989.

[41] W. C. Chew, *Waves and Fields in Inhomogeneous Media*. New York: Van Nostrand Reinhold, 1990.

[42] L. Alatan, M. I. Aksun, K. Leblebicioglu, and T. Birand, "Use of computationally efficient method of moments in the optimization of printed antennas," *IEEE Trans. Antennas Propagat.*, vol. 40, pp. 725-732, April 1999.

[43] D. E. Goldberg, Genetic *Algorithms in Search, Optimization and Machine Learning*, Massachusetts: Addison-Wesley Publishing Co., 1989.

[44] R. F. Pierret, *Modular Series on Solid State Devices Volume IV: Advanced Semiconductor Fundamentals,* Massachusetts: Addison-Wesley Publishing Co., 1985.

[45] D. M. Pozar, Benedikt D. H.Schaubert, "Scan blindness in infinite phased arrays of printed dipoles," *IEEE Trans. Antennas Propagat.*, vol. 32, no.6, pp.602-610, June1984.

[46] G. Dural, M.I. Aksun, "Closed-form Green's functions for general sources and stratified media," *IEEE Trans. Antennas Propagat.*, vol. 43, no. 7, pp. 1545-1552, July 1995.

[47] Y. Rahmat-Samii, "On the question of computation of the dyadic Green's function at the source region in waveguide cavities," *IEEE Trans. Microwave Theory Tech.*, vol. 23, no. 9, pp. 762–765, Sept. 1975.

[48] J. Arsac, *Fourier Transforms and The Theory of Distributions*, New Jersey: Prentice-Hall, 1966.

[49] G. Cano. F. Mesa, F. Medina, M. Horno, "Systematic computation of the modal spectrum of boxed microstrip, finline and coplanar waveguides via an

efficient SDA," *IEEE Trans. Microwave Theory Tech.*, vol. 43, no. 4, pp. 866-872, April 1995.

[50] M. Bozzi, S. Germani, L. Minelli, L. Perregrini, P. de Maagt, Efficient calculation of the dispersion diagram of planar electromagnetic bandgap structures by the MoM/BI-RME method," *IEEE Trans. Antennas Propagat.*, vol. 53, no.1, pp.29-35, January 2005.

[51] V. A. Labay, J. Bornemann, "Matrix singular value decomposition for pole-free solutions of homogeneous matrix equations as applied to numerical modeling methods," *IEEE Microwave and Guided Wave Lett.,* vol. 2, no. 2, pp. 49-51, February 1992.

[52] S. Amari, J. Bornemann, R. Vahldieck, "A technique to locate minima in singular-value decomposition for eigenvalue problems in electromagnetics," *Microwave and Optical Tech. Lett.*, vol. 14, no. 6, April 1997.

[53] W. H. Press, S. A. Teukolsky, W. T. Vetterling, B. P. Flannery, *Numerical Recipes in C*, New York: Cambridge University Press, 1992.

[54] R. Hooke, T.A. Jeeves, "Direct search solution of numerical and statistical problems," *Journal of the Association for Computing Machinery*, vol. 8, pp. 212-229, April 1961.

[55] M. S. Bazaara, H. D. Sherali, C. M. Shetty, *Nonlinear Programming: Theory and Algorithms*, New York: John Willey & Sons., 1993.

[56] K. Sakoda, *Optical Properties of Photonic Crystals*, ch. 8, Berlin: Springer-Verlag, 2001.

[57] L.T. Pillage, R. A. Rohrer, "Asymptotic waveform evaluation for timing analysis," *IEEE Trans. Computer-Aided Design ,* vol. 9, no. 4, pp. 352-366, April 1990.

[58] E. K. Miller, "Model-Based parameter estimation in electromagnetics: Part I. background and theoretical development," *IEEE Trans. Antennas Propagat. Mag.* , vol.40, no.1, pp.42-52, 1998.

[59] F. Ling, D. Jiao, J. M. Jin, "Efficient electromagnetic modeling of microstrip structures in multilayer media," *IEEE Trans. Microwave Theory Tech.,* vol. 47, no. 9, pp. 1810-1818, September 1999.

[60] E. K. Miller, "Model-Based parameter estimation in electromagnetics: Part II. applications to EM observables," *IEEE Trans. Antennas Propagat. Mag.*, vol.40, no.2, pp.51-65, 1998.

[61] M. Davidovitz, "Approach to model order reduction for angular response calculations in periodic structures," *Electronic Lett.*, vol.38, no.8, pp.357-358, April 2002.

[62] W. H. Press, S. A. Teukolsky, W. T. Vetterling, B. P. Flannery, *Numerical Recipes in C*, New York: Cambridge University Press, 1992.

[63] Y. Xiong, D. G. Fang, F. Ling, "Two-Dimensional AWE technique in fast calculation of microstrip antennas," in *3rd Int. Conf. on Microwave Millimeter Tech. Proc.,* 2002, pp.393-396.

[64] J. Karczmarczuk, "Functional Differentiation of Computer Programs", in *Int. Conference on Functional Programming,* 1998, pp. 195-203.

[65] RWTH Aachen University Inst. for Scientific Computing, *Community Portal for Automatic Diff.*, [Online]. Available: http://www.autodiff.org, [Accessed May 2007].

[66] C. Bendtsen, O. Stauning, "TADIFF, a flexible C++ package for automatic differentiation using Taylor series expansion," Department of Mathematical Modeling, Technical University of Denmark, Denmark, IMM-REP-1997-07, 1997.

[67] C. Bendtsen, O. Stauning, "FADBAD, a flexible C++ package for automatic differentiation using forward and backward methods," Department of Mathematical Modeling, Technical University of Denmark, Denmark, IMM-REP-1996-17, 1996.

[68] A. S. Andrenko, Y. Ikeda, O. Ishida, "Application of PBG microstrip circuits for enhancing the performance of high density substrate patch antennas," *Microwave and Opt. Tech. Lett.,* vol. 32, no. 5, pp. 340-344, January 2002.

[69] J. Paul Skinner, Benedikt A. Munk, "Mutual coupling between parallel columns of periodic slots in a ground plane surrounded by dielectric slabs," *IEEE Trans. Antennas Propagat.*, vol. 40, no.11, pp.1324-1335, November 1992.

[70] T. Itoh, R. Mittra, "Spectral domain approach for calculating the dispersion characteristics of microstrip lines," *IEEE Trans. Microwave Theory Tech.,* vol. 21, no. 7, pp. 496-499, July 1973.

[71] T. Güdü, L. Alatan, "A Non-Galerkin spatial domain approach for efficient calculation of the dispersion characteristics of microstrip lines," submitted to *2008 IEEE Antennas and Propagation Society International Symposium.*

[72] J. Bernal, F. Medina, R.R. Boix and M. Horno, "Fast full-wave analysis of multistrip transmission lines Based on MPIE and complex image theory," *IEEE Trans. Microwave Theory Tech.*, vol. 48, pp.445–452, March 2000.

[73] T.H.Ng, L. Ooi and P.S. Kooi, "A Non-Galerkin method of computing the dispersion characteristic of microstrip lines using spectral-domain analysis," *Microwave and Optical Technology Lett.*, vol. 27, pp, 72-77, October 2000.

[74] C. J. F. Bottcher and P. Bordewijk, *Theory of Electric Polarization.* New York: Elsevier, 1978, vol. 2, pp. 476-491.

[75] M. I. Aksun, "A robust approach for the derivation of closed form Green's functions," *IEEE Trans. Microwave Theory Tech.*, vol. 44, pp. 651–658, May 1996.

[76] M. Kobayashi and F. Ando, "Dispersion characteristics of open microstrip lines," *IEEE Trans. Microwave Theory Tech.*, vol. 35, pp. 101–105, February 1987.

[77] C. Shih, R.B. Wu, S.K. Jeng and C.H. Chen, "A Full-wave analysis of microstrip lines by variational conformal Mapping technique," *IEEE Trans. Microwave Theory Tech.*, vol. 36, pp. 576–581, March 1988

APPENDIX-A

VOLUME EQUIVALENCE THEOREM

Consider the scattering problem in Fig. A.1. In the figure the medium has permittivity and permeability constants ε_0, μ_0 respectively. A scattering object with ε_a, μ_a is placed in the medium. The sources $\bar{J}, \bar{M}$ radiate into medium and generate fields $\bar{E}, \bar{H}$.

$$\bar{E} = \bar{E}^s + \bar{E}^i$$

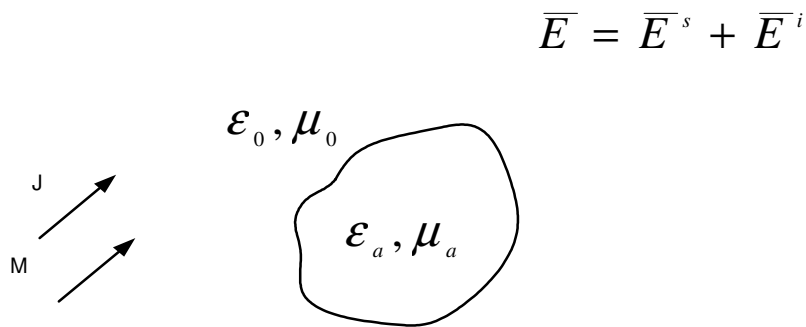**Figure A.1 the scattering problem**

The electric and magnetic field satisfies:

$$\bar{\nabla} x \bar{E}^i = -j\omega\mu_0 \bar{H}^i - \bar{M}$$
$$\bar{\nabla} x \bar{H}^i = j\omega\mu_0 \bar{E}^i + \bar{J} \tag{A.1}$$

Let's define the disturbance fields as:

$$\bar{E}^s = \bar{E} - \bar{E}^i, \quad \bar{H}^s = \bar{H} - \bar{H}^i \tag{A.2}$$

The disturbance fields also satisfy the Maxwell's Equations:

$$\nabla x \overline{E}^{\,s} = \nabla x \overline{E} - \nabla x \overline{E}^{\,i}$$
$$= -j\omega\mu_a \overline{H} + j\omega\mu_0 \overline{H}^{\,i}$$
$$= -j\omega\mu_a \overline{H} + j\omega\mu_0 \overline{H} - j\omega\mu_0 \overline{H}^{\,s} \qquad (A.3)$$
$$= \underbrace{-j\omega(\mu_a - \mu_0)\overline{H}}_{-\overline{M}_{eq}} - j\omega\mu_0 \overline{H}^{\,s}$$

$$\nabla x \overline{H}^{\,s} = \nabla x \overline{H} - \nabla x \overline{H}^{\,i}$$
$$= j\omega\varepsilon_a \overline{E} - j\omega\varepsilon_0 \overline{E}^{\,i} \qquad (A.4)$$
$$= \underbrace{j\omega(\varepsilon_a - \varepsilon_0)\overline{E}}_{\overline{J}_{eq}} + j\omega\varepsilon_0 \overline{E}^{\,s}$$

The equations (A.3) and (A.4) reveal that the scattering object in the original problem could be replaced with equivalent sources, $\overline{J}_{eq}, \overline{M}_{eq}$ such that,

$$\overline{J}_{eq} = j\omega(\varepsilon_a - \varepsilon_0)\overline{E}$$
$$\overline{M}_{eq} = j\omega(\mu_a - \mu_0)\overline{H} \qquad (A.5)$$

The equivalent problem is shown in Fig. A-2.

$$\overline{E} = \overline{E}^{\,s} + \overline{E}^{\,i}$$

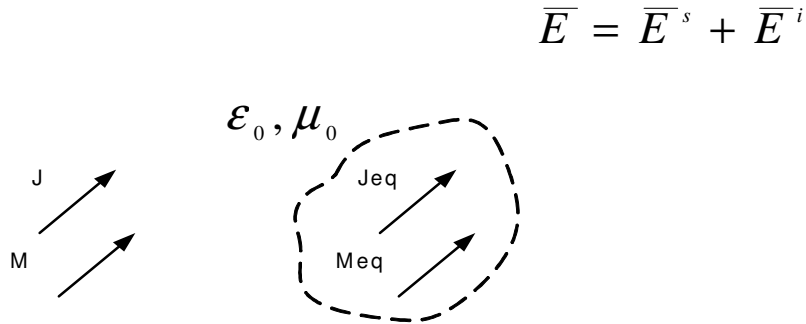**Figure A.2 The volume equivalent problem**

DERIVATION OF GREEN'S FUCTION FOR PERIODIC STRUCTURES

The component's of space domain Green's function which represents the electric field from infinitesimal dipole is equal to the inverse Fourier transform of the spectral domain counterparts, given by:

$$G_{uv}(r,r') = \frac{1}{4\pi^2} \int\limits_{-\infty}^{\infty}\int\limits_{-\infty}^{\infty} \widetilde{G}_{uv}(k_x,k_y,z,z') e^{-jk_x(x-x')} e^{-jk_y(y-y')} dk_x dk_y \qquad (B.1)$$

where, $\widetilde{G}_{uv}$ is the component of the spectral domain electric field Green's function in terms of k_x, k_y, z, z'.

The Floquet's theorem says that for doubly periodic structures the dipole currents in a doubly periodic structure must be phased as:

$$\bar{J}(x+ma, y+nb, z) = \bar{J}(x,y,z).e^{-jmaB_x} e^{-jnbB_y} \qquad (B.2)$$

Therefore the Green's function for the periodic structure is written as:

$$G_{uv}(r,r') = \frac{1}{4\pi^2} \sum_{m=-\infty}^{\infty} \sum_{n=-\infty}^{\infty} e^{-jmaB_x} e^{-jnbB_y} \int\limits_{-\infty}^{\infty}\int\limits_{-\infty}^{\infty} \widetilde{G}_{uv}(k_x,k_y,z,z') e^{-jk_x(x-x'-ma)} e^{-jk_y(y-y'-nb)} dk_x dk_y$$

$$(B.3)$$

(B.3) can be thought of as a Green's function of an infinite phased array of infinitesimal dipoles in stratified media. With this from the equation is not computationally usable because of double integration on the spectral domain Green's function terms. Using the Poisson's sum formula, the expression can be written in more simplified and computationally usable form [45]. Poisson's formula is written as:

$$\sum_m e^{jm\omega_0 t} F(m\omega_0) = T \sum_m f(t+mT) \qquad (B.4)$$

Let $f(t) = h(t)e^{j\omega_1 t}$. Then $F(\omega) = H(\omega - \omega_1)$ and (B.4) is written as:

$$\sum_m e^{jm\omega_0 t} H(m\omega_0 - \omega_1) = T\sum_m h(t + mT)e^{j\omega_1(t+mT)} \qquad \text{(B.5)}$$

Substituting the explicit expression of $H(m\omega_0 - \omega_1)$ into (B.5), we can write:

$$\sum_m e^{jm\omega_0 t} \int_{-\infty}^{\infty} h(t')e^{-j(m\omega_0 - \omega_1)t'}dt' = T\sum_m h(t + mT)e^{j\omega_1(t+mT)} \qquad \text{(B.6)}$$

If the (B.3) is compared with (B.6) the similarities can be seen. By letting $t = \beta_y$, $t' = k_y$, $\omega_0 = a$, $\omega_1 = x - x'$, $h = \tilde{G}_{uv}$ and applying (B.6) twice, (B.3) can be written as:

$$G_{uv}(r, r') = \frac{1}{ab} \sum_{m=-\infty}^{\infty} \sum_{n=-\infty}^{\infty} \tilde{G}_{uv}(k_x, k_y, z, z')e^{-jk_x(x-x')}e^{-jk_y(y-y')} \qquad \text{(B.7)}$$

where, $k_x = 2\pi n / a + \beta_x$, $k_y = 2\pi n / b + \beta_y$.

A NON-GALERKIN SPATIAL-DOMAIN APPROACH FOR EFFICIENT CALCULATION OF THE DISPERSION CHARACTERICTICS OF MICROSTRIP LINES

Introduction

In the analysis of dispersion characteristics of microstrip lines, spectral domain approaches have been preferred as opposed to the spatial domain calculations since the spatial domain Green's functions corresponding to the microstrip structure require the numerical evaluation of inverse Fourier transform integrals which are computationally expensive. However as demonstrated in [72], the discrete complex image representation of the spatial domain Green's functions eliminates the need for the evaluation of numerical integrals and renders the spatial domain method to be more efficient compared to the spectral domain approach. When the discrete complex image method (DCIM) is used, the matrix entries of the eigenvalue problem involve double integrations in the spatial domain. One of them is the convolution integral with the basis function, the other one is the inner product integral with the testing function to impose the boundary conditions. In case a Galerkin approach with basis functions satisfying the edge conditions on the conducting strips is preferred as in [72], these integrals need to be evaluated numerically. However, if a non-Galerkin approach with pulse type testing functions is adopted, one of the integrals could be evaluated analytically and a single numerical integration is required. In this study, the non-Galerkin method is utilized and the accuracy of the method is demonstrated by comparing the results of dispersion characteristics to the ones found in the literature.

Formulation

Consider an infinite microstrip line embedded in a multilayered medium as shown in Figure C-1. By denoting the unknown propagation constant as β, a common phase factor $e^{-j\beta y}$ is assumed for fields and currents, and it is suppressed. By enforcing the boundary condition for the tangential components of the electric field at the surface of the conductor, an integral equation is obtained in terms of the unknown surface currents on the strip. Then, the unknown currents are expanded in terms of known basis functions.
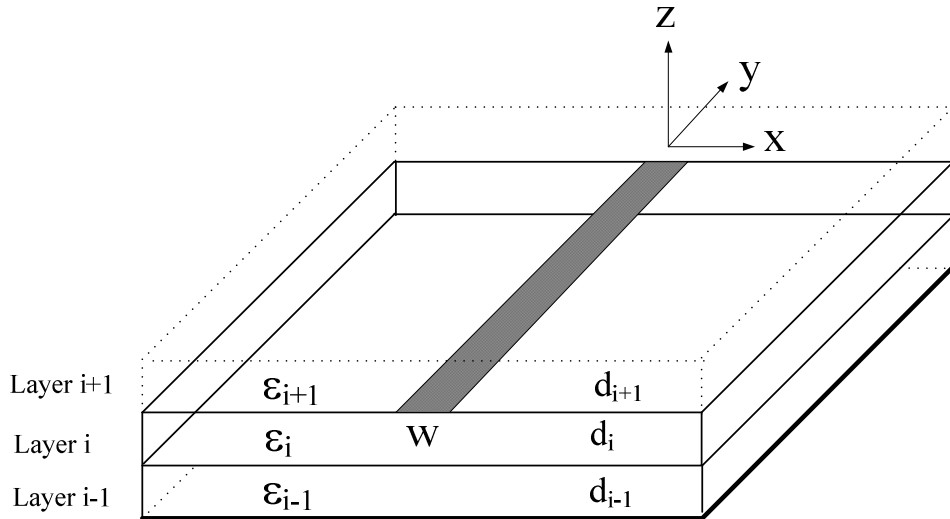
Figure C-1 Geometry of the microstrip line

In this study, only one basis function is assumed for the longitudinal current ($B_y(x)$) and the transverse current is neglected ($B_x(x)=0$), to explore the accuracy limits of the proposed method in the dispersion analysis of microstrip structures with parameters (w,d,ε) that are widely used in practical applications. Although the formulation is easily applicable for both longitudinal and transverse current components as given in [72], here it will be presented only for the longitudinal component for the sake of brevity. The inner product integral of the

119

testing function and the y-component of the electric field are written in the following form:

$$\langle T_y(x), E_y(x) \rangle = -j\omega \int_{D_T} dx T_y(x) \int_{D_B} G_{yy}^E(x - x') B_y(x') dx' \qquad \text{(C.1)}$$

the space domain Green's function for the electric field (G_{yy}^E) can be written in terms of the Green's functions for the vector (G_{yy}^A) and scalar potentials (G_y^q) as follows:

$$G_{yy}^E = G_{yy}^A - \frac{\beta^2}{\omega^2} G_y^q$$

The contribution of surface wave poles ($k_{\rho p}$) are extracted from the spectral domain Green's functions; and the remaining part is cast into a summation of complex exponentials by using the two-level approximation scheme employing GPOF method [75]. Then, the 2D space domain Green's functions are expressed in the following closed form:

$$G \cong \frac{1}{4j} \sum_{i=1}^{N} a_i H_0^{(2)}\left(k_t \sqrt{(x-x')^2 - b_i^2}\right) + \sum_{p=1}^{N_p} \frac{\text{Res}(k_{\rho p}) k_{\rho p}}{\alpha} e^{-\alpha|x-x'|} \qquad \text{(C.2)}$$

where $k_t = \sqrt{k_i^2 - \beta^2}$, $\alpha = \sqrt{\beta^2 - k_{\rho p}^2}$, k_i is the wave number of the observation layer, N is the number of complex exponentials used to approximate the spectral domain Green's functions, a_i and b_i are the coefficients and exponents of the complex exponentials, respectively; N_p is the number of surface wave poles and Res denotes the residue of the corresponding pole.

By changing the order of integrations in equation (C.1), the convolution integral between the basis function and the Green's function can be transferred into a correlation integral between the basis and testing functions as:

$$\langle T_y(x), E_y(x) \rangle = j\omega \int du G_{yy}^E(u) \underbrace{\int T_y(x) B_y(x-u) dx}_{F(u)} \qquad \text{(C.3)}$$

The following basis function that satisfies the singularity condition at the edges of the strip is chosen:

$$B_y(x) = \frac{1}{\sqrt{1-\left(\dfrac{2x}{w}\right)^2}} \quad for \;\; |x| \leq w/2 \tag{C.4}$$

When pulse type testing function is used, the correlation integral in (C.2) can be evaluated analytically as:

$$F(u) = \begin{cases} \dfrac{w}{2}\left[\dfrac{\pi}{2} + \sin^{-1}\left(\dfrac{2u}{w}+1\right)\right] & for \;\; -w < u < 0 \\[2em] \dfrac{w}{2}\left[\dfrac{\pi}{2} - \sin^{-1}\left(\dfrac{2u}{w}-1\right)\right] & for \;\; 0 < u < w \end{cases} \tag{C.5}$$

Finally, the single integral left in equation (C.3) is evaluated numerically after subtracting the singularity of the Hankel function at $u=0$, and then adding its contribution analytically. A code is written in MATLAB to find the β value that makes the result of this integration zero.

Simulation results and conclusions

To verify the accuracy of the proposed method, the β values obtained for the fundamental mode of a microstrip line are compared to the ones presented in [72]. In [72], it is mentioned that four quadrature points are used for numerical integrations. During the simulations, it is observed that our results converge for larger number of quadrature points. Therefore, the results for two different cases are presented. Case A: 4 quadrature points, Case B: numerical integration converges. The results are given in Table C.1

Table C.1 Comparison of β/k_0 results (w=3.0mm, d=0.635mm, ε_r=9.8)

f (GHz)	20	25	30	35	40	45	50
From [72]	2.977	3.006	3.026	3.042	3.054	3.064	3.071
Our results (A)	2.987	3.011	3.028	3.052	3.062	3.071	3.078
Our results (B)	2.994	3.017	3.035	3.048	3.058	3.067	3.074

The results given in [72] are obtained by using 3 basis functions for the longitudinal current and 2 basis functions for the transverse current. However in our analysis, only one basis function is used for the longitudinal current and transverse current is neglected. The only difference between the two approaches is the choice of testing functions. In [72], Galerkin approach is used so the testing functions also posses an edge singularity like the basis functions. The agreement in the results obtained by using a smaller number of basis functions may be due to the pulse type testing function used in this study that gives equal importance to each point on the strip while imposing the boundary conditions, as opposed to the testing function used in [72] that emphasizes the boundary conditions at the edges.

A last example is studied to explore the accuracy limits of the proposed method for electrically wide microstrip lines build on electrically thick substrates. The results are compared to the ones reported in [73], [76], [77], and summarized in Table C.2. To make a fair comparison, from [73] only the results corresponding to one basis function is included in the table. From Table C.2, it can be observed that by using the proposed method very satisfactory results are obtained even for wide microstrip lines which are not generally preferred in practical applications.

Table C.2 Comparison of the effective dielectric constant (ε_r=8, w/d=1)

h/λ_0	From [76]	From [77]	From [73]	Our results
0.005	5.468	5.471	5.467	5.476
0.05	6.124	6.130	6.122	6.145
0.1	6.742	6.753	6.750	6.785
0.3	7.62	7.654	7.660	7.674

In summary, an efficient non-Galerkin spatial domain method is proposed to analyze the dispersion characteristics of microstrip lines build in multilayer substrates. The efficiency of the method is due to the utilization of discrete

complex images in obtaining the 2D space domain Green's functions and the choice of pulse type testing functions that eliminates one of the numerical integrations. It is also observed that very satisfactory results are obtained even with a single basis function. This may be attributed to the better conformity of the boundary conditions achieved by the choice of pulse type testing function.

CURRICULUM VITAE

PERSONAL INFORMATION

Surname, Name: GÜDÜ, Tamer

Nationality: Turkish (T.C.)

Date and Place of Birth: 10 February 1977, Bursa

Marital Status: Married

Phone : +90-262-6481435

email: tgudu@uekae.tubitak.gov.tr

EDUCATION

Degree	Instution	Year of Graduation
MS	METU Electrical and Electronics Eng.	2001
BS	Bilkent U. Electrical and Electronics Eng.	1998
High School	Bursa Cumhuriyet Lisesi	1993

PUBLICATIONS

1. Güdü, T., Alatan L., "A Non-Galerkin spatial domain approach for efficient calculation of the dispersion characteristics of microstrip lines," submitted to *2008 IEEE Antennas and Propagation Society International Symposium.*

WORK EXPERIENCE

Year	Place	Enrollment
2001-Present	TÜBİTAK-UEKAE	Senior Researcher
1999-2000	TÜBİTAK-SAGE	Researcher
1998-1999	Bilkent Univ.	RF Engineer

HOBBİES

Swimming, skiing, motorcycle driving, fitness, reading.